NOAA Technical Memorandum ERL ARL-184

DEVELOPMENT OF A "GENERIC" MOBILE FLUX PLATFORM WITH DEMONSTRATION ON A SMALL AIRPLANE

Timothy L. Crawford
Robert T. McMillen
Atmospheric Turbulence and Diffusion Division
Oak Ridge, Tennessee

R. J. Dobosy
Oak Ridge Associated Universities
Oak Ridge, Tennessee

Air Resources Laboratory
Silver Spring, Maryland
July 1990

UNITED STATES
DEPARTMENT OF COMMERCE

Robert A. Mosbacher
Secretary

NATIONAL OCEANIC AND
ATMOSPHERIC ADMINISTRATION

John A. Knauss
Under Secretary for Oceans
and Atmosphere/Administrator

Environmental Research
Laboratories

Joseph O. Fletcher
Director

NOTICE

Mention of a commercial company or product does not constitute an endorsement by NOAA/ERL. Use for publicity or advertising purposes, of information from this publication concerning proprietary products or the tests of such products, is not authorized.

ATDD Contribution File No. 90/4

For sale by the National Technical Information Service
5285 Port Royal Road, Springfield, VA 22161

CONTENTS

LIST OF FIGURES vi

LIST OF TABLES vii

ACKNOWLEDGMENTS viii

ABSTRACT. 1

1. INTRODUCTION 1

2. THEORY OF AIR VELOCITY MEASUREMENT 4
   2.1 Platform Velocity Measurement 4
   2.2 Relative Velocity Measurement 5

3. SYSTEM DESCRIPTION 5
   3.1 Motion Sensors 6
      3.1.1 Platform Motion Sensors 7
      3.1.2 Relative Air Motion Sensors 9
   3.2 Support Sensors 10
      3.2.2 High Speed Sensors 10
      3.2.3 Low Speed Sensors 12
   3.3 Data Acquisition System 13
      3.3.1 Hardware 14
      3.3.2 Software 14

4. AIRPLANE DESCRIPTION AND OPERATION 15
   4.1 Technical Specifications 15
   4.2 Operational Considerations 16
   4.3 Special Operations 17

5. DATA PROCESSING 17
   5.1 Path Boundary Conditions 17
   5.2 Flux Calculation Corrections 17
   5.3 Sensor Frequency Response and Lag Corrections 18

6. IN-FLIGHT TEST AND CALIBRATIONS 18

7. PRELIMINARY FIELD TESTS 24
   7.1 EPA Spatial Variability Study 24
   7.2 FIFE Field Results 26

8. CONCLUSIONS 29

REFERENCES 30

APPENDIX A: Wind Velocity from a Mobile Platform A1

APPENDIX B: Mixing High- and Low-Frequency Measurements B1

APPENDIX C: Relative Wind Velocity from a 9-Hole Pressure Sphere C1

APPENDIX D: Mobile Flux Platform–Key Routines From FLUX D1

LIST OF FIGURES

Figure 1. ATDD's MFP installed on a LONG-EZ for demonstration. 3
Figure 2. Accelerometers and pressure sensors located in the pressure sphere. 8
Figure 3. Pressure ports and symmetric probe positioning. 9
Figure 4. Temperature sensor inlet and position. 11
Figure 5. Mounting of the infrared H_2O/CO_2 analyzer. 12
Figure 6. Mounting of the net radiometer. 13
Figure 7. Spectral analysis of W'T'. 19
Figure 8. Spectral analysis of W'e'. 20
Figure 9. Spectral analysis of $W'O_3'$ 21
Figure 10. Spectral analysis of $W'CO_2'$. 22
Figure 11. Results of induced pitch motion calibration test. 23
Figure 12. Observed spatial variability of heat, moisture and O_3 flux. 26
Figure 13 Observed profiles of heat, moisture and CO_2 flux during FIFE 28

LIST OF TABLES

Table 1 Sensors Used to Determine V_p and V_a 7
Table 2 Wide-Body Long-EZ N286TS 16
Table 3 EPA Spatial Variability Study: Summary of Airplane Transect Data 25
Table 4 NASA FIFE--AUGUST 10, 1989: Summary of Airplane Transect Data 27

Acknowledgements

This work was supported by the National Oceanic and Atmospheric Administration and the United States Environmental Protection Agency. The authors thank Bruce Hicks not only for his enthusiastic encouragement of this effort but, also for having generated a Division within which talent existed to accomplish such technically complex tasks efficiently. Special recognition goes to David Auble and Robert Mayhew. David designed, built, and tested the electronic circuits and acted as an advisor on all electronic aspects. Without his help, many electrons would have taken an inappropriate path to ground before doing anything useful. Robert completed essential machining, fabrication, and electrical wiring. He had the difficult task of keeping up with the "change-of-the-day" while turning "good" ideas into field-practical hardware.

DEVELOPMENT OF A "GENERIC" MOBILE FLUX PLATFORM WITH DEMONSTRATION ON A SMALL AIRPLANE

ABSTRACT. *The theory, instrumentation and demonstration of a "generic" Mobile Flux Platform (MFP) to measure atmospheric turbulent structure and trace-gas air-surface exchange are described. This development responds to research needs for a low cost system capable of measuring representativeness and spatial variability of air-surface exchange over various ecosystems. The MFP was demonstrated on a small single engine airplane. For this demonstration, the system was configured to measure position, mean temperature, wind, and the fluxes of momentum, heat, moisture, carbon dioxide, and ozone. Additionally, low-frequency sensors document pressure altitude, radar altitude, incoming short-wave radiation, net radiation, and infrared surface temperature. The MFP described is novel in approach, and was designed to be a small low cost, generic "strap down" system. Specific applications require a platform-specific turbulence velocity probe. The low cost and practical nature of ATDD's MFP was made possible by recent technological advances in both low cost miniature sensors and computer technology. Small sensors allowed co-location of both the air velocity and motion sensors. This allows direct measurement of probe motion instead of platform motion. Modern computer technology allows not only channel input, data rate, and storage flexibility, but also mathematical rotation from platform to earth coordinates. Airborne platform utility also benefits from modern technology by use of a high performance canard airplane which is inexpensive to operate and aerodynamically well suited for high fidelity turbulent flux measurements.*

1. INTRODUCTION

The chemical make-up of our atmosphere and the resulting global environment are largely controlled by trace gas air-surface exchange. Considerable efforts are under way to assess the impacts of increasing trace gas concentration on our environment. These efforts are hampered by the spatial variability of trace gas exchange and limitations in existing measurement systems. Development of practical air-surface exchange measurement systems suitable for measuring trace gas exchange and spatial variability over both land and oceans is needed.

The only direct method for air-surface exchange measurement is eddy-covariance. Tower based measurement systems have become convenient and economical (McMillen, 1986), providing much point information on the temporal nature of air-surface exchange (Lenschow and Hicks, 1989). Unfortunately, they reveal little about representativeness of measurement, or spatial variability of exchange. Towers are poorly suited for obtaining representative flux measurements over heterogeneous terrain, and are difficult to install in remote areas such as oceans, forest, swamps, and tundra.

Mobile Flux Platforms (MFPs) instrumented for eddy-covariance measurement are, in principle, a more efficient tool for investigation of air-surface exchange over diverse surface conditions. A wide variety of carrying vehicles may be used. Balloons can probe greater heights than towers and can be more readily deployed from diverse locations. Ships can cover wide

ocean areas, while buoys can provide long-term measurements at remote ocean sites.

These ideas have been partially realized in such works as the balloon-borne turbulence velocity measurement of Lapworth and Mason (1988). Although ships are ideal over the deep oceans, practical application has not been demonstrated. Likewise, buoys carrying simple eddy flux systems which account for platform motion have not been demonstrated. The system described in this report represents further work toward development of a small low-power system suitable for use on many types of platforms. Application to a small airplane will be demonstrated.

For many purposes, the airplane is the most powerful mobile platform. Because an airplane flies at speeds of 50 to 100 m/s, the integration time necessary to obtain statistically steady flux measurements is shorter by more than an order of magnitude than that for earth fixed systems. Also, calm winds are no problem. All types of surface conditions can be explored. An airplane can easily probe the entire depth of the boundary layer. Flux divergence, determined from the difference in exchange measurements at various altitudes, allows for trace gas budget closure with the residual being an estimate of the net chemical production or destruction. Desjardins *et al.* 1982 and 1989, Greenhut 1983, and Lenschow *et al.* 1980 and 1981 give examples of aircraft MFP observations.

In the past, eddy covariance measurement from mobile platforms has been limited to expensive dedicated systems. For example, measurement using aircraft has been accomplished only with complex and expensive systems permanently installed on dedicated research airplanes. Application is expensive and therefore, limited to major research programs. Worldwide, only the National Center for Atmospheric Research (Lenschow, 1972) and the Canadian National Aeronautical Establishment (NAE, MacPherson *et al.*, 1981) have maintained a long-term airplane MFP capability. Due to the power of modern micro-computers and improved sensors, the creation of simple, efficient and flexible measurement systems is now possible. For example, Flinders University of South Australia (Häcker and Schwerdtfeger, 1988) has a relatively new research flux measurement system which is closer to the ATDD approach than the NCAR and NAE efforts. The Australian system uses a motor-glider for the platform. Although their platform and instrumentation are more expensive than that described herein, they are still inexpensive compared to those of the earlier NCAR and NEA efforts. But, from our viewpoint, it is better to directly measure probe motion, and it will be difficult to add trace gases measurements to the tractor engine motor-glider. The obvious extension of the ATDD MFP aboard a ship is in progress.

Both the ATDD MFP system and its airplane implementation are unique, as is readily apparent from Figure 1. The principles presented are generic and can be applied to any moving platform. The description is intentionally complete, so that others may "clone" and improve upon this effort. Although the basic methodology is similar to that described by Lenschow (1972) and MacPherson *et al.* (1981), simplifications in implementation and the use of modern sensors result in a simple low cost system. Light weight and low power demands are also significant advantages because small low cost aircraft can then be used.

The "strap-down" system described weighs 20 Kg and requires 150 watts of 12V DC power. For the demonstration, the MFP was configured to measure position, mean wind, Reynolds stress and the fluxes of heat, H_20, CO_2, CH_4, and 0_3. Additionally, slow response sensors document altitude, incoming short wave radiation, net radiation, and infrared surface

Figure 1. ATDD's MFP installed on a LONG-EZ for demonstration.

temperature. MFP installation in a small airplane is described, along with the results of two field comparisons to tower based eddy-flux systems.

This development effort was guided by a single goal -- the achievement of accurate yet practical vertical flux measurement from mobile platforms. As a result, the primary focus has been on accurate high fidelity vertical velocity measurement. Although both the physical and mathematical approach are generic with respect to wind computation, hardware selection was optimized for vertical winds because of our interest in flux measurements. It is expected that future efforts will improve and validate measurements of horizontal winds. Finally, it should be noted that the system is described as it was initially conceived and configured. Much has been learned in this early endeavor. The system will be continually modified and improved as better and simpler ways are found. Application to other platforms is expected.

2. THEORY OF AIR VELOCITY MEASUREMENT

From an earth-mounted platform, the measurement of air velocity suitable for eddy covariance computation has become straightforward (McMillen, 1986) with the recent availability of inexpensive powerful desktop computers and data acquisition systems. Although measurement from a moving platform is also straightforward in concept, it becomes complex in application. In principle, one simply adds the velocity $\mathbf{V_a}$ of the air relative to the platform to the velocity $\mathbf{V_p}$ of the platform relative to the earth to obtain the velocity $\mathbf{V}$ of the wind relative to the earth.

$$\mathbf{V} = \mathbf{V_p} + \mathbf{V_a} \tag{1}$$

Actually, $\mathbf{V_p}$ is not the velocity of the platform, but rather the velocity of the sensors attached to the platform. Also, $\mathbf{V_a}$ is not the velocity of the air relative to platform, but is the velocity of the air relative to the air velocity sensors. The complete three-dimensional rotational and translational freedom of the platforms provides the new difficulty of the MFP measurement, over tower measurements. Both $\mathbf{V_a}$ and $\mathbf{V_p}$ are necessarily measured from the platform in coordinates relative to the platform. Thus they must be transformed (rotated and translated) to earth coordinates. For reasons to be given later, the translation occurs at each data sampling time step, which is currently 40 Hz for ATDD's MFP. This requires measurement, at the same frequency, of the angular orientation relative to the earth.

As usual, care must be taken to measure $\mathbf{V_a}$ in a region undisturbed by the platform. On aircraft and ships, this requires booms which, unfortunately, amplify sensor motion. The amount of amplification depends on boom length, which in turn depends on both the size and aerodynamic "cleanness" of the platform . Since $\mathbf{V}$ is obtained as the sum of two vectors which often are nearly equal in magnitude but opposite in direction, high accuracy is required, especially on faster platforms.

2.1 Platform Velocity Measurement

The traditional approach for removing sensor motion employs an Inertial Navigation System (INS), which keeps -- using complex mechanical electrical systems -- a gimbaled platform level with respect to local earth. Though well proven, the INS approach is very expensive. It requires significant space and power, limiting application to large platforms and further increasing cost. Its large size precludes co-location with the $\mathbf{V_a}$ air motion sensors that are usually mounted on a boom as previously stated. Thus, relative motion between the INS and the air motion sensors is significant, introducing additional terms into equation (1) that require additional measurements. These measurements, which must be very accurate, allow only partial correction for the relative motion, since boom motions due to vibration and acceleration are not measured. Using "stiff" probes helps, but high frequency response remains limited.

The ATDD system is simplified by co-location of sensors, an approach recently made possible by technological advances in low-cost miniature acceleration (McCarty, 1988) and pressure (Teschler, 1985) sensors. Small size allows mounting of both the air velocity and platform velocity sensors in a small head at the end of the sensor boom. Although orientation

with respect to earth coordinates is presently not measured at the sensor head (a prototype system to do this has been designed but not yet tested), overall accuracy is enhanced by directly measuring the linear translation components of the sensor-head motion. At each time step (40 Hz for the ATDD MFP) the velocity vectors are computationally translated from platform to earth coordinates, obviating the need for a physically oriented measurement platform.

In both the traditional INS approach and in ATDD's MFP scheme, platform velocity $\mathbf{V}_p$ is determined by measuring the three acceleration components and integrating. Since the coordinate system orientation of the mobile platform is continually changing relative to the earth, each acceleration measurement must be rotated to earth coordinates before integrating. Appendix A describes in detail both the coordinate system and an efficient coordinate rotation algorithm developed for this process.

Since integration compounds any error over time, a low-frequency (0.67 Hz) position measurement is blended with the accelerometer data during integration. This technique retains fast response while suppressing the error growth. The third-order scheme employed is similar to that suggested by Blanchard (1971) for vertical velocity, and is described in Appendix B.

2.2 Relative Velocity Measurement

The method for measurement of $\mathbf{V}_a$ relative to the platform is dictated by platform aerodynamics. Sonic or even propeller anemometers are appropriate for low speed platforms such as ships. For the higher speeds associated with airplanes, variable- and fixed-vane and pressure-sphere gust probes have been used. Whatever approach is used, care must be taken not to disturb the flow. To "reach" an undisturbed flow region, long booms are usually employed. On airplanes, booms extending into the undisturbed air ahead of the airplane have been reasonably successful. For ships, the combination of the closeness of the ocean surface and large superstructures make flow disturbance a more difficult problem.

Positioning of the probe for any MFP application (or tower) should be guided by criteria described by Wyngaard (1988a, 1988b). Specifically, the probe should be positioned in a vertically and horizontally symmetric location to minimize cross talk from horizontal flux and where attenuation by flow blockage is negligible. For airplanes, it is relatively easy to position turbulence probes at a symmetric location. Unfortunately, many scalars must be measured close to the airframe. For such scalars, stagnation loss and flow blockage are a more difficult problem that grows at the square of flight speed. For ships the superstructure is large, and there is no vertically symmetric location (all flow must go over or around). But, the lower platform speed mitigates stagnation loss problems. Flow blockage is the major problem in the use of ships as a mobile platform.

3. SYSTEM DESCRIPTION

The basic ATDD design goal was the development of a low cost "generic" methodology for measurement of air-surface exchange on moving platforms such as buoys, ships, and aircraft. Flow measurement hardware would be unique for a specific platform, but the data processing

software and platform motion measurement system could be generic. By using modern technology, the system could be portable, require little space, and have low power demands. Since aircraft and ships are expensive and would not be purchased, system installation must require neither permanent or major modifications to the platform. To meet programmatic needs, a small airplane was chosen as the initial test, development, and demonstration platform. With respect to frequency response, system size, weight and power requirements, application on a small airplane is more demanding and restrictive than other platforms.

The ATDD MFP consists of three major hardware sub-systems: the air and probe motion measurement system, the fast and slow speed support sensors, and the data acquisition system. Physically, these sub-systems are grouped into two assemblies -- the probe, and the strap-down MFP. The probe connects to the MFP electrically and thus can be easily changed for specific applications. The rest of the hardware -- computer, data storage device, sensor electronics, etc. -- simply mounts on a 45 cm by 70 cm plywood board. The following describes the three hardware sub-systems, their application, and physical locations.

3.1 Motion Sensors

As described in Section 2, both the velocity of the sensors, $\mathbf{V_p}$, and the relative air velocity, $\mathbf{V_a}$, must be accurately measured. But, by co-locating the $\mathbf{V_p}$ and $\mathbf{V_a}$ sensors, the $\mathbf{V_p}$ and $\mathbf{V_a}$ coordinate systems are also co-located, which simplifies the physics, hardware and computational algorithm. This approach is unique to the ATDD MFP. The $\mathbf{V_p}$ vector is computed from an algorithm which numerically performs the role of an expensive INS. The $\mathbf{V_a}$ vector is measured with a turbulence probe. Table 1 summarizes -- for $\mathbf{V_a}$ and $\mathbf{V_p}$ -- the sensors used, the range and resolution of the sensors, and their physical location.

Table 1
Sensors Used to Determine V_p and V_a

Variable	Use[1]	Location	Range	Resolution	Sensor
Acceleration[2] Sensors					
X	p	Probe	±1g	.0005g	SenSym-SXL02G
Y	p	Probe	±1g	.0005g	SenSym-SXL02G
Z	p	Probe	+2/-1g	.001g	SenSym-SXL02G
Pressure Sensors					
Dynamic	a	Probe	0-24mb	.005mb	MS[3]-160PC01D37
Yaw	a	Probe	±12mb	.005mb	MS-160PC01D36
Pitch	a	Probe	±12mb	.005mb	MS-160PC01D36
Static	a & p	Probe	700-1100mb	.04mb	Setra System
Delta Static	a & p	Probe	±12mb	.005mb	MS-160PC01D36
GYROS[4]					
Pitch	a & p	CG[5]	±83 deg	.15 deg	Honeywell JG7044A-35
Roll	a & p	CG	±175 deg	.15 deg	
Yaw	a & p	CG	±6 deg/s	.05 deg/s	Honeywell-GG13A
Temperature Sensors					
T'	a	Nose	±15 C	.005C	Thermistor
T Bar	a	Nose	-7/+65 C	.02 C	Hy-Cal BA-507-B

Notes:
1. p-V_p computation and a-V_a computation.
2. ATDD designed and fabricated support circuity for these transducers.
3. Micro Switch, a Honeywell Division.
4. ATDD R&D is developing a more accurate non-gyro approach.
5. Center of gravity.

3.1.1 Platform motion sensors

To determine V_p, the ATDD MFP was specifically designed for resolution of the high frequency probe motion important to turbulent transport measurement. Unlike an INS, the MFP has no particular concern with the motion of the aircraft center of gravity (or, more generally, the platform).

The input signals to the algorithm are those in Table 1 noted with a "p". The high frequency component of the V_p vector is integrated from acceleration measurements, while the

low-frequency portion is determined from a radio navigation receiver. The solid state accelerometers have a flat frequency response from zero to 300 Hz. Figure 2 illustrates the ATDD accelerometer board, which locates the orthogonal matrix of accelerometers at the center of the pressure sphere and provides signal amplification. Since the low frequency position information is separate from low frequency altitude information, it is useful to separate horizontal and vertical wind description.

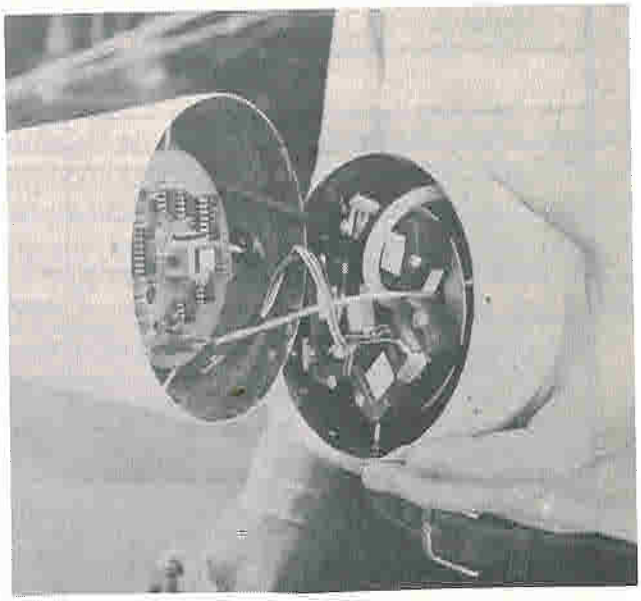

Figure 2. Accelerometers and pressure sensors located in the pressure sphere.

Computation of horizontal $\mathbf{V_p}$ components requires both high frequency acceleration information, (obtained from the $\mathbf{A_p}$ vector) and low frequency position information. The position information keeps the software INS algorithm from drifting with respect to both velocity and position. Position information is obtained from an Apollo II LORAN-C receiver (model 612B). This LOng RAnge Navigation (LORAN) receiver reports latitude and longitude every 1.5 seconds. The receiver determines position from a 100 kHz radio frequency transmitted from chains of land-based stations, with a position repeatability of 13.5 m when in a primary LORAN-C reception area. LORAN coverage is non-existent in some areas of the world, and weak in others. In spite of this limitation, LORAN was chosen because it provides a high-quality low-cost navigation reference for this initial demonstration. However, Global Positioning System (GPS) technology is maturing rapidly, and within a few years it will remove area coverage problems, improve accuracy, and provide an additional altitude reference. Upgrade of the MFP system to a hybrid LORAN/GPS system is under development.

Computation of the vertical $\mathbf{V_p}$ component relies on pressure altitude as the accurate low frequency reference. Pressure altitude is obtained from a Setra Systems model 470 pressure sensor. This sensor was modified by the manufacturer to meet MFP needs. It has a range of 700 to 1100mb (i.e., 3000 m MSL down to the surface) and an accuracy of 0.05 percent. A/D resolution is 0.2 mb, or two meters absolute resolution in pressure altitude. This resolution is further enhanced by the addition of a ±12mb delta pressure sensor. By closing a port on this sensor before a data run, a relative pressure resolution improves to ±0.01 mb, or about 0.1 m at sea level.

Since the accelerometers are rigidly attached to the probe, the observed $\mathbf{A_p}$ is in airplane coordinates. The platform pitch and roll angles, used to rotate $\mathbf{V_a}$ and $\mathbf{A_p}$ to earth coordinates, are obtained from a vertical gyro. This gyro is mounted to the strap-down platform which was located, for the current demonstration, at the airplane's center of gravity. The gyro angular accuracy of ±0.15 degrees limits low frequency vertical velocity accuracy. For example, since

the vertical component of $\mathbf{V_a}$ vector is proportional to the airplane velocity times the tangent of the pitch angle, the lower limit in velocity accuracy would be 10 cm/s at an airplane speed of 57 m/s. Ideally, the roll and pitch angles should also be measured at the center of the probe. Since high frequency velocity information is mostly determined by $\mathbf{A_p}$ and probe delta-pressure information, the turbulent velocity component accuracy is less impaired by gyro limitations. A simple low-cost system to observe probe angles with greater precision has been built, but not yet tested.

High frequency heading information, also required for $\mathbf{A_p}$ and $\mathbf{V_a}$ rotation, is obtained by mixing the high frequency platform yaw rate with low frequency magnetic heading information. High frequency yaw rate information is obtained from a turn rate gyro. Magnetic heading is obtained from a KVH Industries, Inc. flux gate magnetometer. The current sensor has a ±1 degree accuracy which limits horizontal mean wind accuracy but does not affect vertical velocity resolution. The sensor damping has been set for a time constant of 2.7 s. This sensor is being replaced with one having a ±0.01° resolution and a ±0.5° accuracy.

3.1.2 Relative air motion sensors

The ATDD-designed turbulence probe not only houses the accelerometers, but also measures the relative velocity vector $\mathbf{V_a}$. The pressure-sphere turbulence probe approach was chosen for simplicity, ruggedness, and low-cost. Pressure- spheres measure incident flow speed and angle by sensing differential pressure between ports positioned on a hemispherical head. For 50 m/s flight speed, pressure-spheres work well. Implementation was accomplished by design and fabrication of a unique 9-hole pressure-sphere turbulence probe. The positioning of the nine pressure ports on the ATDD pressure sphere is shown by Figure 3, and follows considerations outlined in Brown *et al.* (1983). Appendix C gives a complete review of appropriate theoretical considerations in design and use of the ATDD pressure-sphere turbulence probe, along with results of ATDD wind-tunnel tests. The input signals required for $\mathbf{V_a}$ computation are those in Table 1 noted with an "a". Primary sensors are the pressure sensors, which have flat frequency response from zero to 1000Hz. The pneumatic tubing connections are only a few centimeters long, and do not attenuate frequency response in the range of interest.

Figure 3. Pressure ports and symmetric probe positioning.

ATDD's probe design has several unique advantages. Mounting the pressure and accelerometer sensors within the pressure-sphere allows accurate

high frequency measurement of both probe motion (including vibration and aerolastic) and air motion at the same location. With commercially available probes, long pneumatic tubing combined with unmeasured probe vibration and deflection, limits high frequency response. Also, since probe motion (acceleration) is directly measured, the probe can be positioned at any location on the airplane. This is an advantage, in that low-cost, single-engine airplanes become acceptable platforms by mounting the probe outboard on a wing. A difference relative to commercial probes is the addition of four static ports on the sphere to allow more accurate static and differential pressure measurements. This removes the difficult problem of correcting fuselage static pressure for various errors. Finally, the aerodynamics of the large 12 cm pressure hemisphere is not as easily altered by port holes and "bug strikes" as with smaller 2.5 cm diameter commercial probes.

Positioning of the probe on the airplane was guided by Wyngaard's (1988a and 1988b) criteria. Specifically, the probe is positioned in a vertically and horizontally symmetric location (see Figure 3) to minimize cross talk from horizontal flux and due to amplification or attenuation due to stagnation loss by flow blockage. The flow disturbance at its location, 5 chord lengths forward of the canard, is insignificant. The flow blockage of the streamlined airframe is equivalent to the aerodynamic drag of a 1/5 m^2 flat plate. Typically, one finds aircraft probe lengths which are only two characteristic lengths forward of the major disturbance and airplane speeds that are nearly double that used herein. In general, platform angular resolution demands grow linearly with speed, while pressure disturbance problems grow with the square of the speed.

3.2 Support Sensors

The support sensors are grouped into either fast (40 Hz data logging) or slow response (1 Hz data logging). The first fifteen sensors are fast response (interrogated at 40 Hz). Of these fifteen, the first eleven sensors (3 acceleration, 4 pressure, 3 angles, and 1 temperature) are used in motion and/or velocity computations. Channels eight and twelve through fifteen are used in eddy covariance flux computations. Slow response sensors, consisting of the LORAN and channels 16-23, document the time/space history of other chosen variables. The software is flexible with respect to channel allocation. (Table D1 in Appendix D gives additional detail on channel allocation, operational units, lag, and sensitivity.)

3.2.2 High speed sensors

For the initial test and demonstration, the airplane was instrumented to measure the flux of momentum, heat, H_2O, CO_2, O_3, and CH_4. The following describes each of the fast response sensors. Additional trace gas instrumentation for NO_2, NO and CH_4 is under development. In general, the fast response sensors needed for eddy-flux measurements are available for only a few chemical species.

Regarding momentum, Reynolds stress components are computed in the usual manner. The covariances of the x, y, and z components of the velocity vector, V, from Equation 1, form the Reynolds stress tensor.

In measuring heat flux, fast response temperature is obtained from a micro-bead

thermistor having a 0.1 s still-air time constant. With even a small ambient velocity, time response is greatly improved. Physically, the thermistor is located on the nose of the airplane as illustrated in Figure 4. Tests have been conducted which show that the fast response temperature sensor can be incorporated into the pressure-sphere of the turbulence probe which is a more desirable location.

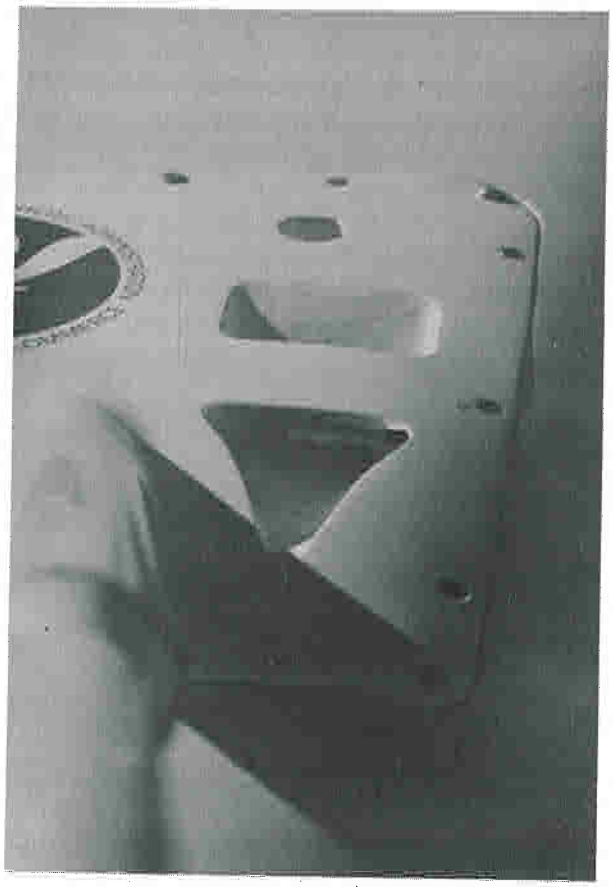

Figure 4. Temperature sensor inlet and position.

To measure water vapor, CO_2, and CH_4, ATDD designed and built an open-path gas analyzer (Auble and Meyers, 1990). This analyzer operates on the principle that H_2O, CO_2, and CH_4 absorb infrared radiation at specific wavelengths. An emission from a broadband infrared source (a halogen lamp operated at about 2400° C) is collimated with calcium fluoride lenses and folded twice with gold-plated front-surface mirrors. Path folding increases the 20 cm open path cell to one with an 80 cm effective path. The beam is then refocused before passing through a rotating chopper wheel that contains four narrow-bandpass infrared interference filters. Since the source is also chopped, the instrument is insensitive to ambient light. The filters for H_2O, CO_2, and CH_4 are centered on wavelengths where these gases are known to have strong absorption and weak interference from other trace species (2.61, 4.26, and 3.31 microns respectively). The reference filter is centered at 2.3 microns. Although CH_4 absorbs 30 times more strongly than CO_2, the low atmospheric concentration (around 350 times less than for CO_2) makes it hard to detect, and no useful data were obtained for CH_4. Future instrument improvements are expected to allow flux detection of CH_4. The amount of energy passing through each filter is detected by a Peltier-cooled lead selenide (PbSe) infrared detector. The signal for each gas is divided by the reference signal, amplified, and output with a frequency response of 20 Hz.

Figure 5 illustrates the positioning of the infrared open-path gas analyzer on the airplane. In both design and mounting, special care was taken to avoid any adverse effects due to airplane vibration. Since the infrared instrument will always be positioned near the probe, it was designed simply to plug into the MFP.

The ATDD ozone sensor was used to measure ozone flux. It too is a hybrid instrument consisting of two components: (1) a very fast response sensor, and (2) a slow response but highly accurate and stable sensor. By appropriately mixing the low-passed portion of the slow response signal with the high-passed portion of the fast response signal (see Appendix B), a

highly stable fast response ozone signal is obtained.

The design of ATDD's fast response ozone sensor follows that of Ray *et al.* (1986). The detection principle is ozone chemiluminescence with eosin Y dye in an ethylene glycol fluid carrier. At a sample rate of 7 l/min, the instrument has an 8 Hz time response, a detection limit of 0.1 ppb, and a sensitivity of 0.1 nA/ppb. The primary limitation of this sensor is its baseline time drift.

The low-speed sensor, which was not used during the demonstrations presented herein, was added to correct this baseline drift problem. The slow-response sensor is a modified DASIBI model 1003AH. Sample flow was increased to 7 l/m to obtain a stable 12 second cycle time. Power supplies, valves and pumps were modified to allow operation on 12 VDC. To suit airplane use, the instruments were designed for light weight and low power demands (40W at 14V DC). Within the airplane, the ozone instruments are mounted with the MFP main assembly, and are positioned near the center of gravity, with a short (50 cm) Teflon inlet sample line which is routed through the floor of the airplane.

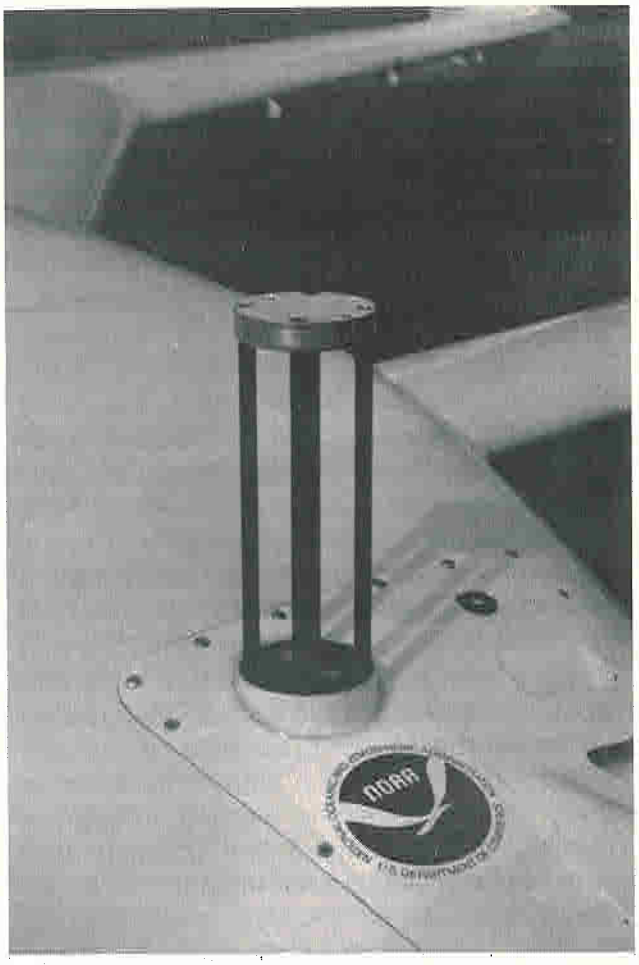

Figure 5. Mounting of the Infrared H_2O/CO_2 analyzer.

3.2.3 Low speed sensors

Since the primary purpose of this effort was the development of practical mobile eddy flux capability, little attention was given to the installation of slow-response sensors. Sensors were primarily limited to those necessary for MFP operation and test. It is likely that additional slow-response sensors will be added. For this demonstration, instrumentation included the slow-speed sensors described below. (Note that "low-speed" sensors are those which are interrogated at 40Hz but only a one-second average is stored).

For accurate mean temperature, a slow-response platinum RTD sensor was mounted beside the high-speed thermistor. The sensor is used for temperature profile measurement, quality control checks, and calibration of the high-speed sensor. The sensor has an operating range of -7° C to +65° C, with a linearity variation of less than 0.06% of span. The sensor and amplifier are a Hy-Cal Engineering model BA-507-B. Air inlet and mounting of the fast and slow response temperature sensors is shown in Figure 4.

Short wave solar radiation was measured with a LI-COR, Inc. LI-200S silicon pyranometer. This sensor is useful in not only documenting solar radiation along the sampling transect, but also in estimating cloud cover and assessing energy balance. The sensor can also be seen in Figure 4. It is mounted vertically. Typical pitch/roll variations are only a few degrees. Although such variations are important, cosine corrections for platform pitch and roll are easily made (MacPherson, 1988).

Net radiation is measured with a Radiation and Energy Balance System, Inc. Q*5 net radiometer. This sensor is mounted on the nose of the airplane, and is visible in Figure 6. Typical pitch/roll variations are only a few degrees. Corrections are necessary but less significant than for the pyranometer. The small airframe size along with the nose location result in very small solid angle interference from the airframe.

Surface temperature is measured with an Everest Interscience Inc. model 4000 microcomputer-based infrared temperature sensor which was mounted through the floor of the airplane and "looks" down. The sensor has a 15° field of view. At 100 m flight altitude, this gives the average surface temperature within a 25 m diameter circular area. The sensor has an accuracy of 0.5%, with a resolution of 0.5°C in its 8 to 14 micron spectral pass range.

Radar Altitude has recently been added to the system. The Terra model TRA 3000/TRI30 radar altimeter has a range of 12 to 762 m, with an accuracy of 5% at typical flight altitudes.

Figure 6. Mounting of the net radiometer.

3.3 Data Acquisition System

There are many possible approaches to data acquisition, all of which would work well. Our approach centers on a desktop personal computer with a high-density storage device and an A/D card. There is nothing special about this approach, but it is simple, low-cost, and works well.

3.3.1 Hardware

The PC, an IBM PS-2 Model 30 (8086 microprocessor), was modified with appropriate 12 volt DC/DC converters and cooling fan. If there is an advantage to this approach, it is that the hardware was available and that the system is easily programmed in Microsoft QuickBASIC. All data are stored on an Iomega Corporation Bernoulli Box II 44MB removable 5.25 inch disk cartridge. An Analog Devices RTI-800 32 channel multifunction board was chosen for data acquisition. A large number of channels is necessary, as well as its Direct Memory Access (DMA) operation. This board contains a 12-bit A/D converter which is configured for a ±5 V signal. All signals are conditioned to operate appropriately within this conversion range.

All fast response analog signals are first conditioned with 10 Hz low-pass anti-aliasing filters before being converted to 40 Hz digital signals. The conservative 40Hz data rate is software controlled and may be changed as indicated by experience. The filters used are single component four-pole Butterworth high performance active filters (Frequency Devices 705L4B-10). Slow response analog signals are digitized directly at 40 Hz and averaged to one second before being recorded. Since typical "slow" response sensors have a frequency response of considerably less than 40 Hz, this block average approach yields a true low-frequency sample without aliasing errors. Recently, Linear Technology Corporation introduced a variable frequency 8th order Butterworth lowpass filter (LTC1064-2). These filters are undergoing ATDD electronic test and may replace the current filter system.

3.3.2 Software

There are two primary MFP software routines -- STORE and FLUX. Complete listings are available upon request. The setup table (Table D1) and a typical program output (Table D2) along with key FLUX routines are reproduced in Appendix D. STORE is hardware specific, and is therefore not reproduced here. A brief description of each follows. It should be noted that FLUX represents initial efforts to reduce flux data from moving platforms and is an evolving program. It is also important to point out that MFP data reduction and interpretation are more difficult and complex than the data collection task.

STORE is primarily a "bookkeeping" and data storage program. It initializes the A-to-D card to continuously dump 32 channels of data at 40Hz via DMA to the PC memory. The advantages of DMA are that there are no data gaps when data is written to disk, and there is no processor overhead associated with obtaining the data. There are two kinds of bookkeeping tasks: system control and data storage. System control is determined either by constants or through the I/O port. Various constants determine data rates, number of high/low rate channels, buffer sizes and so on. The use of setup constants adds significant software control flexibility. Using a toggle switch connected to the I/O port, the operator (pilot for this demonstration) turns data storage on or off. The computer controls gyro erection, static sensor port closure, and lets the operator know if all functions are working properly through the control of a status light. When the operator requests data storage (*i.e.,* switch closure), the PC formats a one-second block of high/low rate data in memory and writes it to disk in a "burst" with a DOS DMA interrupt. The only processing within STORE involves data statistics such as means, standard deviations, and time trends. These statistics are essential for in-field quality control checks, and allow single-

pass post-processing by FLUX. STORE writes two output files which are post-processed by FLUX: one file for the A-to-D data, and one file for the LORAN serial data.

FLUX reduces the two files written by STORE into two processed output files and the path-average results (printed or written to a file). In appendix D, Table D2, gives a typical summary output. The high rate output file contains a traditional time series of U, V, W, T, and associated scalars. Although this processed file looks much like what would be observed on a tower, it has two significant differences; first, because of the high flight speed (in comparison to a tower) the time series is compressed (more high frequency information), and secondly, the time series approximates a space series (it's just recorded in time reference). During generation of the time series, the data are averaged to 20 Hz. The low rate data file contains one-second information on the MFP position and the slow rate channels.

The FLUX data reduction program is complex and is best understood by review of the key BASIC algorithms. The algorithm uses a setup file and file header information (times, start/stop position, and other data statistics) to initialize processing. An important aspect of the initialization routine is the removal of specified (by Table D1) means and time trends. There are many subtle and important sensor alignment adjustments used in the initialization. The "heart" of FLUX is the procedure called PROCESS. Within PROCESS, $\mathbf{V}_p + \mathbf{V}_a$, scalar mixing ratios, and co-variances are computed. The mathematical bases for PROCESS are described in Appendixes A through C.

4. AIRPLANE DESCRIPTION AND OPERATION

A variant of the Rutan Long-EZ (Figure 1), a two passenger high performance canard airplane, was selected as the research platform. The aerodynamic characteristics of the Long-EZ are well suited for high fidelity turbulent flux measurements. The "pusher" configuration leaves the front of the airframe free of propeller-induced disturbance, engine vibration, and exhaust. The small, light-weight, laminar flow airframe has an equivalent "flat plate" drag area of only 1/5 m^2. As a result, the nose region has minimal flow disturbance and is ideal for measurement of winds, temperature, and trace species. The canard design prevents stall and has superior pitch stability in turbulent conditions. This, combined with the low wing loading, allows for a safe low-speed flight of 50 m/s. Since dynamic compressibility disturbance grows with the square of the flight speed, sampling at 50 m/s reduces compressibility disturbances to one-fourth of that which is typical of high-powered twin engine airplanes (Wyngaard, 1988a).

4.1 Technical Specifications

Table 2 presents the specifications and performance characteristics of the Wide-Body Long EZ. With a transit speed of 90 m/s and a range exceeding 3,300 km, measurement at any location in the world is possible. The airplane is IFR equipped and has a ceiling exceeding 9 km. The airframe structure is a space-age composite, and exceeds the G-load requirements of the utility class airframe. This fatigue-resistant and high-strength characteristic is comforting when flying in conditions of significant thermal or mechanical turbulence.

Table 2 Wide-Body Long-EZ N286TS			
SPECIFICATIONS		PERFORMANCE	
Type Certificate	Experimental	Stalling Speed	27 m/s
Powerplant	Lyc O-320 160HP	Maximum Speed	93 m/s
Electrical	45 amp 12VDC	Ceiling	9000 m
Empty Weight	430 kg (950 lb)	Range	3300 km
Gross Weight	725 kg (1,600 lb)	Endurance	10 to 18 hr
Fuel Capacity	200 kg (435 lb)	Fuel Use	8.2 to 19 kg/hr
Wing Area	9.3 m^2	Flow Blockage	1/5 m^2

Traditionally, research instruments installed in aircraft have required both airframe and electrical system modifications. This is not the case with the ATDD system, since it is a "strap down" system and has low power requirements. Although the turbulence probe mount is specific to the Long-EZ, it could easily be adapted to other aircraft. Having the accelerometers and flow direction sensors located in the probe allows the probe to be mounted at any undisturbed flow location. This means that application on other aircraft is simple (on a wing strut for example). By efficient application of state-of-the-art sensors and high efficiency DC-to-DC switching power supplies, only 120 watts are required.

4.2 Operational Considerations

The STORE program was written to control all system functions. This is necessary, since the pilot's primary responsibility is that of flight safety. The only workload imposed by the MFP is that of turning on or off data collection with a switch, and an infrequent check of the go/no-go status light. With the dominant use of solid state sensors, system failure is unlikely.

The airplane is certified for operation under both VFR/VMC (Visual Flight Rules/Visual Meteorological Conditions) and IFR/IMC (Instrument Flight Rules/Instrument Meteorological Conditions). The airplane and instruments are not adversely affected by rain. The airplane is not certified for flight into known icing conditions. Severe turbulence does not affect flight safety, as the modern composite structure is certified for acrobatic maneuvers and is significantly stronger than normal or utility category aircraft.

The single engine operation does impose practical "safety-of-flight" constraints. Operation during "Hard" IFR or marginal night VFR is not appropriate, nor are routine operations requiring the full airplane range or duration. Although the flight duration can exceed 18 hours at 50 m/s, pilot fatigue limits routine flights to six hours or less. The oxygen system and time-to-climb limits operation from surface to 6 km. Night flights are acceptable but only under good night VFR conditions, and with well planned flight paths.

4.3 Special Operations

In general, all flights must comply with Federal Aviation Regulations (FAR) as specified by FAA Part 91, or must obtain a waiver. Of specific interest, Part 91.79 lists restrictions for flights below 300 m AGL. The restrictions require 300 m altitude over "congested areas" and 150 m altitude above an other-than-congested area. Lower altitudes are allowed over open water or "sparsely populated areas." In any situation, any aircraft may not be operated closer than 300 m to any person, vessel, vehicle, or structure. An advantage of low level flight with the Long EZ is that it is quiet and its unusual shape attracts favorable attention rather than citizen complaints. Over-water operations have no special restrictions, except that flight safety concerns would require that appropriate survival and navigation gear be carried.

5. DATA PROCESSING

5.1 Path Boundary Conditions

Simplifying the intended use of ATDD's MFP made it more effective, efficient, and economical. By assuming only straight-line sampling (or piecewise-continuous straight lines), adjustments to the data which reflect these boundary conditions are possible. If at the start and stop of the data path the platform has the same speed, altitude, and heading, then the path-average acceleration can be set to that of gravity. This assumption allows the removal of mean acceleration and time trend. For the pressure sensors, the yaw pressure is adjusted to reflect zero mean cross probe velocity. For vertical pressure, the mean sensor pressure is adjusted to reflect (for sufficiently long paths) $W_p+W_a=W=0$. No such adjustments can be made to probe dynamic pressure since its absolute value is used to calculate probe relative velocity. Although not yet explored, boundary conditions for any simple flight patterns (e.g., circles or Ls) could also be imposed.

5.2 Flux Calculation Corrections

Fluxes of heat, momentum, water vapor, CO_2, and O_3 are computed during data post processing using standard covariance computation techniques. Corrections consist of removing appropriate means and time trends. The need for corrections for pressure, temperature, and water vapor fluctuations as outlined by Webb *et al.* (1980) is eliminated by first converting sensor outputs to mixing ratios; *i.e.* the mass of the species is divided by the mass of dry air. In practice, this is simply accomplished by dividing the measured gas concentration by the density of dry air at every data point (40 Hz).

Nonstationarity can be a problem during long transects. It is addressed, in part, by subtracting a running mean, estimated by a digital recursive filter applied to incoming data. This high-pass filter detrends the data and partially corrects for the effects of nonstationarity. Sources of nonstationarity are not only due to changing meteorological conditions, but also to horizontal gradients and to sensor drift (for instance, due to the change in the angle of attack of the airplane from fuel use). This technique is usually not necessary for transects shorter than about 15 km.

Sensible heat flux computation requires corrections for pressure fluctuations, that result from both altitude and air speed variations. To remove the effects of altitude variations, potential temperature is used in the heat flux covariance computations. Potential temperature is computed from the high speed temperature sensor and the static pressure measured by the turbulence probe. Air speed variations cause a temperature variation through adiabatic compression at the temperature sensor. Correction for probe heating is also made using the observed dynamic pressure at the probe.

To remove the need for Webb *et al.* (1980) corrections in water vapor, CO_2 and O_3 flux, the sensor reported concentrations are converted to mixing ratios at each data time step (*i.e.* 40Hz). Using water vapor as an example, the infrared-sensor-observed mg H_2O/m_3 output is divided by the dry air density in kg/m_3. To compute the run-averaged flux, the run-averaged covariance summation is multiplied by C_p and by the run-averaged dry air density. The correction is similar for CO_2 and O_3.

5.3 Sensor Frequency Response and Lag Corrections

In covariance computation, lag or phase errors between the w' time series and any species of interest must be removed. Use of fast sensors and identical low-pass filters mitigates such problems. Still, phase differences are created by imperfect sensors and spatial separation. The sensors used in this demonstration are very fast and therefore induce little phase lag. Since the turbulence probe is boom mounted, the distance from the boom to the sensor will induce a phase lag proportional to this distance divided by the air speed. With the exception of the ozone instrument, the separation distance is about one meter. At 50 m/s flight speed and 40 Hz interrogation, one data step lag would be expected. Experimentally, the lags can be determined very precisely from the cross-correlation, or cross-correlogram of the two time series. The lags were found to range from 1 data step for H_2O to 5 data steps for O_3. During flux computation, each species' time series is shifted as necessary to remove any phase lags.

Figures 7 through 10 display typical spectra, co-spectra, and cross-correlation spectra for vertical velocity with temperature, moisture, ozone, and CO_2.

6. IN-FLIGHT TEST AND CALIBRATIONS

A truly advantageous aspect of the ATDD MFP system is the independence of the MFP from the platform. This allows very careful in-laboratory calibration, repair, and modification. Even with careful laboratory calibration of each sensor, it is essential that in-flight *system* tests and calibrations be conducted. Such tests are essential because vertical velocity is dependent on many sensors and on a complex computation algorithm. Only through an integrated system test is it possible to demonstrate correct operation. Although a variety of in-flight tests are possible (see Lenschow and Spyers-Duran, 1987), the most demanding is the induced pitch motion. With this maneuver, the pilot induces a pitching motion with the elevator. The pitching motion modulates static pressure, dynamic pressure, accelerometers, probe angles, and airplane angles. As a result, the airplane's vertical velocity, (W_p), airspeed (U_a), and the velocity relative to the airplane (W_a), are modulated. In still air (high altitude/stable conditions) W, which is

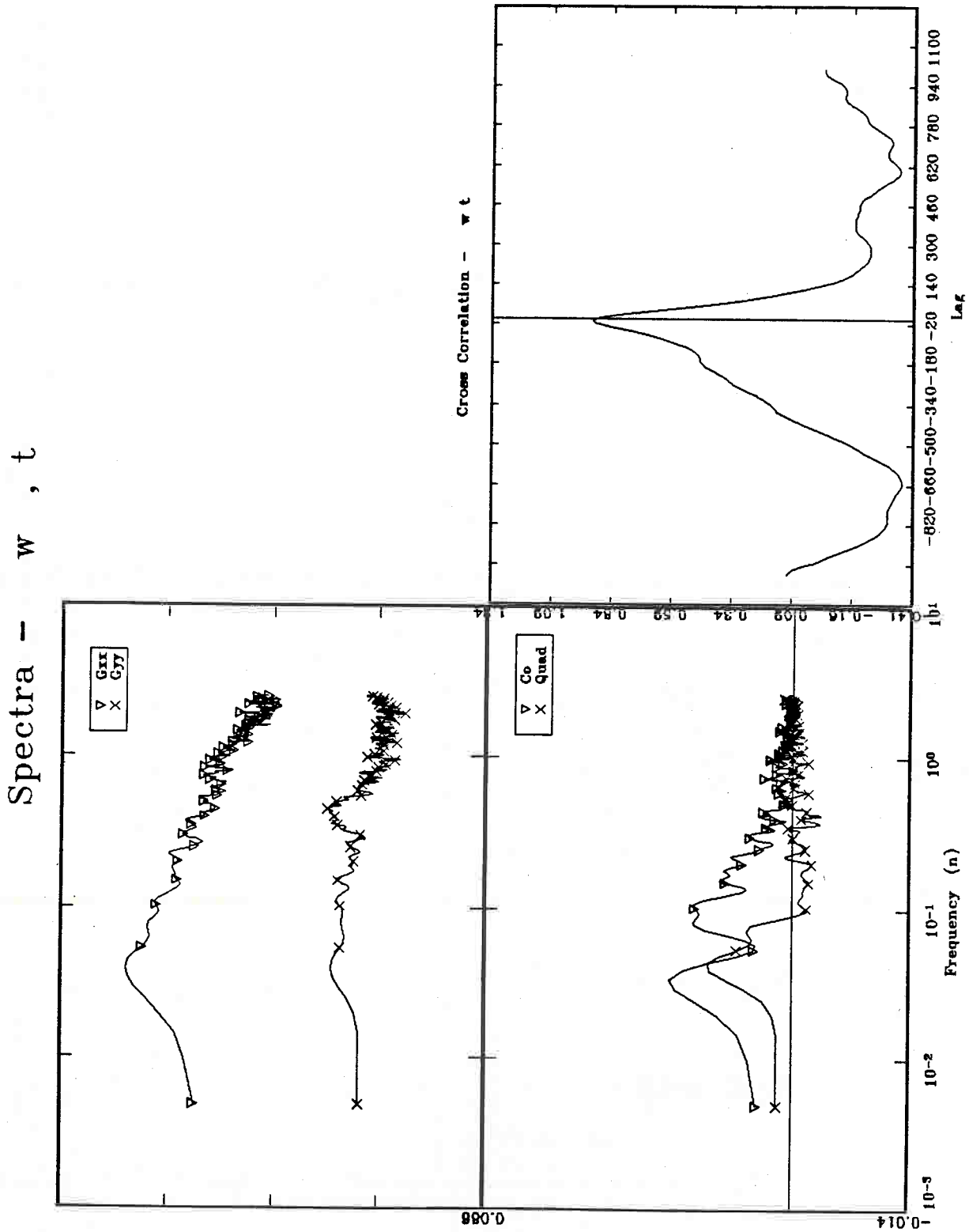

Figure 7. Spectral Analysis of w't'.

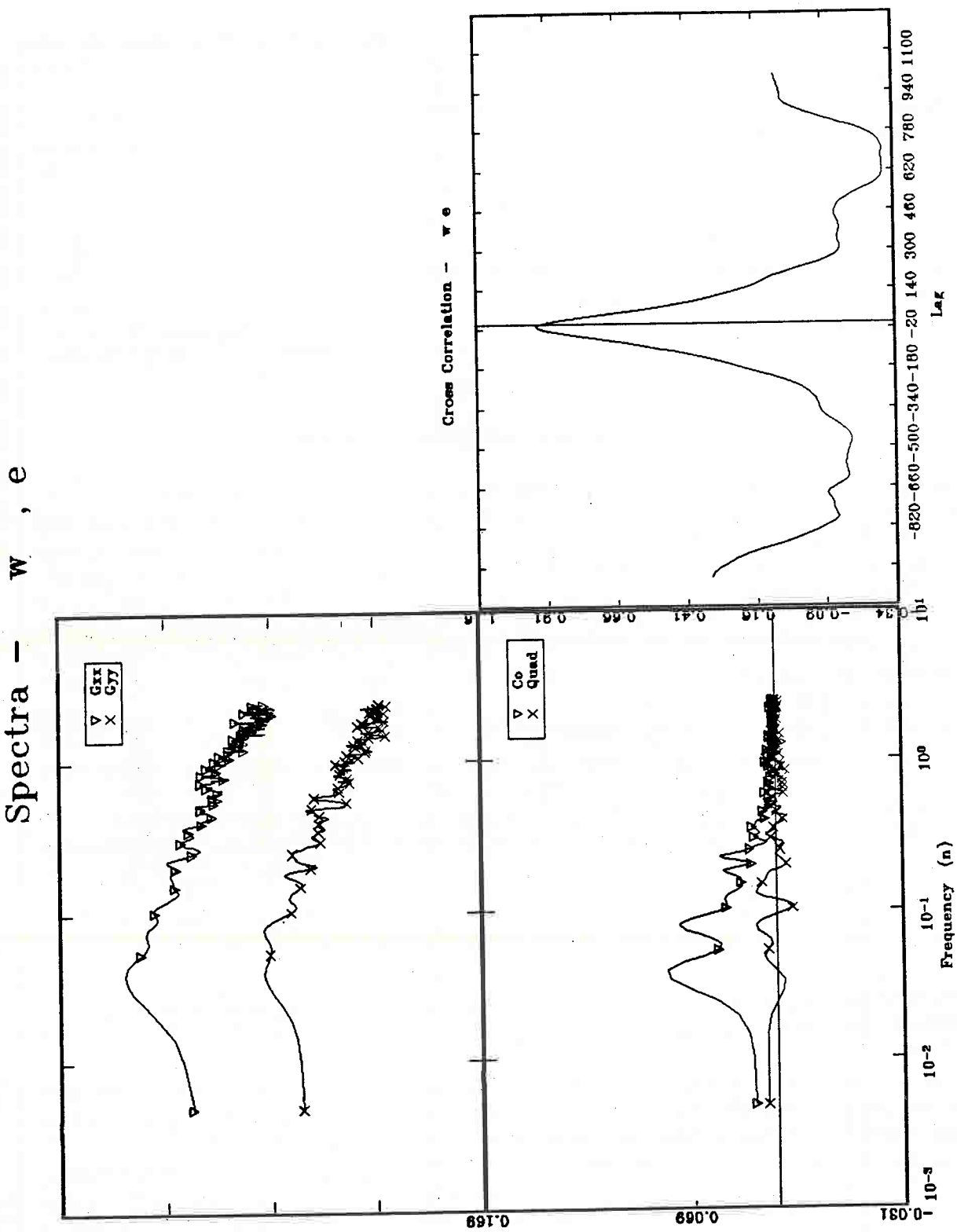

Figure 8. Spectral analysis of w'e'.

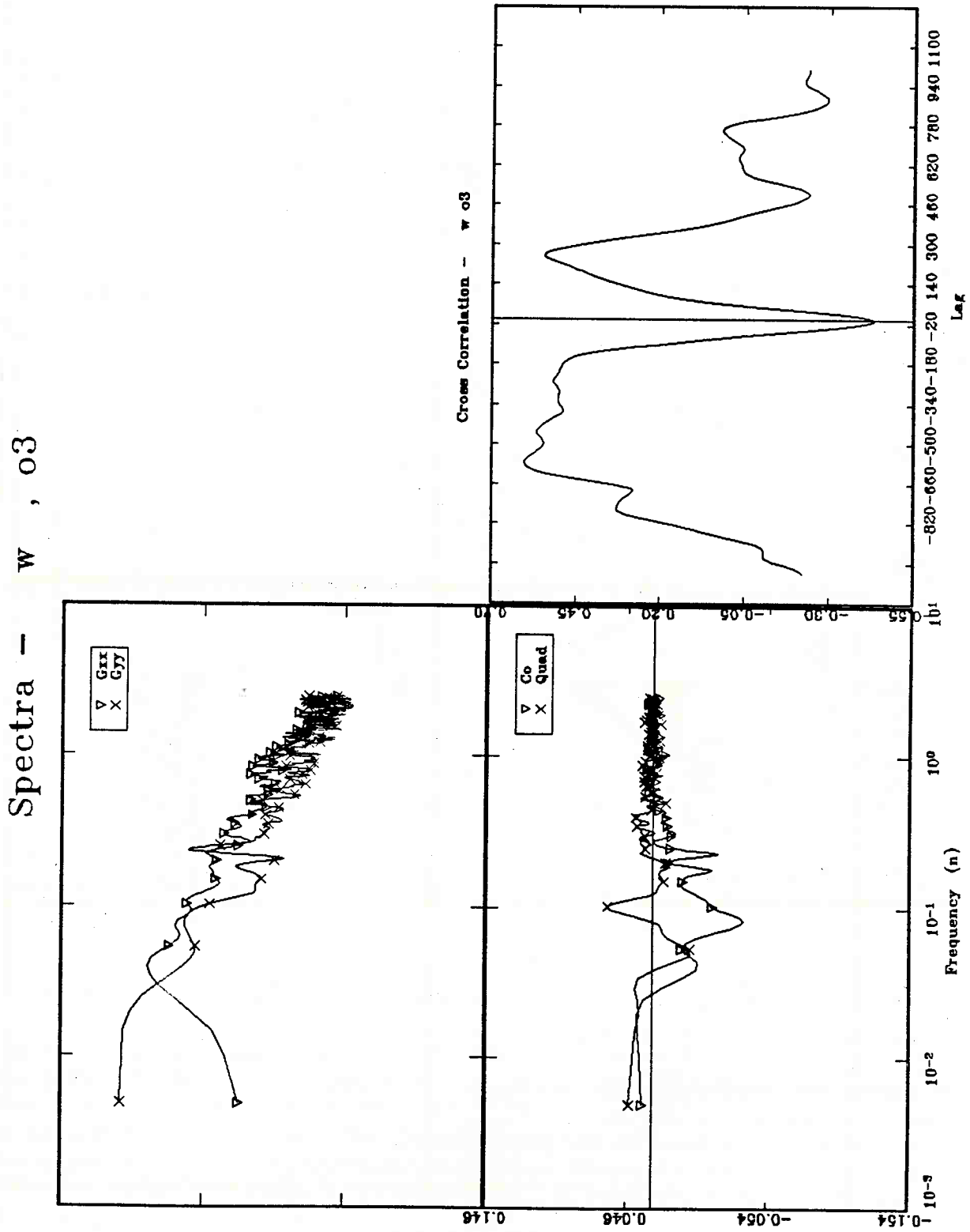

Figure 9. Spectral analysis of $w'o_3'$.

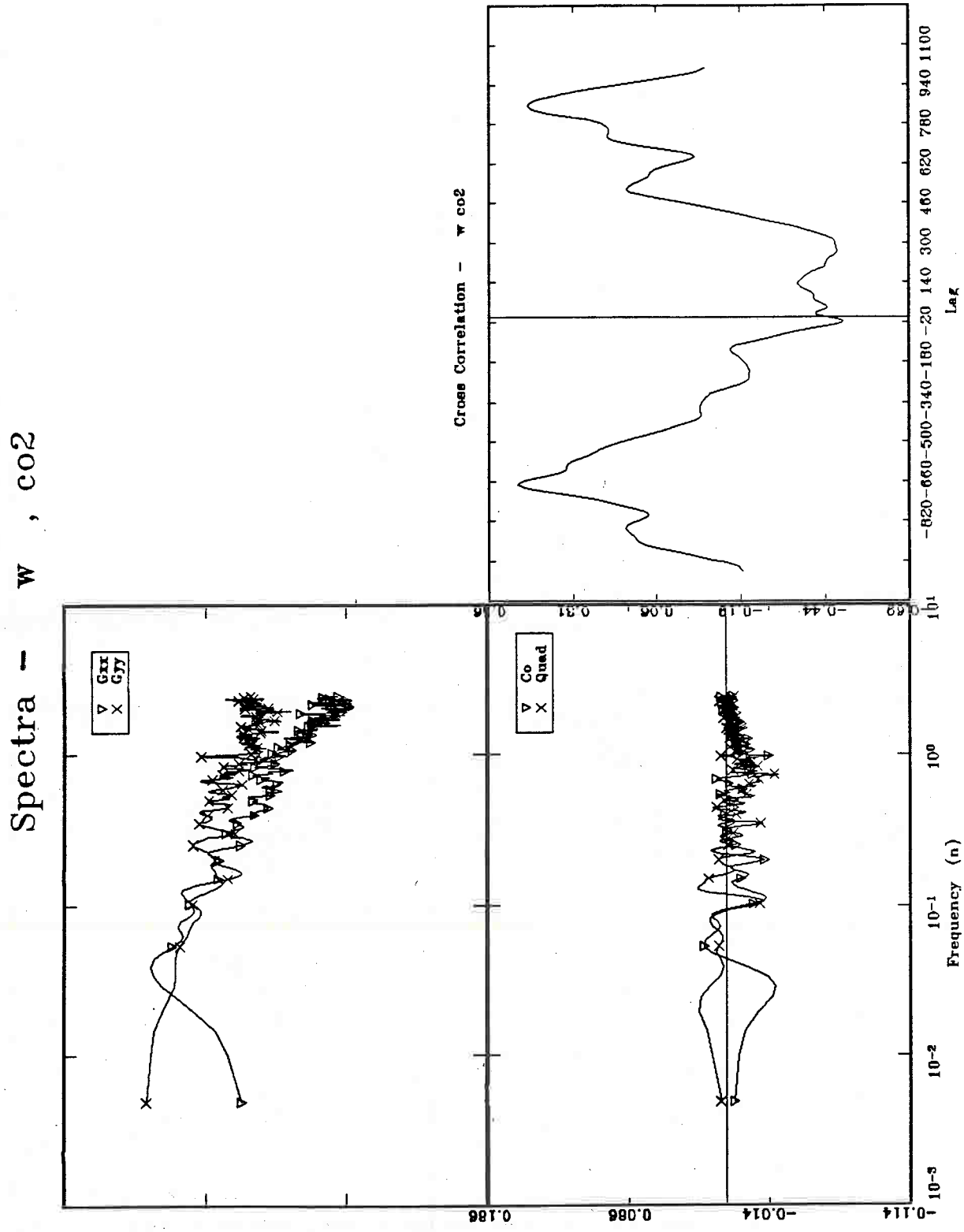

Figure 10. Spectral analysis of $w'co_2'$.

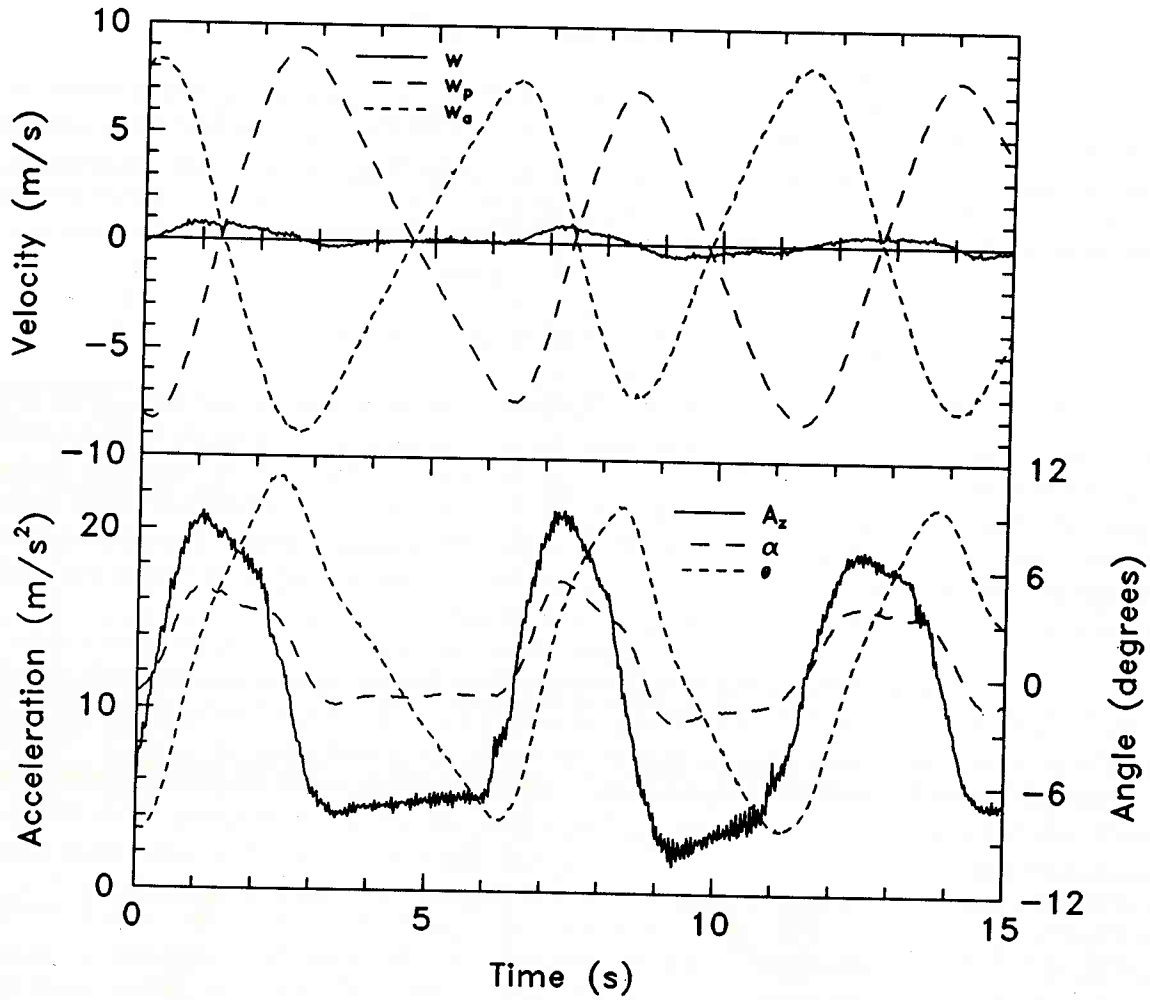

Figure 11. Results of induced pitch motion calibration test.

W_p+W_a, should be zero. Therefore, W_p should be equal to but opposite in sign to W_a. If any sensors have amplitude or phase errors, a periodic error in vertical air velocity will be apparent. Figure 11 illustrates the result of the pitch-induced motion test. Induced yaw motion gave similar results.

From Figure 11, it is apparent that the induced motion modulated vertical acceleration (A_z) to ±1g, the physical probe pitch angle (Θ) to ±10 degrees, and the relative probe angle of attack (α) to +6/-3 degrees. These motions induced extreme W_p and W_a velocities of ±10m/s. It is pleasing that W shows little contamination from all the induced motions. The primary W deflection from zero occurs at extreme probe angle of attack (alpha). (In typical turbulent conditions, such angles are rare.) The displayed result was expected since at such extreme attack angles, the probe response becomes non-linear, as discussed in Appendix C. In response to these test results, the pressure-sphere hole location has been adjusted to force the average alpha closer to zero.

7. PRELIMINARY FIELD TESTS

The system was first tested in two short field experiments during the summer of 1989. Illustrations are taken from these initial tests of the MFP system. These field tests were an EPA July 1989 study of spatial variability, and the NASA 1989 First ISLSCP Field Experiment (FIFE) study. Both presentations are intentionally brief since the purpose is only demonstration and additional analyses and a detailed description of these experiments are in progress.

7.1 EPA Spatial Variability Study

This study was a model validity assessment conducted over a test area of 85 km by 85 km in southeastern Indiana and southwestern Ohio. The object of the study is to determine the spatial variability of dry deposition of trace gases to the surface. It is precisely this kind of question which requires MFP capability. A tower was erected in a soybean field near North Vernon, Indiana, to provide ground truth data for the MFP measurements. It should be noted that this tower location was characterized by a low leaf area index and significant bare soil, and direct comparisons with the airplane should not be expected.

Table 3 presents the average result for each of the ten transects along with the average tower results for the period of transects. Due to the length of the transects, a running mean eddy-flux computation was used in data computation for presentation in Table 3. The airplane momentum fluxes (U*) are too large due to low frequency contamination in u' and v'. Currently winds are not a priority. It is expected future efforts will solve this problem. The energy flux is not in balance due to the large flux divergence and ground storage. The mixed layer depth was low (600m) and it was warming at about 1.8°C per hour. This results in about 80 W of energy storage in the air below the 150 m flight altitude. Eighty Wm^{-2} is the imbalance in heat flux between the airplane and tower. Although ground storage was not measured, it would have been large due to the wet conditions. Unfortunately, neither moisture nor ozone tower flux data were recovered because of instrument problems. Both the moisture and ozone flux data from the airplane appear to be correct.

TABLE 3
EPA Spatial Variability Study
Summary of Airplane Transect Data

TRANSECT			RADIATION		FLUX			
RUN	TIME (EDT)	ALTITUDE (m-AGL)	SHORT (W/m^2)	NET (W/m^2)	U_* (m/s)	H (W/m^2)	LE (W/m^2)	Vd_{O3} (cm/s)
JULY 24, 1989								
1-NE	0931-1004	150	665/45	493/30	0.55	50	180	0.23
1-SW	1006-1041	145	815/60	575/35	0.49	60	210	0.23
2-NE	1057-1131	145	635/265	625/50	0.50	55	285	0.38
2-SW	1134-1207	140	855/260	635/105	0.45	60	275	0.38
3-NE	1324-1355	150	810/290	565/130	0.70	50	390	0.20
3-SW	1359-1432	160	730/276	534/160	1.01	40	260	---
AIRPLANE MEANs		150	750	570	0.6	50	265	0.28
TOWER MEANs		5	730	510	0.1	125	---	---
JULY 25, 1989								
4-NE	1015-1046	130	440/287	460/125	0.59	35	300	0.13
4-SW	1048-1123	120	790/316	570/120	0.51	55	275	0.05
5-NE	1128-1200	130	760/340	620/130	0.30	60	310	0.01
5-SW	1203-1236	240	894/290	685/120	0.40	50	350	0.40
AIRPLANE MEANs		155	720	585	0.45	50	310	0.59
TOWER MEANs		5	730	470	0.13	138	---	---

Note: Standard Deviations follow /s

Figure 12 shows the normalized fluxes of sensible and latent heat and ozone along a flight path from the North Vernon airport to the Eaton, Indiana airport. The transect is a diagonal across the study area. The curves shown are the averages of ten 105 km transects of the study region. In order to have adequate spatial resolution, the fluxes were calculated every 250 m along the transect using a 750 m window of raw data. No running means were removed and fluxes were calculated using Reynolds averaging. Raw data were block-averaged by a factor of two (reducing the data rate effectively to 20 Hz); thus 750 m of flight path at 50 m/s contain 300 time steps of data. The results are noisy, since they are based on only ten transects, but show the effect of major terrain features. The location of Brookville Lake is clearly evident in the fluxes of all three scalars.

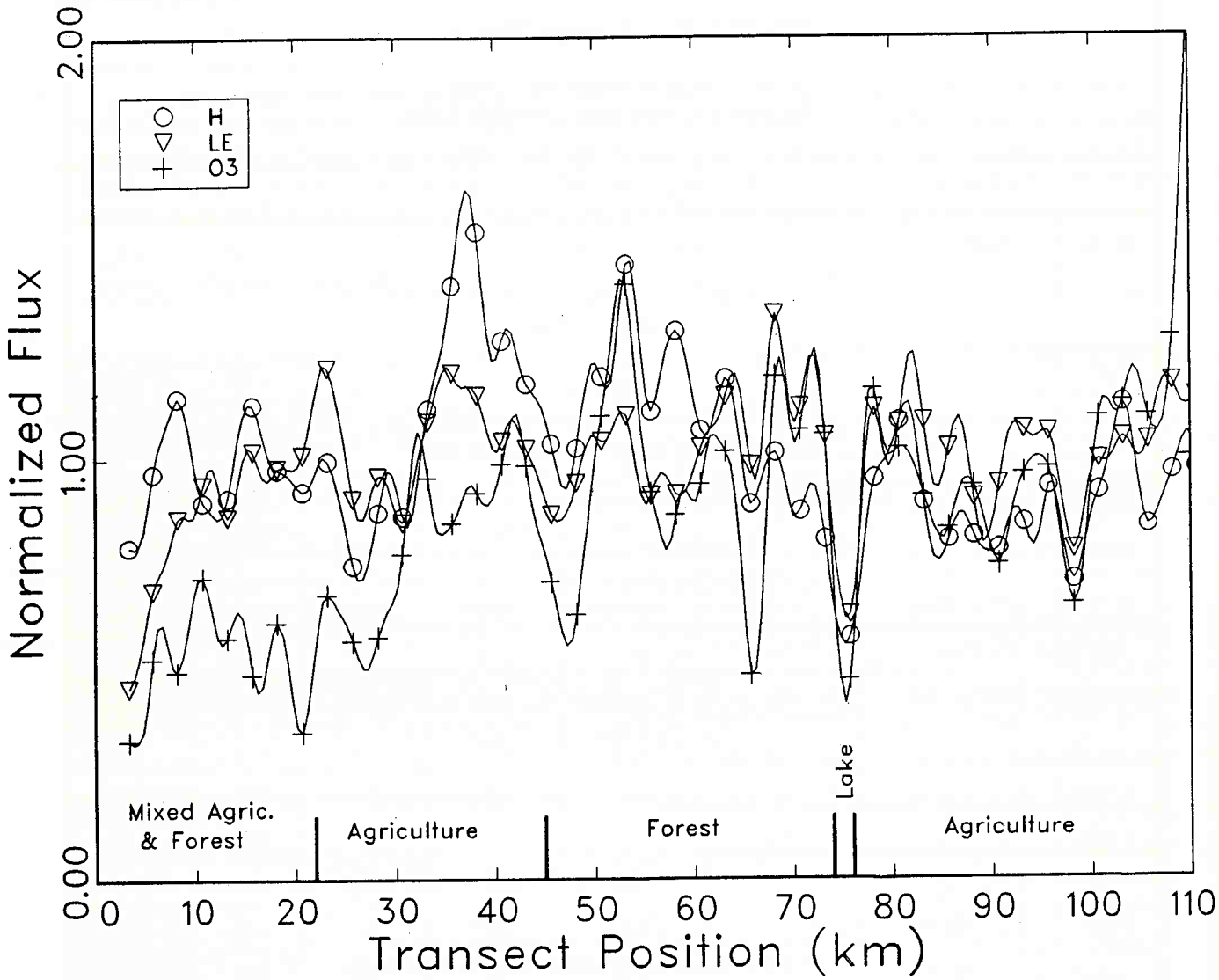

Figure 12. Observed spatial variability of heat, moisture and O_3 flux

7.2 FIFE Field Results

On August 10, 1989, from 1000 to 1400 hours CDT, the airplane made twenty-five 15 km transects as part of the NASA FIFE experiment. All transects were over the study region outflow (north) boundary. Table 4 and Figure 13 present some preliminary results from these transects.

Table 4 presents the results of ten consecutive low altitude transects which were collected during a 75 minute period between 1100 and 1215 local time. The last two rows present the mean result from the aircraft and the ATDD flux tower which operated during FIFE. The tower was located in a reasonably representative, but very dry, portion of the test area. Therefore, the tower data are expected to have a different Bowen ratio than the area average and, due to plant stress, somewhat lower CO_2 flux. Unfortunately, the water vapor sensor was not working properly and the tower system was down for repairs during this flight period. For comparison, the data presented for the tower are for days having similar conditions before and after the aircraft transects, but during the same time period.

TABLE 4
NASA FIFE--August 10, 1989
Summary of Airplane Transect Data

TRANSECT			RADIATION		FLUX		
RUN	TIME (CDT)	ALTITUDE (m-AGL)	SHORT (W/m^2)	NET (W/m^2)	H (W/m^2)	LE W/m^2	CO_2 mg/m^2s
1-E	1105	142	738	534	216	341	0.64
1-W	1118	162	853	549	261	472	0.27
2-E	1133	73	710	512	188	221	0.73
2-W	1148	82	842	549	277	357	0.57
3-E	1163	210	786	570	189	538	0.17
3-W	1177	148	742	477	253	419	0.16
4-E	1192	166	892	635	191	353	0.35
4-W	1205	151	898	635	199	257	0.3
5-N	1218	136	850	611	120	332	0.19
5-SW	1235	413	894	605	175	225	0.65
AIRPLANE MEANs		168	820	567	207	352	0.40
TOWER MEAN		5	753	514	222	---	0.37

For the aircraft data, the ratio of observed sensible plus latent heat flux to net radiation is slightly low, as it should be considering flux divergence and ground storage. The tower-observed short wave radiation, net radiation, along with the fluxes of heat and CO_2 are all within 10% of those observed with the airplane. Due to the depth of the mixed-layer, close agreement would be expected.

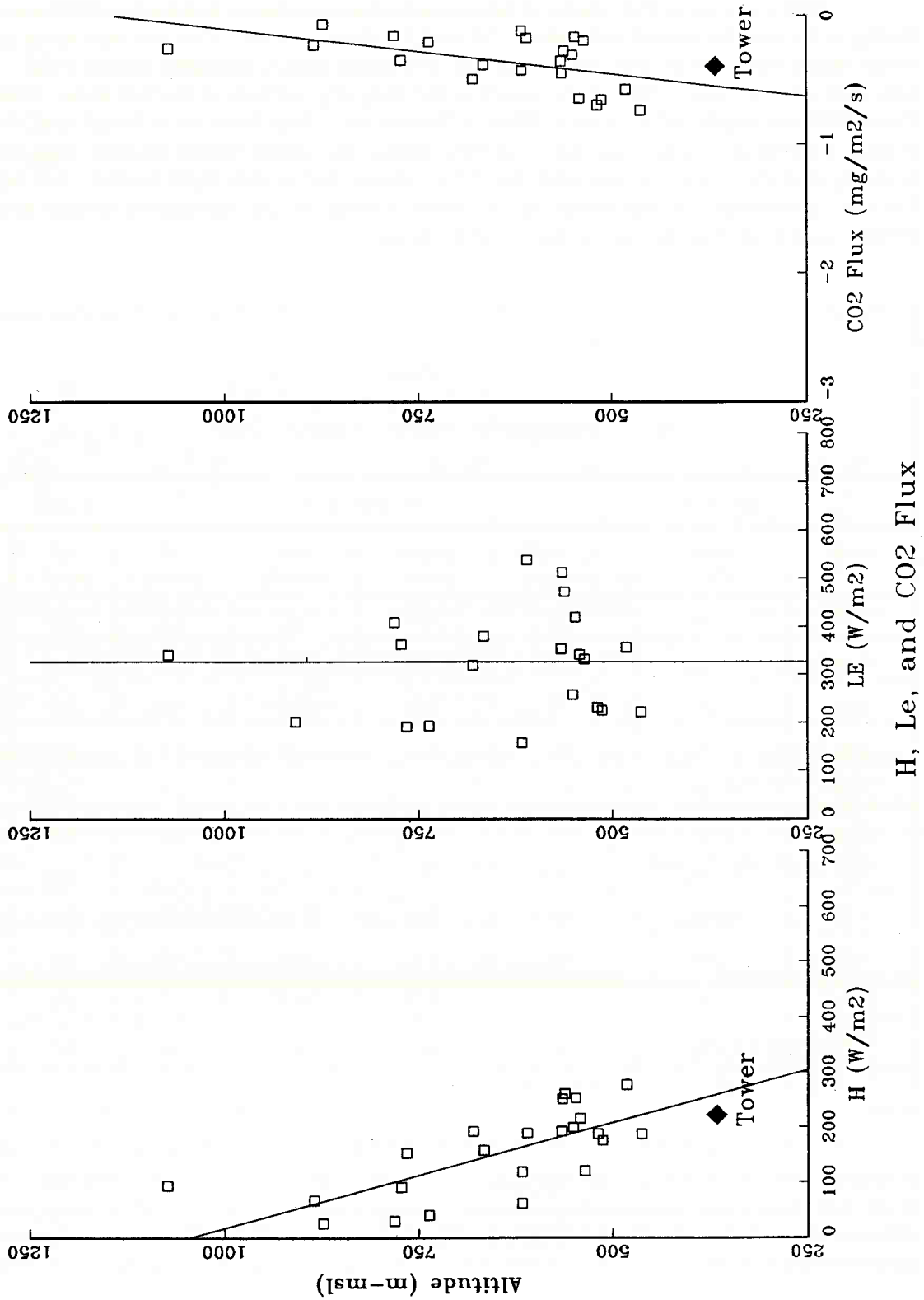

Figure 13. Observed profiles of heat, moisture, and CO_2 flux during FIFE.

Figures 13a, 13b, and 13c display the observed heat, moisture, and CO_2 fluxes for the 25 transects as a function of altitude. The average tower result is noted with a diamond. The mixed-layer depth at 1400 CDT was about 2250 m MSL. Considering the expected mixed-layer growth during the 1000 to 1400 CDT measurement period, the heat flux divergence as illustrated with Figure 13a is a classic example of that which is expected (e.g., Stull, 1988). The observed water vapor flux profile illustrated in Figure 13b suggests no significant gradient, which is also as expected. The low altitude CO_2 flux of -0.4 $mg/m_2/s$ agrees well with the tower observation and with values reported by other FIFE research groups. Figure 13c illustrates the seldom observed flux divergence profile for CO_2. The lack of significant scatter is impressive, especially considering the natural variability and the 6-hour observation period which allows non-stationarity to come into play.

8. CONCLUSIONS

The theory, instrumentation, and demonstration of MFP trace gas air-surface exchange measurement has been presented. Theoretically, such measurements are more complex than tower measurements because sensor motions must be removed. However, important simplifications over traditional INS-based approaches have been achieved and demonstrated. Simplifications were made possible by co-location of the relative velocity sensors with the motion sensors and the development of the necessary mathematical framework. Positioning the motion sensor within the probe allows direct measurement of probe motion removing the need to infer this motion from INS-measured platform motions. The approach described does increase computational demands but this is no problem with modern microcomputers.

The instrumentation used for this demonstration was low cost and light weight. Hardware cost of the MFP described (without chemical sensors) was less than $8,000, and the system weighs 20 kg. The cost and weight advantages derive from modern solid-state sensors and computer hardware, have removed the need for an expensive INS. It is easy to envision an even smaller and lighter MFP -- one that would strap to a variety of mobile platforms including ultra-light airplanes, balloons, buoys, and ships.

The MFP was successfully demonstrated on a small single engine airplane. The system simply "straps" down, requiring no airplane modifications. The important implications of this are: (1) a dedicated "research" aircraft is no longer required, and (2) small aircraft of low operational cost can be used. As a result of this effort, cost no longer prohibits MFP-type measurements for small research programs.

REFERENCES

Auble, D. R., and T. M. Meyers, 1990: An H_2O and CO_2 Open Path Gas Analyzer for Use With Eddy Flux Systems. For submission to *Boundary-Layer Meteorol.*

Blanchard, R. L., 1971: A new algorithm for computing inertial altitude and vertical velocity. *IEEE Trans. Aerosp., Electron. Syst.* **AES-7**:1143-1146.

Brown, E. N., C. A. Friehe, and D. H. Lenschow, 1983: The use of pressure fluctuations on the nose of an aircraft for measuring air motion. *J. Clim. Appl. Meteorol.* **22**:171-180.

Desjardins, R. L., E. J. Brach, P. Alno, and P. H. Schuepp, 1982: Aircraft monitoring of surface carbon dioxide exchange. *Science* **216**:733-735.

Desjardins, R. L., J. I. MacPherson, P. H. Schuepp, and F. Karanja, 1989: An evaluation of aircraft flux measurements of CO_2, water vapor and sensible heat. *Boundary-Layer Meteorol.* **47**:55-69.

Greenhut, G. K., 1983: Resistance of a pine forest to ozone uptake, *Boundary-Layer Meteorol.* **27**:387-391.

Hacker, J. M. and P. Schwerdtfeger, 1988: The FIAMS Research Aircraft System Description. Flinders Institute for Atmospheric and Marine Sciences, The Flinders University of South Australia, S.A., 5042, Technical Report No. 8.

Lapworth, A. J., and P. J. Mason, 1988: The new Cardington balloon-borne turbulence probe system. *Atmos. and Oceanic Tech.*

Lenschow, D. H., and B. B. Hicks, 1989: Global Tropospheric Chemistry -- Chemical Fluxes in the Global Atmosphere. In Report of the Workshop on Measurements of Surface Exchange and Flux Divergence of Chemical Species in the Global Atmosphere.

Lenschow, D. H., and P. Spyers-Duran, 1987: Measurement Techniques: Air Motion Sensing. NCAR-Bulletin No. 23.

Lenschow, D. H., R. Pearson, Jr., and B. B. Stankov, 1981: Estimating the ozone budget in the boundary layer by use of aircraft measurements of ozone eddy flux and mean concentration. *J. Geophys. Res.* **86**:7291-7297, 1981.

Lenschow,D. H., A. C. Delany, B. B. Stankov, and D. H. Stedman, 1980: Airborne measurements of the vertical flux of ozone in the boundary layer. *Boundary Layer Meteorol.* **19**:249-265.

Lenschow, D. H., 1972: The Measurement of Air Velocity and Temperature Using The NCAR Buffalo Aircraft Measuring System. NCAR-TN/EDD-74.

MacPherson J. I., 1988: NEA Twin Otter Operations in Fife. Laboratory Technical Report LTR-FR-104.

MacPherson, J. I., J. M. Morgan, and K Lum, 1981: The N.A.E. Twin Otter Atmospheric Research Aircraft. LTRR-FR-80.

McCarty L. H., 1988: Tiny accelerometer weighs just one gram. *Design News*, February, 1988, by Cahners Publishing Co.

McMillen R. T., 1986: A Basic Program for Eddy Correlation in Non-Simple Terrain. NOAA Technical Memorandum ERL ARL-147.

Ray, J. D., D. H. Stedman and G.J. Wendel, 1986: Fast chemiluminescent measurement of ambient ozone. *Analytical Chemistry* 58:598-600.

Stull, R. B., 1988: Convective Mixed Layer. In *An Introduction to Boundary layer Meteorology*, Chap. 11:441-497. Kluwer Academic Publishers.

Teschler, L. E., 1985: The push into silicon for pressure sensing. *Machine Design*, March, 1985, pg. 71-76.

Wyngaard, J. C., 1988a: Flow-distortion effects on scalar flux measurements in the surface layer: implications for sensor design. *Boundary-Layer Meteorol.* 42:19-26.

Wyngaard, J. C., 1988b: The effects of probe-induced flow distortion on turbulence measurements: extensions to scalars. *J. Atmos. Sci.* 45:3400- 3412.

Webb, E. K., G. I. Pearman, and R. Leuning, 1980: Corrections of flux measurements for density effects due to heat and water vapor transfer. *Quart. J.R. Met. Soc.* 106, *85-100.*

APPENDIX A
WIND VELOCITY FROM A MOBILE PLATFORM

A.1. Governing equation for wind velocity measurement

Obtaining wind velocity from a mobile platform is a problem of transfering coordinates and reference frames. The accelerated reference frame in which the winds are measured undergoes complex motion with full three-dimensional translational and rotational freedom. The reference frame of the earth is treated as inertial, with Coriolis and centrifugal effects included as fictitious forces. Two velocities must be determined: the relative wind velocity, measured by anemometers on the moving platform, and the velocity of the platform itself. The vector sum of these two velocities gives the wind velocity with respect to the earth, also called the absolute wind velocity.

The anemometers may be of any appropriate type. For the airplane demonstration discussed in this report, differential pressure measurements were obtained on a sphere pointed into the airflow. The platform velocity is determined by an inertial navigation system which senses accelerations in three dimensions and integrates in time to yield position and velocity. The accelerometers are at the origin of the relative coordinates, by definition. A key feature of the ATDD MFP is the co-location of the anemometers with these accelerometers. This places the anemometers at the origin of the platform coordinate system, with major advantages that will become evident in the following discussion. To emphasize the difference, we refer to the assembly of anemometers and accelerometers as a *probe*.

The coordinate system of the probe will be indicated by a prime superscript on the symbol denoting the quantity. Quantities in the reference frame of the probe will have subscript $\mathbf{p}$, while quantities in earth reference frame will have no subscript. Thus vector $\mathbf{z_p}$, in earth coordinates, denotes the displacement of a point from the origin of the probe coordinates. The symbol $\mathbf{v'_p}$ denotes the relative wind velocity in relative (*i.e.*, probe) coordinates. Absolute wind velocity is $\mathbf{v}$, with no adornments. The probe velocity will be denoted $\mathbf{C_{pe}}$. Subscripts $\mathbf{pe}$ denote motion, with respect to earth coordinates, of a point fixed in probe coordinates.

The principal advantage to having the relative-velocity sensors at the origin of the relative coordinates is the simplification of $\mathbf{C_{pe}}$. In general, not only must the linear velocity $\mathbf{U_{pe}}$ of a platform be considered, but also its angular velocity $\boldsymbol{\omega}_{\mathbf{pe}}$. Thus

$$\mathbf{C_{pe}} = \mathbf{U_{pe}} + \boldsymbol{\omega}_{\mathbf{pe}} \times \mathbf{z_p}.$$

In earlier systems the displacement $\mathbf{z_p}$ of the relative motion sensors (anemometers) from the accelerometers is as much as several metres. The ATDD system, by contrast, mounts the accelerometers within the array of anemometers, making $\mathbf{z_p}$, and the angular motion term, vanish.

The resultant equation for the absolute velocity of the air with respect to the earth (*i.e.*, the wind) is

$$\mathbf{v} = \mathbf{v_p} + \mathbf{U_{pe}} \qquad (A1)$$

The relative wind velocity in earth coordinates, $\mathbf{v_p}$, is readily obtained from the measured $\mathbf{v'_p}$ by coordinate transformation. Determination of $\mathbf{U_{pe}}$ will now be described.

A.2. Determining probe velocity by inertial navigation

A.2.1. Use of accelerometers:

The velocity of the origin of the relative reference frame is obtained by integration of the readings of three accelerometers, one for each coordinate direction. The three accelerometers, mounted within 1 cm of each other, may be treated as a single instrument. Acceleration is measured by holding a test mass stationary. The forces acting on the test mass are gravity, centrifugal, and Coriolis forces of the earth, and the measured force (per unit mass) $\mathbf{b}$ required to hold the mass stationary within the accelerometer. Thus, by Newton's Second Law of Motion (per unit mass):

$$\dot{\mathbf{u}} = \mathbf{b} + \mathbf{g} - \mathbf{\Omega} \times \mathbf{\Omega} \times \mathbf{R} - 2\mathbf{\Omega} \times \mathbf{u}. \qquad (A2)$$

Here $\mathbf{u}$ is the velocity, with respect to the earth, of the test mass; the dot indicates a time derivative. The force (acceleration) of gravity is $\mathbf{g}$. The angular velocity of the earth is $\mathbf{\Omega}$, while the displacement from the center of the earth is $\mathbf{R}$. Since the test mass is stationary with respect to the accelerometer, which defines the origin of the relative coordinates,

$$\mathbf{u} = \mathbf{U_{pe}}. \qquad (A3)$$

Eq. $(A3)$ considerably simplifies determination of $\mathbf{U_{pe}}$, which otherwise requires measurement both of the rotation rate $\boldsymbol{\omega}_{\mathbf{pe}}$ and its time derivative $\dot{\boldsymbol{\omega}}_{\mathbf{pe}}$ (Lenschow, 1986). In the present form one simply transforms $\mathbf{b}'$ to earth coordinates from the probe coordinates in which it is measured:

$$\mathbf{b} = \mathcal{A}\mathbf{b}'. \qquad (A4)$$

Matrix $\mathcal{A}$ defines the three-dimensional coordinate rotation. Its explicit form will be presented in the next section.

From $(A2)$ and $(A3)$ we obtain an expression for the absolute acceleration of the probe in earth coordinates.

$$\dot{\mathbf{U}}_{\mathbf{pe}} = \mathcal{A}\mathbf{b}' + \mathbf{g} - \mathbf{\Omega} \times \mathbf{\Omega} \times \mathbf{R} - 2\mathbf{\Omega} \times \mathbf{u} \qquad (A5)$$

The two terms containing the earth's rotation are small. Since the earth's radius is about 6×10^6 m, while $|\Omega| = 7.3 \times 10^{-5}$ s^{-1},

$$|\Omega|^2|R| \approx 0.03 \text{ ms}^{-2}$$

$$2|\Omega||u| \approx 0.01 \text{ ms}^{-2}.$$

A typical flux run uses nominally straight flight paths at constant altitude, with attitude and velocity controlled as much as possible. The standard deviation of the acceleration in such a

run is of the order of 1.0 ms^{-2}. A standard deviation of 0.1 ms^{-2}, obtained under particularly smooth conditions above the clouds, is the smallest value likely to be encountered. All rotation terms are thus expected to be less than 10% of the accelerations of interest, except for extremely smooth cases, and are ignored, leaving

$$\dot{\mathbf{U}}_{\mathbf{pe}} = \mathcal{A}\mathbf{b}' + \mathbf{g}, \tag{A6}$$

where the first term on the right-hand side is the output from the accelerometers, rotated to earth coordinates. Since $\dot{\mathbf{U}}_{\mathbf{pe}}$ is in absolute coordinates, its integral is the velocity of the probe with respect to the earth.

A.2.2. Coordinate rotation matrix:

The coordinate rotation matrix $\mathcal{A}$ of $(A4)$ transforms from probe coordinates to earth coordinates, as appropriate to this application. Since this is the reverse of common usage, the signs of the angles will be reversed, a positive angle indicating a counterclockwise rotation *from* probe *to* earth. Otherwise, both coordinate systems are right-handed rectangular Cartesian. Earth coordinates are the conventional east, north, and up.

An airplane will be assumed to carry the probe, although the principles are independent of the carrying system. In relative coordinates, the first axis, z_1', is along the axis of the fuselage, positive toward the nose of the airplane. The second axis, z_2', is along the wings, positive toward the pilot's left. The third axis, z_3', is positive toward the roof of the airplane. Fig A1 shows the two coordinate systems.

Matrix $\mathcal{A}$ of $(A4)$ is most readily explained and derived as a series of three two-dimensional coordinate rotations. The three rotation angles are ϕ, θ, and ψ, called roll, pitch, and yaw, respectively, and are taken sequentially in that order. The sign convention stated above gives the following result:

ϕ: Roll is positive to the pilot's left.

θ: Pitch is positive for nose up.

ψ: Yaw has the same sign convention as the compass heading. Note, however, that yaw angle is zero for east in earth coordinates. Compass headings give $\psi + 90°$.

Although the coordinate rotation is currently done by computation, it helps to imagine a physical system which behaves analogously. The gyro-oriented inertial probe used in earlier mobile-flux-measurement designs provides a useful example. The accelerometers hang in concentric gimbals, each of which allows a two-dimensional coordinate rotation about its axis. The outermost gimbal, axis aligned with the fuselage, rotates through roll angle ϕ until the axis of the next gimbal inward is horizontal. This gimbal then rotates through pitch angle θ about its, now horizontal, axis, until the third gimbal axis is vertical, hence in earth coordinates. This innermost gimbal then rotates about the third axis to align the probe with east and north, completing the transformation.

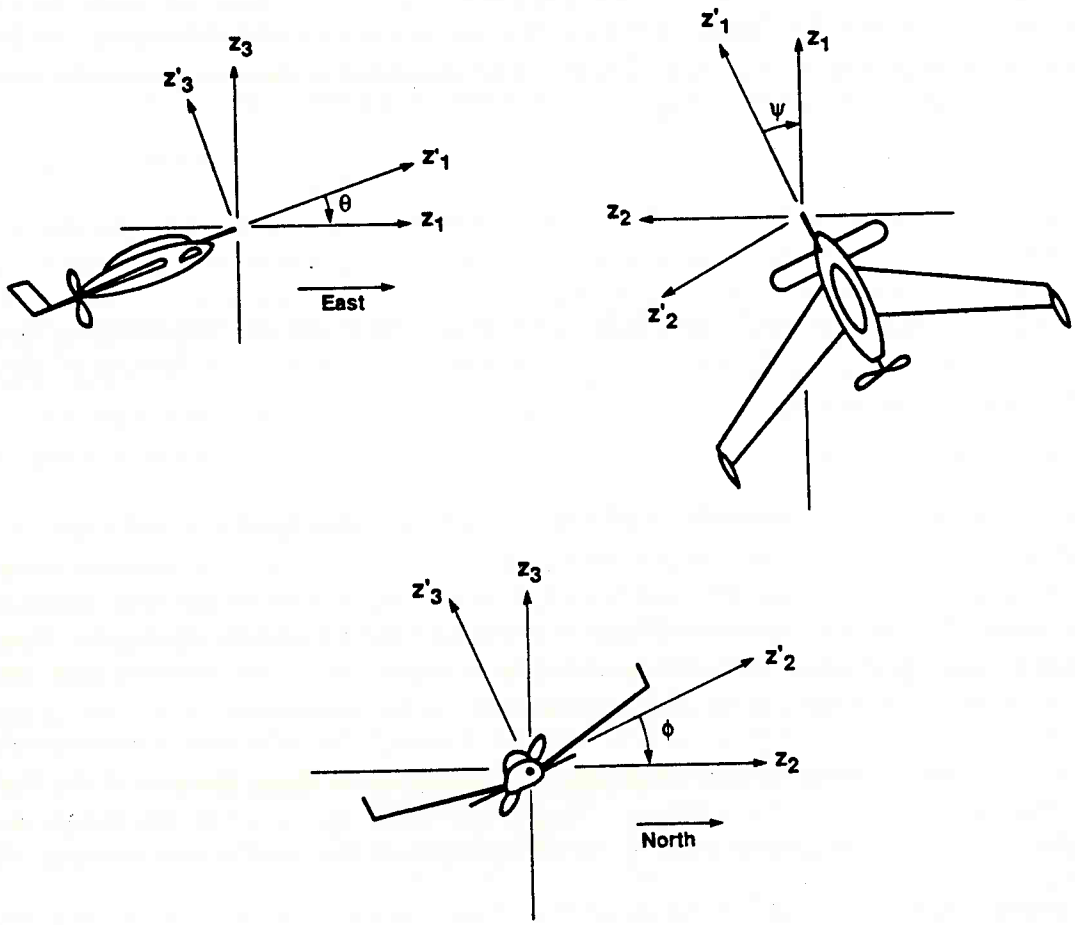

Figure A1: *Earth and probe coordinate systems, shown for an airplane-borne probe with the airplane headed approximately east. Probe coordinates carry prime superscripts and have origin at the center of the probe. The sense of the pitch, yaw, and roll angles is to rotate from probe to earth coordinates.*

For the present system, each of the three serial coordinate rotations is a matrix multiplication, the order of which is significant, analogous to the hierarchy of gimbals just described.

$$\begin{pmatrix} z_1 \\ z_2 \\ z_3 \end{pmatrix} = \begin{pmatrix} cos\psi & sin\psi & 0 \\ -sin\psi & cos\psi & 0 \\ 0 & 0 & 1 \end{pmatrix} \begin{pmatrix} cos\theta & 0 & -sin\theta \\ 0 & 1 & 0 \\ sin\theta & 0 & cos\theta \end{pmatrix} \begin{pmatrix} 1 & 0 & 0 \\ 0 & cos\phi & sin\phi \\ 0 & -sin\phi & cos\phi \end{pmatrix} \begin{pmatrix} z'_1 \\ z'_2 \\ z'_3 \end{pmatrix} \quad (A7)$$

Eq. $(A7)$ is readily reduced to a series of multiplications by 2×2 matrices through cyclic permutation of the z-vector components, thus halving the number of computations required for the coordinate rotation (P.A. Coppin, CSIRO, Australia; personal communication, 1989). At each of the three steps the cyclic permutation places at the bottom of the vector that component of z which lies along the rotation axis. Thus the three steps have the form:

Step 1. Rotate about z_1' (roll)

$$\begin{pmatrix} \tilde{z}_2 \\ \tilde{z}_3 \end{pmatrix} = \begin{pmatrix} cos\phi & sin\phi \\ -sin\phi & cos\phi \end{pmatrix} \begin{pmatrix} z_2' \\ z_3' \end{pmatrix}$$

Step 2. Rotate about $\tilde{z}_2$ (pitch)

$$\begin{pmatrix} \hat{z}_3 \\ \hat{z}_1 \end{pmatrix} = \begin{pmatrix} cos\theta & sin\theta \\ -sin\theta & cos\theta \end{pmatrix} \begin{pmatrix} \tilde{z}_3 \\ z_1' \end{pmatrix}$$

Step 3. Rotate about $\hat{z}_3 = z_3$ (yaw)

$$\begin{pmatrix} z_1 \\ z_2 \end{pmatrix} = \begin{pmatrix} cos\psi & sin\psi \\ -sin\psi & cos\psi \end{pmatrix} \begin{pmatrix} \hat{z}_1 \\ \tilde{z}_2 \end{pmatrix}$$

Note that after the three permutations the **z**-vector has returned to its original order and has been transformed to earth coordinates. The three stages of the algorithm are implemented in a computer program simply by recursive calls to the same subroutine.

A.3. Theoretical wind-velocity equation in final form

Integrating $(A6)$ from a specified initial probe velocity, $\mathbf{U_{pe}}^{(0)}$, and substituting into $(A1)$ gives

$$\mathbf{v} = \mathcal{A}\mathbf{v}_\mathbf{p}' + \mathbf{U_{pe}}^{(0)} + \int_0^t \dot{\mathbf{U}}_\mathbf{pe}\, dt^\star. \qquad (A8)$$

with $\dot{\mathbf{U}}_\mathbf{pe}$ given by $(A6)$. The measurement technique for the wind velocity relative to the probe, in probe coordinates, $\mathbf{v}_\mathbf{p}'$, depends on the carrying vehicle. Differential pressure measurements were used for the airborne system demonstrated in this report. The mathematical development is described in Appendix C.

Although $(A8)$ is correct in principle, implementation is not straight-forward. Naïve integration of $(A6)$ results in unbounded error growth in $\mathbf{U_{pe}}$ over time. This drift, common to many high-frequency measurements, is overcome by a modified integration algorithm in which position data obtained at low frequency are used to control the error growth. The altitude is currently given at low frequency by a pressure altimeter, while horizontal position is given by a LORAN-C system. The algorithm is described in Appendix B.

REFERENCES

Lenschow, D. H., 1986: Aircraft measurements in the boundary layer, in *Proving the Atmospheric Boundary Layer* (D. H. Lenschow, ed.), Am. Meteor. Soc., Boston: 39-55.

Synge, J. L., and A. Schild, 1949: *Tensor Calculus*, University of Toronto Press, Toronto, 324 pp.

APPENDIX B
MIXING HIGH- AND LOW-FREQUENCY MEASUREMENTS

B.1. Governing differential equation

B.1.1. Fundamental concept and equation:

Modern studies of the dynamics and chemistry of the atmosphere require measurement of both long-term mean quantities and turbulent departures. Turbulence measurement from a platform undergoing rapid and complex translation and rotation in all three dimensions requires fast-response instruments (on the order of 40 Hz). But such instruments often drift significantly over time, due to instabilities in the instruments themselves or to the way in which the measurements are used. Accelerometer-derived velocities and positions, discussed in Appendix A, are an example. A commonly-used technique to mitigate the drift is to blend the high-frequency data with additional measurements which do not drift. These additional measurements need not be, and generally are not, accurate at high frequency. Since a differential equation governs the blending, the two types of instrument may directly measure the same physical quantity, such as concentration of O_3, or may measure different quantities, related by time differentiation, such as acceleration and position.

The use of a low-frequency signal to limit error accumulation in a high- frequency signal constitutes a classical problem of control-systems engineering (*e. g.*, Di Stefano *et al.*, 1967). We use a third- order scheme represented by an ordinary differential equation with constant coefficients. Two forms of the equation are currently used, depending on the quantities being determined. For linear motions (acceleration and position) the equation is of the form

$$\frac{d^3z}{dt^3} + c_1\frac{d^2z}{dt^2} + c_2\frac{dz}{dt} + c_3 z = \frac{da_z}{dt} + c_1\frac{d^2z_p}{dt^2} + c_2\frac{dz_p}{dt} + c_3 z_p. \qquad (B1)$$

All quantities are in earth coordinates and reference frame. The platform position (altitude, for example) is z. Acceleration, the $\dot{\mathbf{U}}_{\mathbf{pe}}$ of (A6), is represented by its (vertical) component a_z. The directly-measured position (here, pressure altitude) is z_p. The high- frequency input appears in the higher-order derivatives of the right-hand side, the low-frequency in the lower. Both are appropriately differentiated to achieve physical consistency with the corresponding terms from the left- hand side. The second form of the equation is used for all remaining quantities. For example,

$$\frac{d^3\psi}{dt^3} + c_1\frac{d^2\psi}{dt^2} + c_2\frac{d\psi}{dt} + c_3\psi = \frac{d^2r_y}{dt^2} + c_1\frac{dr_y}{dt} + c_2\frac{d\psi_c}{dt} + c_3\psi_c, \qquad (B2)$$

where ψ is the platform heading. The inputs are r_y, the yaw rate, and ψ_c, the compass heading. Again the high- and low-frequency inputs appear, respectively, in the higher- and lower-order terms on the right-hand side. The two forms, $(B1)$ and $(B2)$, differ in the shape of their frequency response, as will be shown later. The symmetrical response of $(B2)$ was preferred when there was no apparent advantage to use of $(B1)$. We selected $(B1)$ for the linear-motion calculations because the platform velocity is conveniently extracted from $(B7)$, in which form $(B1)$ is actually solved.

The coefficients, $c_1, ..., c_3$, are chosen such that there are three equal roots to the characteristic equations associated with $(B1)$ and $(B2)$, thus prescribing a single characteristic (crossover) frequency α_f for each system.

$$\begin{aligned} c_1 &= 3\alpha_f \\ c_2 &= 3\alpha_f^2 \\ c_3 &= \alpha_f^3. \end{aligned} \tag{B3}$$

Above α_f, low-frequency input is damped by $(B1)$ and $(B2)$, leaving the high-frequency input dominant, where the benefits of its fast response are realized. Below α_f high-frequency input is damped, realizing the benefits of long-term stability in the low-frequency measurements.

B.1.2. Frequency response:

These selective damping properties of $(B1)$ and $(B2)$ are illustrated by postulating oscillatory input at frequency ω. Since for each equation both sensors sample the same oscillation,

$$\begin{aligned} a_z &= -\omega^2 A_z e^{i\omega t} \\ z_p &= Z_p e^{i(\omega t + \phi_z)} \\ r_y &= i\omega R_y e^{i\omega t} \\ \psi_c &= \Psi_c e^{i(\omega t + \phi_\psi)}. \end{aligned} \tag{B4}$$

Here $i = \sqrt{-1}$, t is time. Ideally a_z, z_p, r_y, and ψ_c are related as

$$\begin{aligned} a_z &= \frac{d^2 z_p}{dt^2} \\ r_y &= \frac{d\psi_c}{dt}. \end{aligned} \tag{B5}$$

Since the sensed amplitudes and phases may differ in practice, however, $(B4)$ provides four separate amplitudes, A_z, Z_p, R_y, and Ψ_c, along with two phases, ϕ_z and ϕ_ψ. Eq. $(B5)$ holds when $A_z = Z_p$, $R_y = \Psi_c$, and $\phi_z = \phi_\psi = 0$.

The output will respond to this forcing at the same frequency. Thus the solution will have the form

$$\begin{aligned} z &= \mathcal{Z} e^{i\omega t} \\ \psi &= \mathcal{P} e^{i\omega t}. \end{aligned}$$

where the coefficients $\mathcal{Z}$ and $\mathcal{P}$ may be complex, allowing response amplitude and phase to differ from that of the input. We substitute these expressions into $(B1)$ and $(B2)$, take derivatives and solve for $\mathcal{Z}$ and $\mathcal{P}$ to obtain

$$\begin{aligned} \mathcal{Z} &= \frac{-i\omega^3 A_z + (-3\alpha_f\omega^2 + 3i\alpha_f^2\omega + \alpha_f^3) Z_p e^{i\phi_z}}{(\alpha_f + i\omega)^3} \\ \mathcal{P} &= \frac{(-i\omega^3 - 3\alpha_f\omega^2) R_y + (3i\alpha_f^2\omega + \alpha_f^3)\Psi_c e^{i\phi_\psi}}{(\alpha_f + i\omega)^3}. \end{aligned} \tag{B6}$$

These equations are versions of the transfer function of $(B1)$ and $(B2)$ for analysis of frequency response, excluding transients. If the two inputs are consistent, that is if $(B5)$ holds, then the gains (moduli of $\mathcal{Z}$ and $\mathcal{P}$) are unity for all frequencies, and the phase differences between output and input (arguments of $\mathcal{Z}$ and $\mathcal{P}$) are zero. Inconsistant amplitudes and phases between the two inputs at the given frequency, ω, represent error in the sampling of the true signal by at least one system.

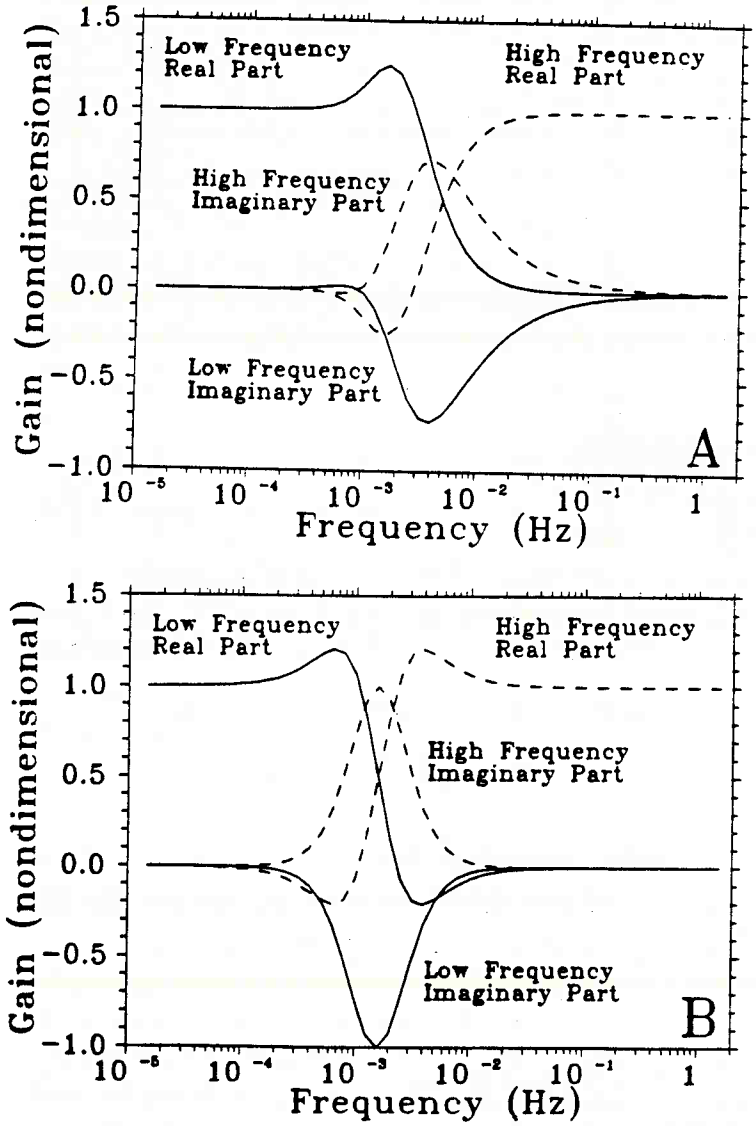

Figure B1: *Frequency response from $(B6)$ for asymmetric* **A** *and symmetric* **B** *blending algorithms showing relative contribution of high- and low- frequency input as a function of frequency. At any frequency the real parts add to unity, the imaginary parts to zero.*

The primary difference between the two forms in $(B6)$ is in how the two inputs are treated in the numerators. In the first equation A_z enters only in the third-order term in ω, while in the second the corresponding R_y term enters in both the third and second-order terms in ω. The effect of this difference is seen in Fig B1A and B, where the contribution to the output signal from each input is displayed as a function of frequency. In these figures, with α_f = .0016 Hz, the real and imaginary parts of the expressions in $(B6)$ are plotted. High- and low-frequency contributions to the output have been separated by setting the inputs to zero in turn. At any frequency, the real parts of the two contributions sum to unity, while the imaginary parts sum to zero. Fig B1A, corresponding to $(B1)$, has an asymetrical frequency response. The low-frequency input still has significant influence on the output, through its imaginary part, up to about $20\alpha_f$. The high-frequency input, by contrast is damped by about $0.3\alpha_f$. Fig B1B, corresponding to $(B2)$ has a symmetric

frequency response with the influence of low-frequency extending up to about $10\alpha_f$ and of high-frequency down to about $0.1\alpha_f$.

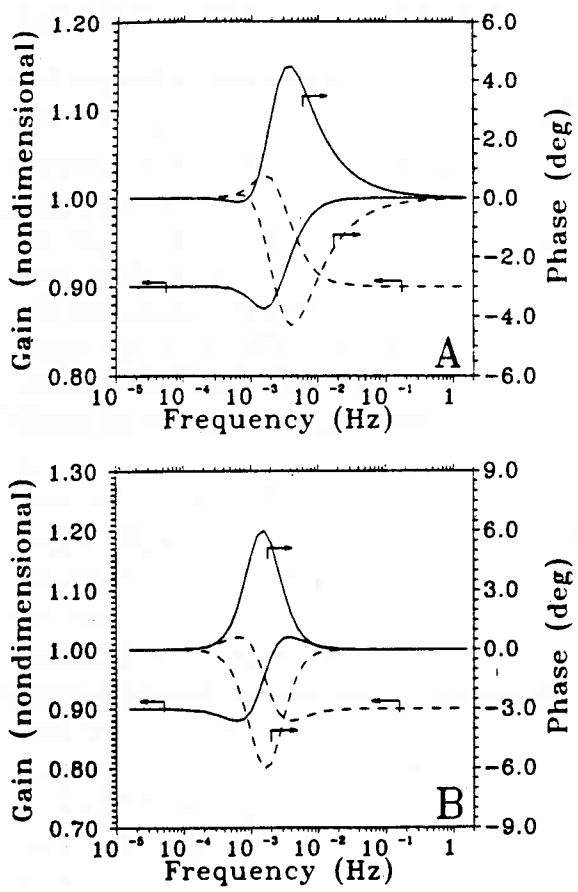

Figure B2: *Consequence of inconsistent amplitudes between high- and low-frequency inputs to the asymmetrical* **A** *and symmetrical* **B** *blending algorithms. The solid lines show runs with low-frequency input at 90% of nominal; dashed lines high-frequency input at 90% of nominal. Axes have been scaled and shifted to align zero phase with unit gain. With consistent amplitudes each graph collapses to a single straight line.*

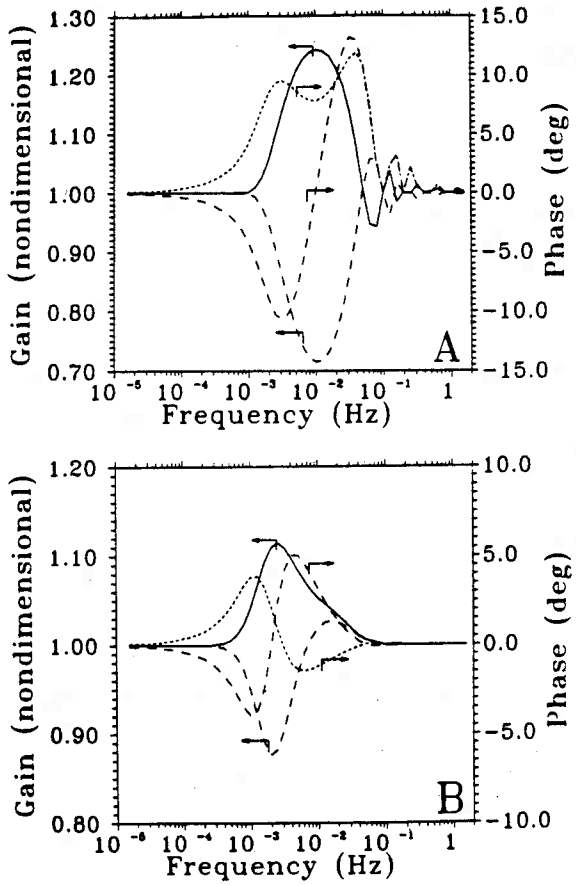

Figure B3: *Same as B2 except the inconsistency is in phase. The phase incongruity is specified as a 10 s time lag, making the phase lag vary with frequency. In the vicinity of the crossover frequency α_f (1.6×10^{-3} Hz) gain exceeds unity, and phase is nonzero.*

In Fig B1 the amplitudes and phases of the two inputs are consistent. More likely, there will be inconsistencies, causing amplitude and phase errors, especially within a factor of ten

of the crossover frequency, α_f. The effect can be seen by adjusting amplitudes and phases of the two inputs in turn. In Fig B2 each of the input amplitudes in turn is set at 90% of its consistent value. With the amplitude of the high-frequency input, for exarnple, set 10% low, the output amplitude (gain) is unity below some neighborhood of α_f and is (properly) 0.9 above this neighborhood. Within the neighborhood, the gain exceeds unity, and the phase becomes nonzero. By comparison with Fig. B1 we see that the gain curves of Fig B2 have the shape of the real part, while the phase curves have the shape of the imaginary part from the stronger of the two inputs. Fig B3, showing the effect of a 10 s time lag in one of the two inputs is considerably more complex. The phase shift implied by a fixed time lag depends on the frequency. For reasons unknown, the symmetric blender appears to recover better at high frequencies, while the asymmetric blender is better at low frequencies. Since inconsistencies between the two inputs are expected in normal operation, the crossover frequency should be chosen as low as possible to include all relevent scales of atmospheric turbulence, but not so low as to fail to control drift in the high-frequency data. The choice of an actual value requires considerable judgement and experience. A typical value for an airplane at 50 ms^{-1} is $\alpha_f = 0.02$ Hz.

B.2. Implementation

B.2.1. Integral form of the equation:

The control system is implemented following common practice (Lenschow, 1986; MacPherson *et al.*, 1981), with some modifications. The algorithm used is derived by integrating $(B1)$ and $(B2)$ three times and nesting the integrals. From $(B1)$ is obtained

$$\begin{aligned} I_z(t') &= \int_0^{t'} \alpha_f^3 z_d \, dt^\star + I_z(0) \\ v_z(t) &= \int_0^{t} [a_z - 3\alpha_f^2 z_d - I_z(t')] \, dt' + v_z(0) \\ z(t_1) &= \int_0^{t_1} [-3\alpha_f z_d + v_z(t)] \, dt + z(0). \end{aligned} \qquad (B7)$$

Here

$$z_d = z - z_p$$

expresses the discrepancy between the computed position (altitude) and that directly measured (by altimeter). The equation corresponding to $(B2)$ becomes

$$\begin{aligned} I_\psi(t') &= \int_0^{t'} \alpha_f^3 \psi_d \, dt^\star + I_\psi(0) \\ y_r(t) &= \int_0^{t} [3\alpha_f r_y - 3\alpha_f^2 \psi_d - I_\psi(t')] \, dt' + y_r(0) \\ \psi(t_1) &= \int_0^{t_1} [r_y - 3\alpha_f \psi + y_r(t)] \, dt + \psi(0) \end{aligned} \qquad (B8)$$

with

$$\psi_d = \begin{cases} \psi - \psi_c - 360^\circ & \text{for } \psi - \psi_c > 180^\circ \\ \psi - \psi_c + 360^\circ & \text{for } \psi - \psi_c < -180^\circ \\ \psi - \psi_c & \text{otherwise.} \end{cases}$$

The definition of ψ_d allows for passage through north.

In each equation of $(B7)$ and $(B8)$ the initial values are indicated by the zero argument. Transients are avoided by specifying initial conditions consistent with the state of the system. Position and heading, up to and at initial time, are clearly given by the low-frequency input. The remaining quantities are less obvious. In $(B7)$, v_z is equal to the platform velocity, given $z_d = 0$, and may be initially so set. Initial velocity is adequately given by the average over the measurement path if real-time output is not required. For vertical velocity this average is usually zero. In $(B8)$ y_r is not equal to the yaw rate, but contains absolute heading information. Its consistent initial value cancels the $3\alpha_f\psi$ in the third equation of $(B8)$ so that ψ is initially given entirely by integration of the measured yaw rate r_y. Summarizing the initial conditions:

$$\begin{aligned} I_z(0) &= 0 & I_\psi(0) &= 0 \\ z(0) &= z_p(0) & \psi(0) &= \psi_c(0) \\ v_z(0) &= 0 & y_r(0) &= 3\alpha_f\psi(0) \neq 0. \end{aligned} \qquad (B9)$$

If transients appear, experience shows them to be damped over a time period comparable to $2\pi/\alpha_f$.

B.2.2. Signal path diagram and departures from previous practice:

Fig B4 (Lenschow, 1986) illustrates the signal path for $(B7)$ using standard notation of control systems. Circles are summation points, boxes are components operating on the signal passing through them. The inputs are a_z and z_p; the outputs v_z, vertical velocity, and z, inertial altitude. The expression for the inertial altitude may be traced from the diagram with two exceptions. Neither the branch containing the Schuler frequency ω_s (defined below) nor that containing lag-correction coefficient c_4 is included in the present system.

The Schuler frequency is that of an error oscillation characteristic of gyro-oriented inertial navigation systems. If the inertially-determined horizontal position is in error, the vertical orientation of the platform will also be in error due to the curvature of the earth. Thus the measured horizontal components of acceleration will be contaminated by gravity components. These have compensating sign, producing an oscillation of the platform position about its correct orientation with frequency

$$\omega_s^2 = \frac{g}{R_0}$$

where g is the acceleration of gravity and R_0 is the radius of the earth. This oscillation does not occur in the present system, which senses the vertical direction by gravity, rather than by position on the earth. The feedback between computed position and orientation which drives the Schuler oscillation is thus absent from the present system.

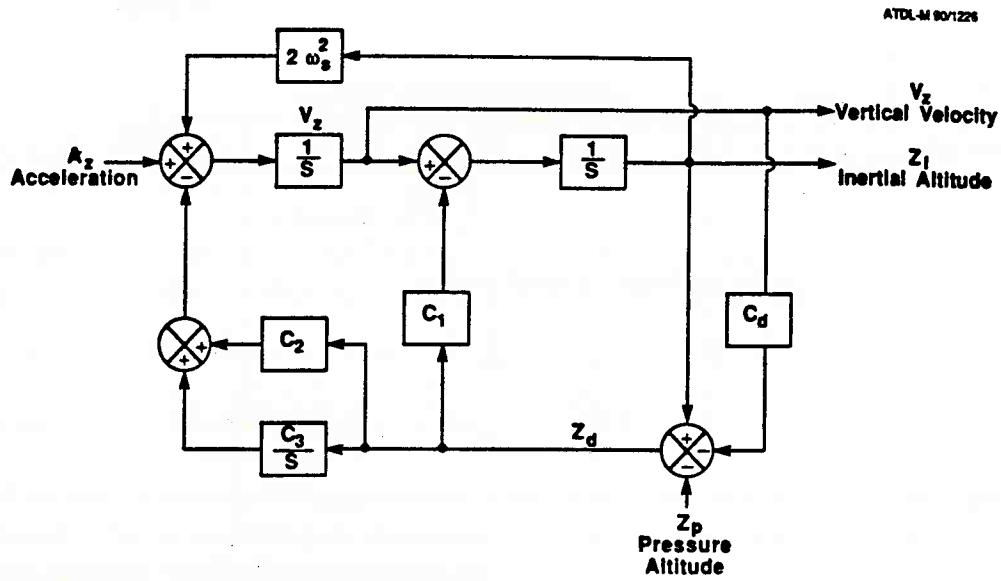

Figure B4: *Signal-flow diagram for the asymmetrical algorithm used by Lenschow (1986). Circles are summation points. Boxes are operations on the Laplace-transformed signal. Time integration is denoted $1/s$. In the current application, ω_s and c_d are set to zero. See text.*

The lag-correction coefficient c_4, having time units, appears in the z_d term of $(B7)$

$$z_d = z - (z_p + c_4 v_z).$$

Here v_z is given by $(B7)$. The $(z_p + c_4 v_z)$ provides a "forecast" of z_p, given the current v_z and z_p, thus partially compensating for lag in the measurement of z_p. We have found gain and phase to be badly distorted by this term for all frequencies above the crossover frequency. We are primarily interested in the high frequencies. Furthermore, the probe design eliminates many sources of lag. Remaining lag in sensor readings can be more directly compensated by other means. Thus, we have chosen to ignore this term.

The signal path for $(B8)$ is given in Fig B5. The primary differences from $(B7)$ are in the two points of input for the yaw rate r_y and in the takeoff of the c_1 branch from ψ rather than from $\psi - \psi_c$. This is because in $(B8)$ only ψ, not ψ_c, appears in the outermost integral.

B.2. Computing the platform velocity

In principle, the computed platform velocity should at all times be equal to the time derivative of the platform position. This can be assured by defining, for example, the vertical component of the platform velocity to be equal to the integrand of the outermost integral in $(B7)$. Thus

$$\mathcal{U}_z = v_z - c_1 z_d \qquad (B10)$$

where v_z is defined by $(B7)$. This, however, introduces unfiltered signal into $\mathcal{U}$ from the low-frequency sensors. Typically these are considerably less accurate than the high-frequency sensors for individual measurements. For example, the horizontal position may be determined

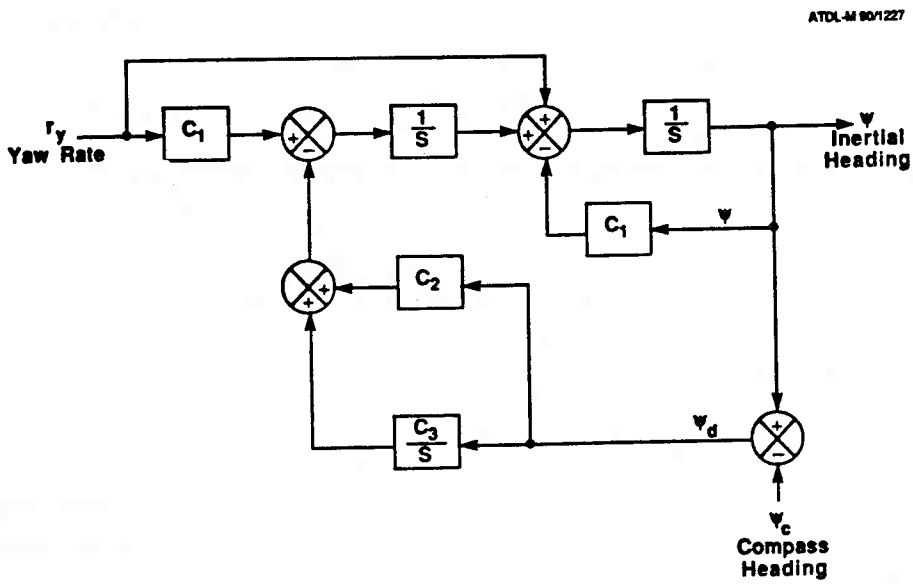

Figure B5: *Same as B4, but for the symmetrical filter*

from LORAN, accurate only to tens of metres. We have judged the increased noise to outweigh any advantages derived from linking platform velocity and position at every sampling time. Thus we simply use v_z, and its corresponding forms for the other components, as the platform velocity, following Blanchard (1971) and Lenschow (1986).

REFERENCES

Blanchard, R. L., 1971: A new algorithm for computing inertial altitude and vertical velocity. *IEEE Tran. Aerosp. Electron. Syst.*, **AES-7**:1143-1146.

DiStefano, J. J., III, A. R. Stubberud and I. J. Williams, 1967: *Feedback and Control Systems*, Schaum Outline Series, McGraw-Hill, New York, 371 pp.

Lenschow, D. H., 1986: Aircraft measurements in the boundary layer, in *Proving the Atmospheric Boundary Layer* (D. H. Lenschow, ed.), Am. Meteor. Soc., Boston: 39-55.

MacPherson, J. I., J. M. Morgan and K. Lum, 1981: The N.A.E. Twin Otter Atmospheric Research Aircraft. National Aeronautical Establishment, **LTR-FR-80**, National Reserch Council, Canada, Ottawa, 86 pp.

APPENDIX C
RELATIVE WIND VELOCITY FROM A NINE-HOLE PRESSURE SPHERE

C.1. Basic concepts

Determination of wind velocity with respect to the earth from (A8) requires measurement of the air velocity relative to the probe in probe coordinates, $\mathbf{v}'_{\mathbf{p}}$, in (A8). Which technique is preferrable, among several choices, depends on the carrying vehicle. In the demonstration described in this report that vehicle is an airplane, capable of relatively slow flight at 40-50 ms^{-1}. Yet this flight speed remains fast enough to require a rugged instrument, which can sustain dynamic pressures around 15 mb and be insensitive to impacts from small objects. A very satisfactory approach is to measure the pressure distribution on a sphere extended from a boom into the undisturbed airstream ahead of the airplane (Brown *et al.*, 1983). Such pressure spheres are easily constructed, have good physical basis, and are readily fitted with accurate, low-cost pressure sensors.

The pressure distribution around a sphere in an airstream may be specified from potential-flow theory for any given incident velocity (Brown *et al.*, 1983):

$$p_\gamma - p_\infty = q(1 - \frac{9}{4} sin^2\gamma). \qquad (C1)$$

Here p_γ is the air pressure at angle γ from the stagnation point; p_∞ is the ambient air pressure far from the sphere, also called the static pressure; and q is the dynamic pressure, the excess above static pressure at the stagnation point. The dynamic pressure is related to the incident speed by

$$q = \frac{1}{2}\rho U^2, \qquad (C2)$$

where ρ is the local density of air, and U is the incident airspeed. Experiment shows fully turbulent flow to follow this pressure distribution very closely for at least 60° of arc around the sphere from the stagnation point (Schlichting, 1968). Therefore, measurement of p_γ, p_∞, and ρ at specified γ allows calculation of the incident air speed from $(C1)$.

The incident airflow direction is measured relative to the probe coordinates, described in Appendix A. The origin is at the center of the pressure sphere with axes z'_1, z'_2, and z'_3, oriented forward, leftward (facing forward), and upward, respectively. The z'_1-axis passes through a reference point on the sphere. The boom is oriented such that, at nominal sampling airspeed, the stagnation streamline of the incident flow strikes this reference point. Departure of the actual stagnation point from nominal may be kept small by the pilot's maintaining nominal airspeed and minimizing heading correction, allowing the airplane its natural orientation directly into the airstream. The turbulence-induced departure from nominal can be held well within 10° and may be sensed by differential pressure measurements around the sphere.

A significant difference between the current pressure-sphere design and other similar systems is the placement of the static-pressure sensing ports on the pressure sphere itself. This design is a major simplification, avoiding complex corrections required for time delay and flow

distortion in systems which locate the ports on the fuselage or behind the probe head. From $(C1)$ there is an angle $\gamma = \gamma_s = 41.81°$ at which

$$p_s = p_\infty.$$

Pressure measurements on the sphere displaced 41.81° of arc from the reference point thus provide the static pressure in principle, with a few practical adjustments to be discussed later.

C.2. Design

The quantities to be determined are air density, ρ, static pressure, p_∞, stagnation-point pressure, and the departure of the actual stagnation point from its nominal position. The actual location of the stagnation point is given in spherical coordinates on the pressure sphere. Using the same conventions as for the earth, the origin is at the center of the sphere, the "north pole" is upward in airplane (probe) coordinates, and the nominal stagnation point is at zero "latitude" and zero "longitude." The "latitude" is then the negative of the angle of attack α of the sphere, following aeronautical sign conventions, and will be so named in the following. The "longitude" is the negative of the sideslip angle β. Fig C1 shows these conventions. Design of the measurement system assumes α and β are smaller than 10°. Density is determined from air temperature and static pressure. Static pressure is measured at ports drilled into the sphere at the appropriate angle from the (nominal) stagnation point, as previously stated. Four ports, appearing as crosses in Fig C1, are evenly spaced around the sphere. This allows averaging, which compensates to first order when the stagnation point is displaced from its nominal position. Stagnation point pressure, from which incident air speed is determined, is derived from a pressure measurement through a port at the reference point.

The attack and sideslip angles α and β, being small, may be treated independently. Through (C1), the difference between two pressures p_U and p_D, measured at coordinates $-\theta$ and $+\theta$ above and below the reference point gives the vertical angular departure α of the stagnation point from its nominal position. Apparent sign reversal is due to the convention in use.

$$\begin{aligned} \frac{(p_U - p_D)}{q} &= \frac{9}{4}[sin^2(\theta - \alpha) - sin^2(\theta + \alpha)] \\ &= -\frac{9}{4} sin2\alpha \; sin2\theta. \end{aligned} \qquad (C3)$$

By design θ is 45° to maximize the sensitivity of $(C3)$ to changes in α. Likewise, β is given by the difference between two pressure measurements p_L and p_R at 45° to left and to right of the reference point. Defining

$$\Delta p_\alpha = p_U - p_D$$
$$\Delta p_\beta = p_L - p_R$$

gives

$$\begin{aligned} \alpha &= -\frac{1}{2} sin^{-1}(\frac{4}{9}\frac{\Delta p_\alpha}{q}) \\ \beta &= -\frac{1}{2} sin^{-1}(\frac{4}{9}\frac{\Delta p_\beta}{q}). \end{aligned} \qquad (C4)$$

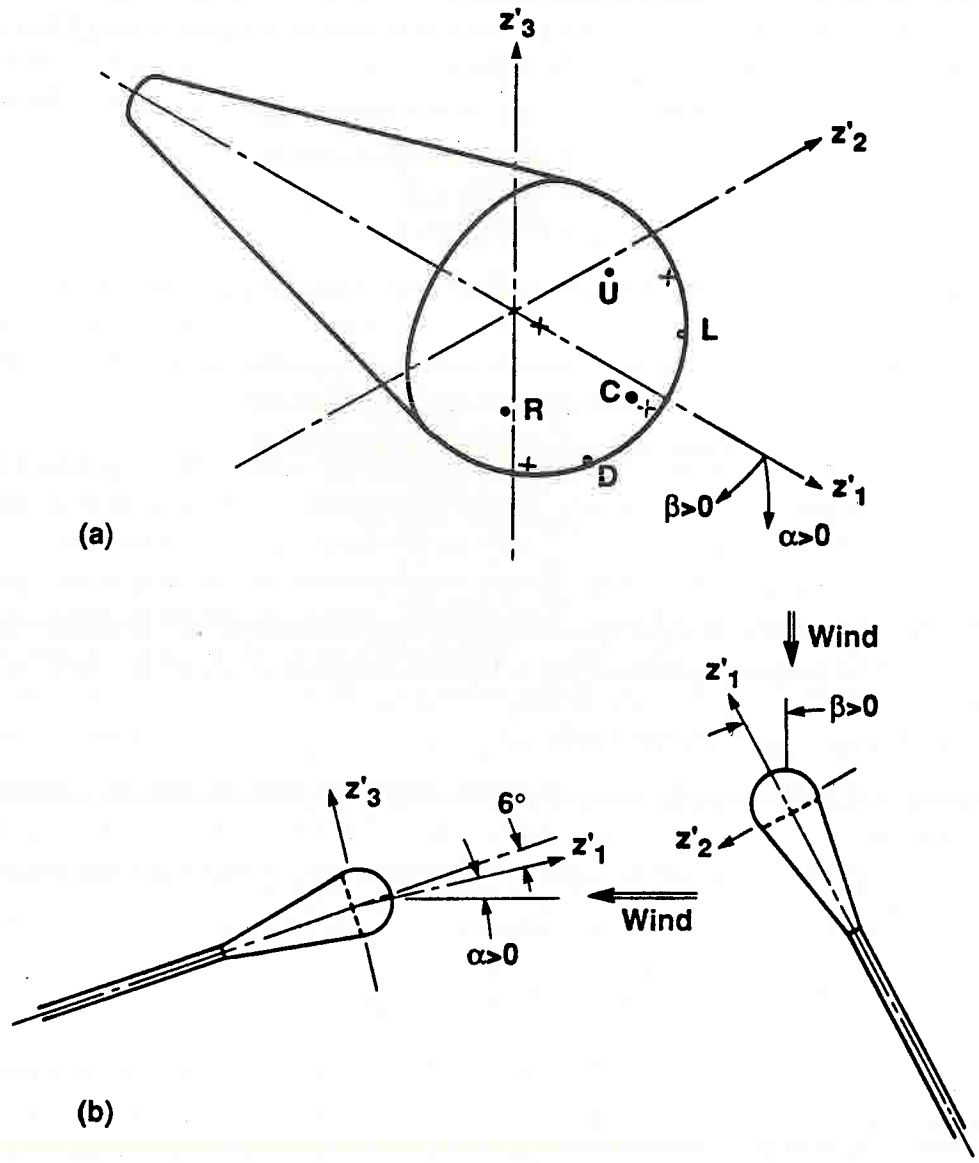

Figure C1: (a) *The pressure sphere, showing the relative coordinate system (same notation as in Appendix A), the port locations, and the sign convention for the angles of attack and sideslip, equivalent to negative latitude and longitude on the sphere with "north pole" along* z_3'. *Crosses indicate static ports.* **(b)** *Detail of the sign convention, viewing attack and sideslip from the position of the pilot. The 6° displacement of the central port below the axis of the probe allows the airplane an adequate angle of attack on its wings for slow flight, while retaining near-zero angle of attack on the sphere.*

The three components (u_a, v_a, w_a) of the air velocity relative to the sphere in probe coordinates are computed from the relative air speed U and the direction of the stagnation streamline. This streamline is parallel to the incident flow and would pass through the center of the sphere if extended. Its direction is given by angles α and β with signs already correct because of the sign convention in use. Conversion from spherical to rectangular probe coordinates gives:

$$\begin{aligned} u_a &= U cos\alpha cos\beta \\ v_a &= U cos\alpha sin\beta \\ w_a &= U sin\alpha. \end{aligned} \tag{C5}$$

C.3. Sources of uncertainty: Theory

The success of much of the determination of relative air velocity from pressure measurements on a sphere depends on the validity of the assumption of small angles of attack and sideslip. Violation of this assumption has two types of consequences: those due to nonlinear interactions between α and β, and those due to displacement of the stagnation point from the stagnation pressure port. In a typical flux run only gentle correction maneuvers are used to maintain the planned ground path. Thus the primary source of non-zero α and β is high-frequency turbulent eddies. Experience indicates average values of 0.5° for α and 1° for β. Extremes for both angles infrequently reach 10°.

Nonlinear interactions between α and β affect the determination both of these angles themselves and of the static and dynamic pressures. The full nonlinear relations among α, β, p_∞, and q are derived from an expression, used in navigation, for the angular great-circle distance between two points on a sphere, given the latitude and longitude of these points

$$cos\gamma = sin\alpha_1 sin\alpha_2 + cos\alpha_1 cos\alpha_2 cos(\beta_2 - \beta_1). \tag{C6}$$

Here subscripts 1 and 2 refer to the two points while γ is the distance in great-circle radians between the two points. The sign convention for this appendix follows standard aeronautical practice: positive pitch (nose up) means positive angle of attack, while having the nose to the left of the flight path results in positive sideslip. As a consequence of this convention, α and β are negatives of latitude and longitude. Since $(C6)$ is an even function of latitude and longitude, however, there is no effect. In view of $(C6)$ it will be convenient to express $(C1)$ in terms of the cosine

$$p_\gamma - p_\infty = \frac{q}{4}(9cos^2\gamma - 5). \tag{C7}$$

C.3.1. Angles α and β:

Eq $(C3)$ for α and its counterpart for β assume that the angle not being measured is zero. When this is not the case, the angular distances between the stagnation point and the pressure ports are no longer $\pi/4 \pm \alpha$ or $\pi/4 \pm \beta$, but something rather more complicated. Define the pressure ports U, D, R, and L as in Fig C1, where "left" and "right" are defined facing the

airflow. The great-circle angular distance from the stagnation point to each port is indicated by a corresponding subscript. Thus, from $(C6)$

$$\begin{aligned} cos\gamma_U &= -sin\alpha sin\theta + cos\alpha cos\theta cos\beta \\ cos\gamma_D &= sin\alpha sin\theta + cos\alpha cos\theta cos\beta \\ cos\gamma_R &= cos\alpha cos(\theta - \beta) \\ cos\gamma_L &= cos\alpha cos(\theta + \beta). \end{aligned} \tag{C8}$$

Note that in $(C8)$, as in $(C3)$, signs opposite to those of the latitudes and longitudes of the U, D, L, and R ports have been affixed to $\theta = \pi/4$. If expressions $(C8)$ are inserted into $(C7)$, the appropriate differences taken, and the results put into a form resembling $(C3)$:

$$\begin{aligned} p_U - p_D = \Delta p_\alpha &= -\frac{9}{4} q \; sin2\alpha cos\beta \\ p_L - p_R = \Delta p_\beta &= -\frac{9}{4} q \; sin2\beta cos^2\alpha. \end{aligned} \tag{C9}$$

Simultaneous solution of $(C9)$ yields α and β, but this is unnecessarily complicated for small angles. The best use of $(C9)$ is to determine the error incurred using $(C3)$.

C.3.2. Static pressure:

Correct measurement of the static pressure requires an incident airflow directly into the reference point, $\alpha = \beta = 0$. Consequences of violating this condition, mitigated by averaging over four ports, are investigated using $(C6)$ and $(C7)$. Their polar coordinates on the pressure sphere may be computed by first determining their positions in the rectangular probe coordinate system, with origin at the center of the sphere, and then transforming to polar coordinates. The result, using subscripts 1,...,4 to denote the individual ports, are

$$\begin{aligned} (\alpha_1, \beta_1) &= (28.1°,\ 32.3°) \\ (\alpha_2, \beta_2) &= (-28.1°,\ 32.3°) \\ (\alpha_3, \beta_3) &= (-28.1°, -32.3°) \\ (\alpha_4, \beta_4) &= (28.1°, -32.3°). \end{aligned} \tag{C10}$$

Clearly all α's and β's of $(C10)$ have the same measure, differing only in sign. Except for the cosine term, $(C7)$ is linear and unchanged from one port to another. The cosine term in the composite form of $(C7)$ is, therefore, the average of the squared cosines of the angular separations between the stagnation point and the individual static pressure ports

$$\overline{cos^2\gamma_i} = sin^2\alpha sin^2\alpha_1 + cos^2\alpha cos^2\alpha_1(cos^2\beta_1 cos^2\beta + sin^2\beta_1 sin^2\beta). \tag{C11}$$

Here (α, β) are the negatives of the latitude and longitude of the stagnation point on the sphere. The overbar indicates that an average of the squared cosines has been taken. The α_1 and β_1 in $(C11)$ carry all necessary information from $(C10)$. The averaging has cancelled the

cross-product terms in $(C11)$ leaving the error only quadratic dependence on the sines of α and β. The fixed quantities in $(C11)$, involving α_1 and β_1, may be given exactly as:

$$\begin{aligned} sin^2\alpha_1 &= \frac{2}{9} & cos^2\alpha_1 &= \frac{7}{9} \\ sin^2\beta_1 &= \frac{2}{7} & cos^2\beta_1 &= \frac{5}{7} \end{aligned} \qquad (C12)$$

Using $(C11)$ and $(C7)$ with $(C12)$:

$$\overline{p_\gamma} - p_\infty = \frac{q}{4}\left\{\left[2sin^2\alpha + cos^2\alpha(5cos^2\beta + 2sin^2\beta)\right] - 5\right\}. \qquad (C13)$$

If $\alpha = \beta = 0$ the right-hand side is zero and the average $\overline{p_\gamma}$ is equal to the static pressure. The error otherwise depends on α, β, and q. A plot of this relation is given later (Fig. C4).

C.3.3. Stagnation pressure:

The displacement of the stagnation point from the stagnation pressure port erroneously decreases the reported stagnation pressure. The error may be computed from the following expression, obtained from $(C6)$ and $(C7)$ assuming an infinitesimal pressure port:

$$p_C - p_\infty = \frac{q}{4}(9cos^2\alpha\ cos^2\beta - 5). \qquad (C14)$$

Here p_C is the indicated stagnation pressure, equal to the true stagnation pressure if $\alpha = \beta = 0$. A plot of this relation is given later (Fig. C5).

C.4. Sources of uncertainty: Wind-tunnel measurements

The characteristics of the actual sphere were examined in a wind tunnel. Since an environmental wind tunnel was used, capable of no more than about 17 ms^{-1} over its full 1 m^2 cross section, a plywood sheet was inserted to reduce the cross-section area. This sheet covered the entire cross section of the tunnel except for a 0.3 m^2 hole at its center. Close to 40 ms^{-1} was achieved with this plate, the flow velocity remaining homogeneous to within 2% over the core of the jet passing through the plate. The 12-cm diameter probe and a corroborating pitot tube were placed about 0.3 m downstream from the plate for the tests.

The tests were of two types, the first varying only the flow speed at zero angle of attack, the second varying only the angle of attack at the highest flow speed. The sideslip angle was kept at zero for these tests. All results are assumed to depend uniformly on $\sqrt{\alpha^2 + \beta^2}$.

C.4.1. Angles α and β:

The accuracy of determination of the attack and sideslip angles was tested by directly measuring the probe orientation at each of seventeen attack angles. Fig C2 shows the comparison between the set probe orientation and that measured by the probe. A theoretical proportionality constant between α and $\Delta p_\alpha/q$ of -0.22 follows from (C4). Linear regression between -4° and 4°, the range of α normally encountered in practice, gives a value of -0.27.

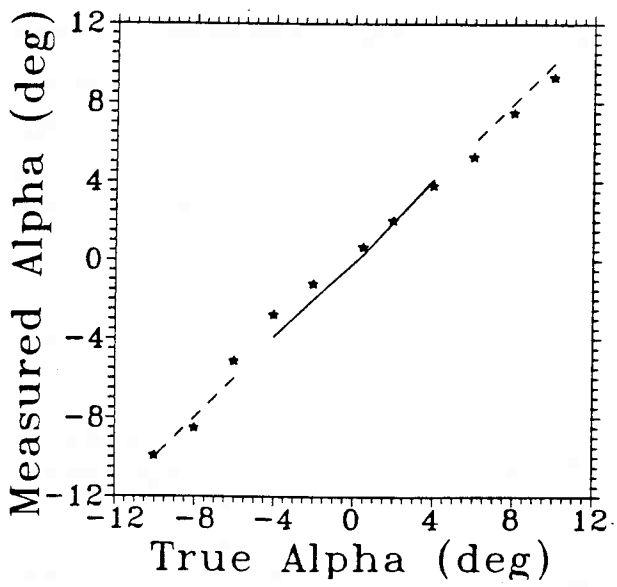

Figure C2: *Angle of attack as set in the wind tunnel by orientation of the pressure sphere, "True Alpha," and as measured by the pressure sphere. Stars are α as computed from (C4), while the solid curve represents a calibration derived from these wind-tunnel measurements. A perfect correspondance between "true" and indicated attack angle is given by the line connecting the two dashed segments.*

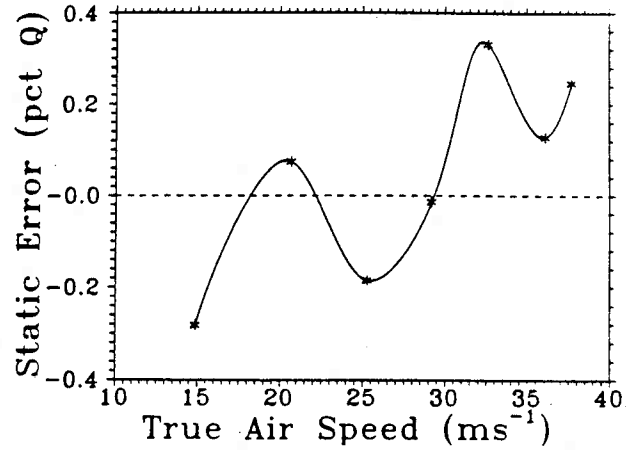

Figure C3: *Error in static pressure determined as the indicated static pressure from the sphere minus the static pressure measured by the pitot probe. The error is less than 0.5%.*

The theoretical value was used for the demonstrations described in this report. No test of cross- dependence between α and β was made.

C.4.2. Static pressure:

Dependence of indicated static pressure on flow speed for zero angle of attack was tested in two runs. In the first, with the static pressure ports at the theoretical 41.81° behind the stagnation point, the error in static pressure increased nearly linearly with q and had a positive offset of about $0.11q$. This error was found by subtracting the static pressure measured on a pitot probe from the indicated static pressure on the sphere, set in the same flow. It was speculated that the downstream rims of the pressure ports on the sphere obstructed the flow slightly, elevating the sensed pressure at these ports and causing the offset for $\alpha = 0$. We compensated by moving the static pressure ports to 45° from the stagnation point, the same as for the ports used to determine α and β. Fig C3 shows the resulting static error at $\alpha = 0$. It has almost been eliminated, being only about 0.3% to 0.4% of q, but a slight nonlinear dependence on q remains in the empirical data, becoming more sensitive to further increase in q as q becomes larger. Adjustment of data from the second run for the plots presented in the

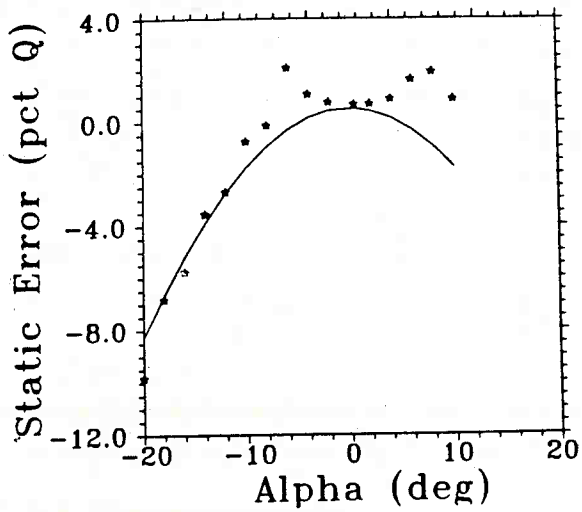

Figure C4: *Error in static pressure as a function of angle of attack. The solid line is the theoretical curve (C13). The "ears" between ±10° have not yet been explained. Pressure ports are actually 45° from the central port, not 41.81° specified by theory. See text.*

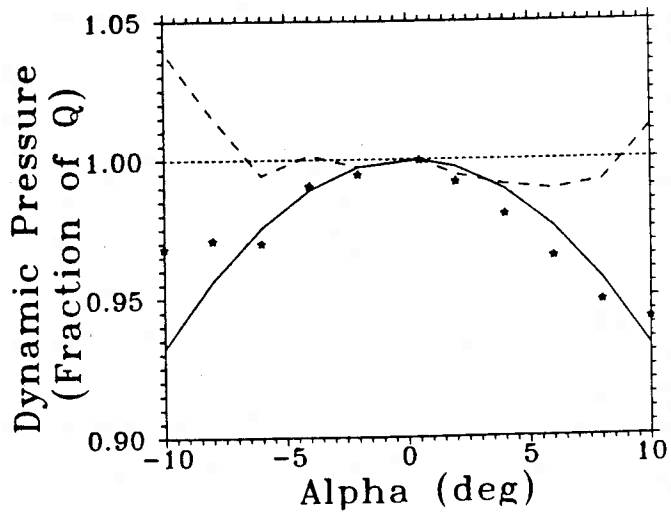

Figure C5: *Indicated dynamic pressure as a function of angle of attack. All quantities are normalized by the true dynamic pressure, which appears as unity on this plot. The solid curve is the theoretical relation (C14). The dashed curve is a correction to the data, based on (C14). Corrected dynamic pressure is held within ±1%.*

remainder of this appendix, assume a static error of $0.005q$.

The *ad hoc* compensation for the non-ideal shape of the pressure ports might unpredictably affect the dependence of indicated static pressure on attack and sideslip angles. The effect was tested by measuring static error as a function of α. Fig C4 shows a remarkably good fit to the theoretical curve beyond $-10°$, and a set of symmetrical "ears" within $10°$ of $\alpha = 0$. The region of the "ears" coincides with that of primary practical interest, and maximum static error of about $0.02q$ is found at about $\pm 6°$. More will be said about this in discussion of the dynamic pressure measurement.

C.4.3. Dynamic pressure:

Fig C5 shows the dependence of the indicated dynamic pressure on α. The data, restricted to the range of interest ($-10° \leq \alpha \leq 10°$), are normalized by the "true" dynamic pressure q, measured by the pitot probe alongside the sphere. A composite of the two runs is shown as the measured dynamic pressure.

The composite is not a direct average because of two conditions: the static error differed in the two runs, as already noted, and the first run had a defect which rendered the data invalid for $\alpha < -2°$. The differing static error in the two runs was adjusted by adding appropriate constants such that the dynamic pressure at $\alpha = 0$ for each run was equal to the "true"

dynamic pressure q. The average of the two runs was then taken for $\alpha \geq -2°$. For negative angles, only data from the second run are plotted.

MacPherson (1985), in a similar test, observed a range $-10° < \alpha < 10°$ where the indicated dynamic pressure was equal to q. He was using the Rosemont commercial probe, having a sphere of 2.54 cm (1") diameter with a central hole of 0.423 cm (1/6"). Such a relatively large central hole covers $\pm 10°$ of arc from the nominal stagnation point, allowing the probe to sense stagnation pressure although the stagnation point departs from its nominal position. The central port of the present probe covers only about $\pm 2°$ from the nominal stagnation point. The result, shown in Fig C5, has the correct dynamic pressure sensed only at $\alpha = 0$. With a coverage of $\pm 2°$, the central port might have a 4° neighborhood about $\alpha = 0$ where the correct dynamic pressure is sensed. The two runs differed on this, however: the first run showing such a region from $-2°$ to $+2°$, the second run not. We conclude that the region probably exists, having width slightly less than 4°, centered on $\alpha = 0$.

A theoretical adjustment for off-angle measurements of the dynamic pressure is readily derived from $(C14)$. The formulas, using small-angle approximations for α and β in radians, are:

$$
\begin{aligned}
q &= p_C - p_\infty \\
q &= \left[1.0 - \frac{1}{3}(0.04 - \sqrt{\alpha^2+\beta^2})\right](p_C - p_\infty) && \sqrt{\alpha^2+\beta^2} \leq 0.04 \\
q &= \frac{4(p_C - p_\infty)}{9(1-\alpha^2)(1-\beta^2) - 5} && 0.04 < \sqrt{\alpha^2+\beta^2} < 0.07 \qquad (C15) \\
& && 0.07 < \sqrt{\alpha^2+\beta^2}.
\end{aligned}
$$

This formulation provides a central region of width 0.08 radians (4.5°) over which the indicated dynamic pressure is not adjusted. Beyond this central region is an intermediate region of linear interpolation between no adjustment and adjustment by $(C14)$. Beyond ± 0.07 radians (4°) adjustment is by $(C14)$. In practice, the central region is so small that ignoring it and the interpolation region to simplify the program logic introduces no significant error. Thus only the third equation of $(C15)$ is actually used. The resulting corrected dynamic pressure measurement is shown in Fig C5. Except on the rarely-encountered negative end of the region of interest, the error in adjusted indicated dynamic pressure remains within $\pm 1\%$.

This remarkably small error is, in fact, less than the 2% reported earlier for the static pressure. The compensation mechanism, partially correcting for the static error in the computed dynamic pressure, has not yet been identified.

C.5. Overall uncertainty in the velocity components

The uncertainty analysis has so far considered error in the indicated dynamic pressure and attack and sideslip angles. This needs to be put in terms of the ultimate output, indicated wind speed and direction. The analysis will ignore error in measurements not covered in section C.3. and C.4., giving only that component of error contributed by the pressure sphere measurements. The result may be less than the total error in the wind measurements, but will indicate the order of magnitude to be expected.

Error in the dynamic pressure and in α and β is first put into terms of error in the relative velocity components u_a, v_a, and w_a of $(C5)$. These errors are then propagated through the transformation to earth coordinates and reference frame (see Appendix A) and scaled by typical magnitudes for horizontal and vertical wind. A convective day is chosen for reference, having horizontal wind speed of 10 ms^{-1} and vertical wind speed of 1 ms^{-1}.

From Section C.4.3., the error in dynamic pressure over the range of interest can be held to within $\pm 1\%$. Therefore, the error in indicated air speed can be estimated from $(C2)$.

$$\begin{aligned} U' &= \sqrt{\frac{2q(1+\epsilon)}{\rho}} \\ &\approx U(1+\frac{1}{2}\epsilon), \end{aligned} \tag{C16}$$

where $\epsilon \leq .01$, giving an error in U of less than about 0.5%.

Error in the relative-velocity components includes error in indicated air speed and in the attack and sideslip angles. From $(C5)$

$$\begin{aligned} u_a &= U(1+\frac{1}{2}\epsilon)cos(\alpha+\delta_\alpha)cos(\beta+\delta_\beta) \\ v_a &= U(1+\frac{1}{2}\epsilon)cos(\alpha+\delta_\alpha)sin(\beta+\delta_\beta) \\ w_a &= U(1+\frac{1}{2}\epsilon)sin(\alpha+\delta_\alpha). \end{aligned} \tag{C17}$$

where ϵ is that in $(C16)$. We may estimate δ_α and δ_β, the error in α and β respectively, by estimating

$$\delta = \frac{1}{2}\left[sin^{-1}(s_I) - sin^{-1}s\right] \tag{C18}$$

where δ is either δ_α or δ_β, and s is either of

$$\begin{aligned} s_\alpha &= sin2\alpha \\ s_\beta &= sin2\beta, \end{aligned} \tag{C19}$$

representing the true angles of attack and sideslip. The s_I is either of

$$\begin{aligned} s_{I\alpha} &= sin[2(\alpha+\delta_\alpha)] \\ s_{I\beta} &= sin[2(\beta+\delta_\beta)] \end{aligned}, \tag{C20}$$

representing the indicated angles of attack and sideslip obtained from adjusted dynamic pressure $(C15)$ and the approximate form $(C3)$ for α and β. We estimate $(C19)$ and $(C20)$ using small-angle approximations in $(C9)$

$$\begin{aligned} s_\alpha &\approx -\frac{4}{9}\frac{\Delta p_\alpha}{q\sqrt{1-\beta^2}} \\ s_\beta &\approx -\frac{4}{9}\frac{\Delta p_\beta}{q(1-\alpha^2)}. \end{aligned} \tag{C21}$$

$$s_{I\alpha} \approx -\frac{4}{9}\frac{\Delta p_\alpha}{q}(1-\epsilon)$$
$$s_{I\beta} \approx -\frac{4}{9}\frac{\Delta p_\beta}{q}(1-\epsilon). \qquad (C22)$$

The ϵ term of $(C22)$ comes from a truncated binomial expansion of $q^{-1}(1+\epsilon)^{-1}$. Further simplification of $(C21)$ retains only terms linear in α^2 and β^2 in binomial expansion:

$$s_\alpha \approx -\frac{4}{9}\frac{\Delta p_\alpha}{q}(1+\frac{1}{2}\beta^2)$$
$$s_\beta \approx -\frac{4}{9}\frac{\Delta p_\beta}{q}(1+\alpha^2). \qquad (C23)$$

The coefficients in $(C21)$ through $(C23)$ are seen from $(C23)$ to be well approximated by

$$\frac{4}{9}\frac{\Delta p_\alpha}{q} \approx -2\alpha$$
$$\frac{4}{9}\frac{\Delta p_\beta}{q} \approx -2\beta \qquad (C24)$$

for α and β smaller than 0.2 radians.

We expand the inverse sine function

$$sin^{-1}(s) = s + \frac{1}{6}s^3 + \ldots. \qquad (C25)$$

to find δ_α and δ_β from $(C18)$, retaining only terms linear in ϵ, α^2, or β^2.

$$\delta_\alpha \approx \frac{4}{9}\frac{\Delta p_\alpha}{q}(\epsilon+\frac{1}{2}\beta^2)$$
$$\delta_\beta \approx \frac{4}{9}\frac{\Delta p_\beta}{q}(\epsilon+\alpha^2).$$

Substituting from $(C24)$

$$\delta_\alpha \approx -\alpha(2\epsilon+\beta^2)$$
$$\delta_\beta \approx -2\beta(\epsilon+\alpha^2) \qquad (C26)$$

Expanding $(C17)$, retaining only linear terms in α, β, δ_α, and δ_β,

$$u_a = U cos\alpha cos\beta(1-\frac{1}{2}\epsilon)$$
$$v_a = U\left[cos\alpha sin\beta\left(1-\frac{1}{2}\epsilon\right)+\delta_\beta cos\alpha\right] \qquad (C27)$$
$$w_a = U\left[sin\alpha\left(1-\frac{1}{2}\epsilon\right)+\delta_\alpha\right].$$

These may be written in the form

$$\mathbf{v_a} = U(\mathbf{v_u} + \mathbf{v}^\star),$$

where

$$\mathbf{v}^\star = \begin{pmatrix} -\frac{1}{2}\epsilon\ cos\alpha cos\beta \\ -\frac{1}{2}\epsilon\ cos\alpha sin\beta + \delta_\beta cos\alpha \\ -\frac{1}{2}\epsilon\ sin\alpha + \delta_\alpha \end{pmatrix}$$

is the vector containing the error terms of $(C27)$. Thus $U\mathbf{v}^\star$ is the error vector in the relative wind $\mathbf{v_a}$, given in probe coordinates.

The important question is the significance of this error to the measurement of wind in earth coordinates and reference frame. We refer for this to (A8) in Appendix A, where the term $\mathcal{A}\mathbf{v}'_\mathbf{p}$ is the relative velocity in earth coordinates, while the rest of the right-hand side is the motion $\mathbf{v_p}$ of the probe in earth coordinates. Equation (A8) for the wind $\mathbf{v}$ is rewritten in the present context as

$$\begin{aligned} \mathbf{v} &= \mathcal{A}\mathbf{v_a} + \mathbf{v_p} \\ &= \mathcal{A}U(\mathbf{v_u} + \mathbf{v}^\star) + \mathbf{v_p}. \end{aligned} \qquad (C28)$$

Matrix $\mathcal{A}$, described in A.2.2., changes only the direction of a vector, not its magnitude. Mathematically, its induced Euclidian norm is unity, as would be expected for a pure rotation of coordinates. In particular, the (Euclidian) magnitude of the error vector $U\mathbf{v}^\star$, denoted $Uv^\star$ and given as the square root of the sum of squares of its components, is unchanged by the rotation.

The error vector will be important according to its relation to the wind vector $\mathbf{v}$. Bounding cases occur when $\mathcal{A}U\mathbf{v}^\star$ is parallel to, and perpendicular to $\mathbf{v}$. In the first case the magnitude of the wind measurement is maximally affected; in the second, the direction. Since $\mathcal{A}U\mathbf{v}^\star$ is in earth coordinates, it will have a horizontal and a vertical component, determined by the pitch angle of the airplane, approximately α. Thus, with subscripts H and V denoting horizontal and vertical,

$$\begin{aligned} v^\star_H &= Uv^\star cos\alpha \\ v^\star_V &= Uv^\star sin\alpha. \end{aligned} \qquad (C29)$$

We assume a convective day with horizontal wind speeds of 10 ms^{-1} and vertical wind speeds of 1 ms^{-1} at the flight altitude of about 150 m above ground (AGL). From Fig C5 we may take $\epsilon = \pm 0.01$. We may estimate δ, assuming the rare, extreme values of $\alpha = \beta = 0.2$ (11.5°). Then $(C26)$ gives

$$\begin{aligned} \delta_\alpha &= -0.012 \ \ (0.7°) \\ \delta_\beta &= -0.02 \ \ (1.2°). \end{aligned}$$

However, even with $\beta = 0$, Fig C2 shows the largest δ_α (at -4°) to be 1.2°. The source of this rather large error between the "true" angle (as set in the wind tunnel) and that given by (C4) has not yet been traced. Using this value as an outer bound for both δ_α and δ_β we find $v^\star = 0.03$ ms^{-1}. If $U = 50$ ms^{-1}, a typical flight speed, then error component $v^\star_H$ is 15% of the magnitude of the horizontal wind, while, with $\alpha = 11.5°$, $v^\star_V$ is 30% of

the vertical. The maximum direction error in reported horizontal wind, with the horizontal error component perpendicular to the true horizontal wind, is $\pm 8.5°$. The errors from the probe-velocity computation must be added to these. Probe-velocity errors have not yet been computed but are probably similar in magnitude to these. The error values given here are outer bounds on error, having been estimated from rare worst cases in theory, field and wind tunnel. They are typically second-order errors, the first-order errors having been removed by averaging over symmetrically placed sensor ports. Thus reducing α and β by a factor of two, to reach more commonly-encountered values, reduces the error by a factor of about four.

REFERENCES

Brown, E. N., C. A. Friehe and D. H. Lenschow, 1983: The use of pressure fluctuations on the nose of an aircraft for measuring air motion. *J. Clim. Appl. Meteor.*, **22**: 171-180.

MacPherson, J. I., 1985: Wind Tunnel Calibration of a PMS Canister Instrumented for Airflow Measurement. Aero. Note **NAE-AN-32**, **NRC** no. **24922**, National Research Council, National Aeronautical Establishment, Ottawa, Canada

Schlichting, H., 1968: *Boundary-Layer Theory*, McGraw-Hill, New York, 747 pp.

APPENDIX D
MOBILE FLUX PLATFORM--KEY ROUTINES FROM FLUX

Table D1

CHANNEL ALLOCATION AND CALIBRATIONS--01-21-1990

OHIO 7-24-89 EPA SPATIAL VARIABILITY STUDY

# Inputs # HI	#LO	Airport Altitude (m)	Airport Pressure (mb)	MagVar (rad)	Vs (mv)
15	8	230	998	2.5 W	12040

Channel P	L	Raw Input Instrument	Scale	Lag	Span	Offset	Min	Max	TND	Note
1	1	Ax (m/s2)	1	0	0.0040	0.00	19.0	-19	1	A
2	2	Ay (m/s2)	1	0	0.0043	0.00	19.0	-19	1	A
3	3	Az (m/s2)	1	0	0.0059	0.00	0.0	0	1	A
4	4	Px (mb)	1	0	39.4900	-3683.00	24.9	-1	0	R
5	5	Py (mb)	1	0	39.5900	-456.00	12.4	-12.4	1	R
6	6	Pz (mb)	1	0	40.0500	36.00	12.4	-12.4	0	R
7	7	Del P (mb)	1	0	39.6800	-176.00	12.4	-12.4	0	R
8	8	T' (K)	20	2	-0.0037	28.20	0.0	0	0	A
9	9	Pitch(rad)	5	0	2.9090	527.00	0.0	0	0	R
10	10	Roll (rad)	5	0	5.9710	653.00	0.0	0	1	R
11	11	YawRt(r/s)	0	0	0.2524	0.00	0.0	0	1	R
12	12	e' (g/m3)	20	1	-0.0024	10.88	0.0	0	1	A
13	13	CO2(mg/m3)	20	4	-0.0435	0.00	0.0	0	1	A
14	14	O3 (ppb)	20	5	0.0300	-10.00	0.0	0	1	A
15	15	CH4(ug/m3)	0	0	1.0000	0.00	0.0	0	1	A
17	16	P Alt (mb)	10	0	0.1339	549.00	0.0	0	0	A
18	17	T-bar (K)	10	0	0.0766	0.32	0.0	0	0	A
19	18	HEAD (rad)	5	0	0.0013	0.00	0.0	0	0	A
20	19	Py(W/m2-s)	1	0	0.2620	0.00	0.0	0	0	A
21	20	Net Rad	1	0	0.2400	0.00	0.0	0	0	A
22	21	IR SFC TEM	1	0	0.0690	0.00	0.0	0	0	A
23	22	IR DET TEM	1	0	-0.0625	-51.61	0.0	0	0	A
24	23	Clino(rad)	7	0	-0.0005	0.00	0.0	0	0	A

NOTES:
1 A-ABSOLUTE CALIBRATION and R-RATIOMETRIC CALIBRATION
2 P Alt must be physical CH-17 and T-bar must be physical CH-18
3 The 1st channel # is the physical channel--the 2nd is the logical channel #

Table D2

STATISTICAL SUMMARY OF FILE--07241057
COLLECTED 07-24-1989 10:57:33 to 11:31:37

DATA STATISTICS #SCANS= 2036 SCAN RATE= 39.84253 Hz

CH	VARIABLE	MEAN	STD DEV	MAX	MIN	TREND	% A/D
1	Ax (m/s2)	-1.99	0.16	-1.08	-2.81	-0.01*	4
2	Ay (m/s2)	-2.11	0.96	1.90	-7.01	-0.19*	21
3	Az (m/s2)	-10.74	1.20	-2.08	-16.82	-1.23*	25
4	Px (mb)	15.29	0.90	18.89	12.25	0.77	20
5	Py (mb)	-0.49	1.08	5.27	-6.03	-0.02*	34
6	Pz (mb)	3.85	0.84	8.31	-0.83	-0.23	27
7	Del P (mb)	-2.53	1.83	2.69	-6.78	-3.78	29
8	T' (K)	27.65	0.39	28.80	26.25	0.70	7
9	Pitch(rad)	0.03	0.02	0.12	-0.09	0.00	8
10	Roll (rad)	0.00	0.05	0.30	-0.22	-0.01*	11
11	YawRt(r/s)	0.00	0.03	0.10	-0.10	0.00*	100
12	e' (g/m3)	18.44	0.62	21.11	15.73	0.27*	22
13	CO2(mg/m3)	622.15	6.61	612.38	584.25	-12.92*	7
14	O3 (ppb)	32.02	3.06	40.76	22.15	7.76*	6
	SLOW RATE DATA						
16	P Alt (mb)	982.74	1.74	987.05	978.23	0.36	1
17	T-bar (K)	27.30	0.45	28.00	25.75	0.51	0
18	HEAD (rad)	1.10	0.82	6.28	0.01	-0.22	50
19	Py(W/m2-s)	634.91	267.28	1044.55	163.75	-159.36	34
20	Net Rad	625.48	49.42	722.46	431.25	25.78	12
21	IR SFC TEM	3.96	3.71	21.23	-4.04	-5.64	4
22	IR DET TEM	28.49	0.66	29.41	26.97	2.70	0
23	Clino(rad)	-0.01	0.01	0.02	-0.04	0.00	1

* TIME TREND REMOVED DURING ANALYSIS

Average probe angle of attack 1.46 (Deg)
Pressure Altitudes= 354 to 394 Wp = 0.02
Average TAS 53.5 (m/s) @ 45 (Deg True)

CORRECTED SENSOR OFFSETS AND CHANGE

Ax(m/s)	Ay(m/s)	Az(m/s)	Py (mb)	Pz (mb)	DelP(mb)	T'(C)	Rol(Deg)
2.24	2.11	10.74	1.99	-1.99	985.85	27.86	
2.24	2.11	10.74	0.49	-1.87	985.27	-0.34	-0.19

LORAN SUMMARY INFORMATION

SCANS= 1346 @ 1.523304 s/scan
START LATITUDE= 39 2.8
START LONGITUDE= 85 36.8
LATITUDE m/deg= 111470.3
PATH LENGTH= 106034 (m)
GROUND SPEED= 51.9 (m/s)
START SNR M243 W198 X230

SYNC ERR = 0
END LATITUDE= 39 42.1
END LONGITUDE= 84 43
LONGITUDE m/deg=-86167.84
AVG Up $ Vp 37.7 35.7
TRUE COURSE= 47
END SNR M245 W162 X233

Table D3

ANALYSIS OF FILE--07241057
COLLECTED 07-24-1989 10:57:33 to 11:31:37

DATA STATISTICS #SCANS= 2036 SCAN RATE= 39.84253 Hz

STATISTICAL ANALYSIS -- EARTH COORDINATES

VARIABLE	MEAN	STD DEV	MIN	MAX	TREND
ALTITUDE(m)	372.707	16.179	354.460	408.773	34.159
Ax (m/s2)	0.009	0.624	0.183	3.374	-0.009
Ay (m/s2)	0.002	0.912	-0.178	4.310	-0.004
Az (m/s2)	9.796	1.148	7.254	18.021	0.014
Up (m/s)	37.681	13.798	37.666	92.055	6.970
Ua (m/s)	-43.630	3.948	0.000	0.000	1.749
Vp (m/s)	35.826	9.762	35.669	66.112	1.876
Va (m/s)	-29.391	6.460	-47.459	-0.343	-6.992
Wp (m/s)	0.026	1.068	-0.064	4.819	0.052
Wa (m/s)	-0.005	1.188	-0.592	5.889	-0.272
ALPHA(deg)	1.466	0.636	-1.949	4.803	0.000
W (m/s)	0.021	0.800	-2.680	3.874	-0.221
U (m/s)	-5.948	13.832	-70.289	47.259	8.715
V (m/s)	6.435	8.589	-24.437	44.864	-5.118
Ta (k)	300.982	0.000	299.424	301.870	0.574
e' (g/m3)	16.568	0.559	14.031	18.992	0.102
O3 (ppb)	25.984	1.703	15.395	32.038	-0.316

	MEAN UP-DRAFT	MEAN DOWN-DRAFT	WS/WD	
velocity (m/s)	0.7000	-0.5723	---	area
(%)	44.9835	55.0165	---	

FINAL Palt 401.3 FINAL Zi 401.9 Pressure 978.6

PATH AVERAGE CO-VARIANCE ANALYSIS

VARIABLE	MEAN	VARIANCE	CO-VAR	FLUX
W'U' (m2/s2)	-0.6974	145.3831	0.2365	0.26
W'V' (m2/s2)	0.9110	66.3529	-0.1859	-0.21
Heat flux (W/m2)	0.0753	0.0402	0.0421	47.05
Latent flux (W/m2)	-0.1013	0.2376	0.1092	295.97
O3 flux (ppm/m2)	-0.0434	1.7599	-0.2226	-0.25

Path Average Density 1.112645 kg/m3
Cd= 0.001 U*= 0.548 m/s Vd=.773352 cm/s

```
*************************************************************************
' *                                                                 1/90   *
' *                                FLUX                                    *
' *          AIRCRAFT EDDY-COVARIANCE FLUX COMPUTATION PROGRAM             *
' *                                                                        *
' *    TIMOTHY L. CRAWFORD, ROBERT T. McMILLEN  and RONALD J. DOBOSY       *
' *                                                                        *
' *             ATMOSPHERIC TURBULENCE AND DIFFUSION DIVISION              *
' *            NATIONAL OCEANIC AND ATMOSPHERIC ADMINISTRATION             *
' *                                                                        *
' *  FILE ALLOCATION                                                       *
' *  #1--ACFILES        LIST OF INFILE$ NAMES TO RUN                       *
' *  #2--setup.sup      INITIAL CALIBRATION SETUP INFORMATION              *
' *  #3--INFILE$.RAW    RTI A-to-D data                                    *
' *  #4--INFILE$.LRN    LORAN POSITION DATA                                *
' *  #5--INFILE$.TND    TREND ANALYSIS INFO                                *
' *  #6--lpt1:/scrn:    GENERAL OUTPUT TO PRINTER OR SCREEN                *
' *  #7--INFILE$.FAO    SLOW ANALYSIS OUTPUT FILE                          *
' *  #8--INFILE$.SAO    FAST ANALYSIS OUTPUT FILE                          *
' *  #9--INFILE$.FFT    OUTPUT FOR FFT ANALYSIS                            *
' *                                                                        *
'*************************************************************************
OPTION BASE 1
TYPE RegTypeX
     ax AS INTEGER: bx AS INTEGER: cx AS INTEGER: dx AS INTEGER
     bp AS INTEGER: si AS INTEGER: di AS INTEGER: flags AS INTEGER
     ds AS INTEGER: es AS INTEGER
END TYPE

DECLARE SUB DETREND ()
DECLARE SUB Response (Ta)
DECLARE SUB SPIKE ()
DECLARE SUB GRAPH (n%, k%, p() AS SINGLE, scal!(), lab$())
DECLARE SUB TEST ()
DECLARE SUB RETRIEVE ()
DECLARE SUB INTERRUPTX (intnum AS INTEGER, in AS RegTypeX, ot AS RegTypeX)
DECLARE SUB DSPMENU ()
DECLARE SUB STATISTICS (jump!)
DECLARE SUB LORAN ()
DECLARE SUB INITIALIZE ()
DECLARE SUB SETUP (infile$)
DECLARE SUB ROTATE (ang!)
DECLARE SUB PROCESS ()
DECLARE SUB SCREEN (jump%)
DECLARE SUB PrcOut (k%)
DECLARE FUNCTION ASIN! (x!)
DECLARE FUNCTION ATN2! (x1!, X2!)
DECLARE FUNCTION DM$ (D!)
DECLARE FUNCTION HMS$ (s!)
DECLARE FUNCTION stddev! (n!, x!, X2!, Xt)
```

```
'DEFINE GLOBAL CALIBRATION FACTORS
CONST Rftr = .0693                      'temp sensor pres rec fact (C/mb)
CONST Kftr = 11.95 / 57.3               'pressure sphere sensitivity factor
CONST SEftr = .0624                     'static error factor

'DEFINE GLOBAL CONSTANTS
CONST RHz = 1 / 39.8                    'Scan rate (s)
CONST nchf% = 15                        'Number of high speed channels
CONST nchs% = 8                         'Number of slow speed channels
CONST nfv% = 8                          'Number of fast variables output
CONST nsv% = 6                          'Number of slow variables output
CONST nch% = nchf + nchs                'Total number of channels
CONST fsr% = 40                         'Fast to slow scan ratio
CONST Siz% = 2 * nchf * fsr             'vf() buffer size
CONST nmf% = 17                         'Length of spike remover (slow scans)
CONST g0 = 9.81                         'Gravitational Acceleration (m/s2)
CONST Rd = 287.04                       'Gas Constant for Dry Air (J/K-kg)
CONST Rdd = 2.8704                      'Gas Constant for Dry Air (mb m3/gm K)
CONST Rv = .00461                       'Gas Constant for H2O Vapor (mb/g/m3-K)
CONST Cp = 1004                         'Specific Heat dry air (J/K-kg)
CONST Cv = 717                          'Specific Heat dry air (J/K-kg)
CONST lam = 1.4                         'Ratio of specific heats
CONST T0 = 273.16
CONST Pi = 3.14159
CONST dr = 180 / Pi                     'Degrees/radian
CONST Gama = .0098                      'Virtual temperature lapse (C/m)
CONST Tv0 = 300                         'move to setup table!!!!!
CONST C0 = Gama * Rd / g0               'Altitude computation constant
CONST C1 = Rd / Cp
CONST C2 = 2 * Cv / Rd
CONST C3 = lam * Rd
CONST AnlSw% = 0                        '0 no analysis; -1 analysis
CONST AnOut% = -1                       '0 no analysis output; -1 output
CONST RotSw% = -1                       '0 no rotation; -1 3D rotation
CONST DelPSw% = -1                      '0-1s;          -1-40Hz Pres sensor
CONST OutDiv$ = "LPT1:"                 'NUL, SCRN: or LPT1:
CONST DISK$ = "D:"                      'Drive to find .RTI and .LRN data
CONST Fh = 6.28 / 45                    'Psi-LOOP mixing frequency (45s)

'DIMENSION GLOBAL VARIABLES
DIM SHARED inary AS RegTypeX, outary AS RegTypeX, stor(Siz + nchs) AS INTEGER
DIM SHARED i3pt AS LONG, ptr AS INTEGER, vf(Siz) AS SINGLE
DIM SHARED infile$, gnit, dsp, ln AS LONG
DIM SHARED idmy AS INTEGER, idmx AS INTEGER, igh AS LONG, H(nmf) AS SINGLE
DIM SHARED dmx AS SINGLE, dmy AS SINGLE, dmz AS SINGLE
DIM SHARED r(32) AS SINGLE, ml(32) AS SINGLE, mt(nch) AS SINGLE, lct AS INTEGER
DIM SHARED sec AS SINGLE, hz AS SINGLE', RHz AS SINGLE
DIM SHARED nscnl AS INTEGER, nscn AS INTEGER, Zr, Pr, MagVar
DIM SHARED s(32) AS SINGLE, B(32) AS SINGLE, bb(32) AS SINGLE, rlb$(32)
```

```
DIM SHARED rscal(32) AS SINGLE, lag(32) AS INTEGER, mxr(32), mnr(32)
DIM SHARED lat AS SINGLE, lon AS SINGLE, tn, tinc, Yerr, Xerr, clat, clon
DIM SHARED PosSW, Yr, XerrB, YerrB
DIM SHARED fcdat AS STRING * 10, dstim AS SINGLE, detim AS SINGLE
DIM SHARED fadat AS STRING * 10, astim AS SINGLE, Wpp
DIM SHARED Q, Ps, Palt, alpha, Xi, Yi, Zi, Ua, Va, Wa, Up, Vp, Wp, U, V, W, Psi
DIM SHARED C3Xx, C3Yx, C3Zx, C3Hx, Zx, Hx                          'FILTER
DIM SHARED flab$(8), cov(8), cov2(8), avg(8), var(8), jscn, ftr(8), RhoA
DIM SHARED x(8), Xlb$(8), Xscal(8), Xrm(8)
DIM SHARED WS, nspike AS INTEGER, nfail AS INTEGER, isquash AS INTEGER
DIM SHARED Ta, Ta0, Timm, Tim, Ti0                                 'RESPONSE
DIM SHARED TND(nch) AS INTEGER
PosSW = -1                                  '0 or -1 Position computation
VIEW PRINT 1 TO 20
CLS
ON KEY(1) GOSUB DISPLAY
KEY(1) ON
dsp = 1                                     'Starting dislpay
OPEN "i", 1, "A:ACFILES"                    'List of files to run
restart:
CLOSE #2, #3, #4, #5, #6, #7, #8, #9
SCREEN (0)
INPUT #1, infile$                           'Get file name to run
infile$ = LEFT$(infile$, 8)
SETUP (LEFT$(infile$, 4) + ".sup")          'Read setup information
OPEN "b", 3, DISK$ + infile$ + ".RTI"       'RTI A to D DATA
OPEN "b", 4, DISK$ + infile$ + ".LRN"       'LORAN DATA
'OPEN "O", 9, "\grapher\TEMP.dat"           'ANALYSIS OUTPUT
'OPEN "O", 9, "fftfile"                     'ANALYSIS OUTPUT"
IF AnOut THEN PrcOut (0)
INITIALIZE
IF NOT AnlSw THEN GOTO restart
IF nscn < 100 OR hz = 0 THEN GOTO restart
SCREEN (-dsp)
FOR i = 1 TO nscn - 1
    sec = dstim + fsr * i * RHz
    RETRIEVE                                   'retrieves data
    IF PosSW THEN SPIKE                     'despike compass data
    DETREND                                 'remove time trends
    FOR j = 1 TO fsr
        jscn = j
        PROCESS                             'Process one scan of data
        IF AnOut THEN PrcOut (-1)           'Write reduced output files
        IF tn < sec AND nscnl >= lct THEN LORAN
        IF dsp = 2 THEN SCREEN (2)
        IF dsp = 3 THEN CALL GRAPH(8, 0, r(), rscal(), rlb$())
        IF dsp = 4 THEN CALL GRAPH(8, 8, r(), rscal(), rlb$())
        IF dsp = 5 THEN CALL GRAPH(8, 16, r(), rscal(), rlb$())
        IF dsp = 6 THEN CALL GRAPH(8, 0, x(), Xscal(), Xlb$())
```

```
        IF dsp > 6 THEN TEST
    NEXT j
IF dsp = 1 THEN
        PRINT USING "\        \"; HMS$(sec); DM$(Yi); DM$(Xi);
        PRINT USING " #######"; CINT(Zi); CINT(Psi * dr);
        PRINT USING " #####.#"; U; V; W
    END IF
NEXT i
STATISTICS (3)                                  'sum statistical summary
IF AnOut THEN PrcOut (1)
PRINT #6,
PRINT #6, USING "FINAL Palt####.#   FINAL Zi####.# Pressure ####.#"; Palt; Zi;
Ps
PRINT #6,
PRINT #6,
PRINT #6, TAB(20); "PATH AVERAGE CO-VARIANCE ANALYSIS"
PRINT #6,
PRINT #6, "       VARIABLE"; TAB(25); " MEAN     VARIANCE     CO-VAR     FLUX";
PRINT #6, "  FLUX COV %"
RhoA = RhoA / (nscn - 1) / fsr
FOR i = 2 TO 8
    avg(i) = avg(i) / (nscn - 1) / fsr
    var(i) = var(i) / (nscn - 1) / fsr
    cov(i) = cov(i) / (nscn - 1) / fsr
    cov2(i) = cov2(i) / (nscn - 1) / fsr
    dmx = 100 * SQR(cov2(i) - cov(i) ^ 2) / cov(i)
    PRINT #6, USING "& "; flab$(i);
    PRINT #6, USING "#####.#### "; avg(i); var(i); cov(i);
    PRINT #6, USING "######.## "; RhoA * ftr(i) * cov(i); dmx
NEXT i
PRINT #6,
PRINT #6, "Path Average Density"; RhoA; " kg/m3"
IF PosSW THEN
    tau = RhoA * SQR(cov(2) ^ 2 + cov(3) ^ 2)
    Cd = tau / (RhoA * WS ^ 2): ustar = SQR(tau / RhoA)
    PRINT #6,
    PRINT #6, USING "Cd=###.###  U*=###.### m/s"; Cd; ustar;
END IF
PRINT #6, "   Vd="; 100 * RhoA * cov(7) / ml(14); " cm/s"
PRINT #6,
PRINT #6, "Ending Inertial Conditions"
PRINT #6, "   Palt     Zi     err"; : IF NOT PosSW THEN PRINT #6,
IF PosSW THEN PRINT #6, "       Xerr     Yerr"
PRINT #6, USING " ######.#"; Palt; Zi; Zi - Palt; XerrB / nscnl; Yerr / nscnl
PRINT #6, "Spikes removed "; nspike; "  Unremovable spikes "; nfail
PRINT #6, " Path mean HEADING substituted "; isquash; " times."
dmy = TIMER - astim: PRINT #6, "   Analysis time-"; dmy; " or ";
PRINT #6, dmy / (detim - dstim); "time real time"
END
```

```
SUB SETUP (infile$)
' ************************************************************************
' * PURPOSE:                                                             *
' *      TO READ INSTRUMENT CHANNEL ALLOCATION AND CALIBRATIONS          *
' *                                                                      *
' * INPUT:                                                               *
' *      nchf  -number of fast channels     nsch -number of slow channels *
' *      Zr    -airport altitude (m-msl)    Pr   -airport preSsure (mb)   *
' *      MagVar-Magnetic variance (Deg)     vs   -Excitation voltage (mv) *
' *      lab$  -label for variable r(i)     rscal-scale for screen plot   *
' *      s(i)  -sensor sensitivity          bb(i)-sensor intercept        *
' *      mnr(i)-sensor under-range limit    mxr()-sensor over range limit *
' *                                                                      *
' ************************************************************************
'
CONST Vscale = 10000 / 4096   'RTI A-to-D scale factor (mv/count)
STATIC oinfile$

'READ CHANNEL ALLOCATION AND CALIBRATION
OPEN "i", #2, "A:" + infile$
PRINT #6, TAB(15); "CHANNEL ALLOCATION AND CALIBRATIONS--"; DATE$
PRINT #6,
LINE INPUT #2, A$: PRINT #6, A$
LINE INPUT #2, A$: PRINT #6, A$
LINE INPUT #2, A$: PRINT #6, A$
INPUT #2, idmy, idmx, Zr, Pr, MagVar, MV$, vs
IF idmy <> nchf THEN PRINT "setup error nchf="; idmy: STOP
IF idmx <> nchs THEN PRINT "setup error nchs="; idmx: STOP
IF MV$ <> "E" AND MV$ <> "W" THEN PRINT "setup err E/W="; MV$: STOP
A$ = "      ###   ###     #####          ######        ###.# &      #####"
PRINT #6, USING A$; nchf; nchs; Zr; Pr; MagVar; MV$; vs
MagVar = MagVar / dr: IF MV$ = "W" THEN MagVar = -MagVar
LINE INPUT #2, A$: PRINT #6, A$
LINE INPUT #2, A$: PRINT #6, A$
LINE INPUT #2, A$: PRINT #6, A$
A$ = "## ##   &    ###   ##  ###.####  #####.## ###.#  ###.# ## &"
FOR i = 1 TO nch
  INPUT #2, dmx, dmy, rlb$(i), rscal(i), lag(i), s(i), bb(i), mnr(i)
  INPUT #2, mxr(i), TND(i), c$: TND(i) = -TND(i)
  PRINT #6, USING A$; dmx; dmy; rlb$(i); rscal(i); lag(i); s(i); bb(i); mxr(i);
  PRINT #6, mnr(i); -TND(i); c$
  IF dmy <> i THEN PRINT "LOGICAL CHANNEL ERROR": STOP
  IF lag(i) > fsr THEN PRINT "ERROR---lag>fsr": STOP
  IF c$ = "R" THEN                        'for ratiometric calibrations
     s(i) = s(i) / vs
     bb(i) = -bb(i) * s(i)
  END IF
   s(i) = s(i) * Vscale                   'RTI-100 A-to-D sensitivity factor
   B(i) = bb(i)
```

```
   lag(i) = nchf * lag(i)
   rscal(i) = .02 * rscal(i) / s(i)
NEXT i
WHILE NOT EOF(2)
    LINE INPUT #2, A$: PRINT #6, A$
WEND
oinfile$ = infile$
CLOSE #2, #6
IF OutDiv = "NUL" OR OutDiv = "SCRN:" OR OutDiv = "LPT1:" THEN
    OPEN "O", #6, OutDiv$
ELSE
    OPEN "A", #6, OutDiv$
END IF
END SUB
```

```
SUB INITIALIZE
'
' ************************************************************************
' *                                                                      *
' * PURPOSE:                                                             *
' *     INITIALIZE FOR AIRCRAFT DATA PROCESSING REMOVING SENSOR OFFSETS  *
' *                                                                      *
' * INPUT File #3--INFILE$.RAW:                                          *
' *    fcdat - file creation date                                        *
' *    dstim - data start time (sec from midnight)                      *
' *    detim - data end time (sec from midnight)                         *
' *    nchf  - number of channels on fast scan rate                      *
' *    nchs  - number of channels on slow scan rate                      *
' *    nscn  - # high rate scans                                         *
' *    fsr   - fast to slow scan ratio                                   *
' *    Hz    - RTI board scan rate (scans/sec)                           *
' *    nscn  - number of fsr scans                                       *
' *    m1-m2 - data set 1'st through 2'nd moments (local)                *
' *    mt    - data time trend                                           *
' *    mx-mn - data set maximum and minimum values                       *
' * OUTPUT:                                                              *
' *    fadat - file analysis date                                        *
' *    astim - analysis start time (sec past midnight)                   *
' *    b(i)  - adjusted offsets                                          *
' *    sec   - initialized start sec - sec past midnight                *
' *                                                                      *
' ************************************************************************

DIM m2(nch) AS SINGLE, mx(nch) AS INTEGER, mn(nch) AS INTEGER
DIM sother AS STRING * 104, eother AS STRING * 104
DIM nse AS INTEGER

'*** READ SETUP FOR RTI FAST/SLOW OUTPUT FILE ***
fadat = DATE$                          'analysis date
astim = TIMER                          'analysis time
GET #3, , fcdat                        'file creation date
GET #3, , dstim                        'file creation time
GET #3, , detim                        'file close time
GET #3, , idmy                         'number of Ch @ fast scan rate
A$ = "SETUP--CHANNEL INPUT ERROR"
IF idmy <> nchf THEN PRINT A$: STOP
GET #3, , idmy                         'number of Ch @ slow scan rate
IF idmy <> nchs THEN PRINT A$: STOP
GET #3, , idmy                         'fast to slow Ch scan ratio
IF fsr <> idmy THEN PRINT A$: STOP
GET #3, , nscn                         'number of complete fsr scans(LOC=27)
FOR i = 1 TO nch                       'read mean's and std.dev.'s
    GET #3, , m1(i)                    ' 1'st moment
    GET #3, , m2(i)                    ' 2'nd moment
```

```
    GET #3, , mn(i)                          ' maximum
    GET #3, , mx(i)                          ' minimum
    GET #3, , mt(i)                          ' time trend
NEXT i

'PRINT FILE STATISTICS
dt = detim - dstim: hz = 0
IF dt * fsr = 0 THEN EXIT SUB
hz = nscn / dt * fsr
IF ABS(1! / hz - RHz) > .002 THEN STOP
PRINT #6, CHR$(12)
PRINT #6, TAB(20); "STATISTICAL SUMMARY OF FILE--"; infile$;
PRINT #6,
PRINT #6, "  COLLECTED "; fcdat; " "; HMS$(dstim); " to "; HMS$(detim);
PRINT #6, "     ANALYSIS "; fadat; " "; HMS$(astim)
PRINT #6,
PRINT #6, TAB(14); "DATA STATISTICS    #SCANS="; nscn; " SCAN RATE="; hz;
PRINT #6, "Hz"
PRINT #6,
PRINT #6, "CH    VARIABLE      MEAN    STD DEV    MAX      MIN    TREND   % A/D"
ln = fsr: ln = ln * nscn + 1
FOR i = 1 TO nch
IF i = nchf + 1 THEN PRINT #6, : PRINT #6, TAB(25); "SLOW RATE DATA"
    dmx = m2(i) - m1(i) ^ 2
    IF i <= nchf THEN
        mt(i) = s(i) * (12 * mt(i) - 6 * ln * m1(i)) / (RHz * (ln - 2) * ln)
    ELSE
        ln = nscn + 1
        mt(i) = s(i) * (12 * mt(i) - 6 * ln * m1(i)) / ((ln - 2) * ln)
    END IF
    m1(i) = s(i) * m1(i) + B(i)
    IF dmx > 0 THEN dmx = SQR(dmx) ELSE dmx = 0
    dmx = ABS(s(i)) * dmx
    dmy = s(i) * mn(i) + B(i)
    dmz = s(i) * mx(i) + B(i)
    IF s(i) < 0 THEN SWAP dmz, dmy
    PRINT #6, USING "##  \        \"; i; rlb$(i);
    PRINT #6, USING " #####.##"; m1(i); dmx; dmz; dmy; mt(i) * nscn;
    c$ = " ": IF TND(i) THEN c$ = "*"
    PRINT #6, USING "&  ###"; c$; (mx(i) - mn(i)) / 40.96;
    A$ = ""
    IF i = 4 THEN
        IF m1(4) < 3 THEN A$ = " STATIC TEST"
        IF mt(4) > 8 THEN A$ = " TAKE OFF"
    END IF
    IF mx(i) >= 2047 THEN A$ = " OVER RANGE"
    IF mn(i) <= -2047 THEN A$ = " UNDER RANGE"
    IF mxr(i) <> 0 AND dmz > mxr(i) THEN A$ = " OVER RANGE"
    IF mnr(i) <> 0 AND dmy < mnr(i) THEN A$ = " UNDER RANGE"
```

```
    PRINT #6, A$
NEXT i
PRINT #6, "* TIME TREND REMOVED DURING ANALYSIS"
'ADJUST CALIBRATION OFFSETS BASED ON MEAN VALUE
B(1) = bb(1) - ml(1) + g0 * SIN(ml(9))        'remove mean Ax acceleration
B(2) = bb(2) - ml(2)                          'remove mean Ay acceleration
B(3) = bb(3) - ml(3) + g0 * COS(ml(9))        'remove mean Az acceleration
B(5) = bb(5) - ml(5)                          'Py correction
B(7) = bb(7) - ml(7) + ml(nchf + 1)           'Del P Correction (mb)
B(8) = bb(8) - ml(8) + ml(nchf + 2) + T0      'correction to T' sensor
B(10) = bb(10) - ml(10)                       'remove mean roll
B(11) = bb(11) - ml(11)                       'remove mean turn rate (rad/s)
s(14) = .00175 * ml(nchf + 2) - .02           'adjust O3 s() for temperature
s(14) = s(14) * 10000 / 4096

'COMPUTE MEAN TRAVERSE Wp BASED ON FIRST and LAST SCAN and b(6) CORRECTION
IF DelPSw THEN                                'using DelP +Palt sensor
    GET #3, 506, idmy                         'starting Q
    dmy = SEftr * (s(4) * idmy + B(4))        'starting Q correction to Ps
    GET #3, , idmy                            'starting Py
    dmy = dmy - .099 * ABS(s(5) * idmy + B(5))  'Py correction to Ps
    GET #3, , idmy                            'starting Py
    dmy = dmy + .054 * ABS(s(6) * idmy + B(6))  'Pz correction to Ps
    GET #3, , idmy                            'starting pressure altitude
    Ps = s(7) * idmy + B(7) - dmy             'starting corrected Ps
ELSE
    dmy = B(nchf + 1) - SEftr * ml(4)         'using Palt sensor
    GET #3, 500 + Siz, idmy                   'Starting Palt
    Ps = s(nchf + 1) * idmy + dmy
END IF
ln = LOF(3) - Siz - 4 * nchs + 1
GET #3, ln, idmy                              'Get Ending Palt
dmx = SEftr * ml(4) + .054 * ABS(ml(6))       'mean static error
Psend = s(nchf + 1) * idmy - dmx + B(nchf + 1)  'ending Ps
Palt = 30612 * (1 - (Ps / Pr) ^ C0) + Zr      'starting pressure alt
Zi = 30612 * (1 - (Psend / Pr) ^ C0) + Zr     'ending pressure alt
Wp = (Zi - Palt) / dt                         'path avg Wp
Q = ml(4) + dmx                               'Mean Dynamic Pressure (mb)
Ps = ml(nchf + 1) - dmx                       'Mean static pressure (mb)
dmy = C2 * ((1 + Q / Ps) ^ C1 - 1)            'Mean Mach number^2 (m/s)
Ta = ml(nchf + 2) - Rftr * Q + 273.12         'Ambient temp  (K)
Tas = 99                                      'Mean True Air Speed (m/s)
IF dmy > 0 THEN Tas = SQR(C3 * Ta * dmy)
dmy = Q / Kftr * (ml(9) - Wp / Tas)           'alpha=theta-Wp/TAS
B(6) = bb(6) - ml(6) + dmy

PRINT #6,
PRINT #6, USING "Average probe angle of attack##.## (Deg)"; ml(9) * dr
PRINT #6, USING "Pressure Altitudes= #### to ####  Wp = #.## "; Palt; Zi; Wp
```

```
PRINT #6, USING "Average TAS ###.# (m/s) @ ### (Deg True)"; Tas; ml(18) * dr
A$ = "#####.## "
PRINT #6, : PRINT #6,
PRINT #6, TAB(18); "CORRECTED SENSOR OFFSETS  AND CHANGE": PRINT #6,
PRINT #6, "   Ax(m/s)   Ay(m/s)   Az(m/s)   Py (mb)   Pz (mb) DelP(mb)   T' (C)
Rol(Deg)"
PRINT #6, USING A$; B(1); B(2); B(3) - g0; B(5); B(6); B(7); B(8) - T0
PRINT #6, USING A$; B(1) - bb(1); B(2) - bb(2); B(3) - bb(3) - g0; B(5) - bb(5);
PRINT #6, USING A$; B(6) - bb(6); B(7) - bb(7); B(8) - bb(8) - T0;
PRINT #6, USING A$; (B(10) - bb(10)) * dr

'INITIALIZE THE SPIKE REMOVER
nspike = 0: nfail = 0: isquash = 0
igh = 500 + Siz + 4
FOR ih = 1 TO (nmf + 1) / 2
  GET #3, igh, idmy
  H(ih + (nmf - 1) / 2) = s(18) * idmy + B(18)
  igh = igh + Siz + nchs * 2
NEXT ih
FOR ih = 1 TO (nmf - 1) / 2
  H(ih) = H((nmf + 1) / 2)
NEXT ih

'READ LORAN INITIAL FILE INFO
lct = 0
GET #4, , fcdat                        'file date                LOC 1-10
GET #4, , dmy                          'file start time          LOC 11-14
GET #4, , dmx                          'close time               LOC 15-18
GET #4, , nscnl                        'number of scans          LOC 19-20
GET #4, , nse                          '# loran sync errors      LOC 21-22
GET #4, , sother                       'starting receiver info   LOC 23-126
GET #4, , eother                       'ending receiver info     LOC 127-230
Yerr = 0: Xerr = 0: XerrB = 0: YerrB = 0
IF nscnl = 0 THEN
    nscnl = 1
    PRINT #6, : PRINT #6, TAB(20); "NO LORAN DATA"
    tn = 99999: Yi = 0: Xi = 0
    clat = 1: clon = 1
    GOTO skip
END IF
'INITIALIZE clat, clon, Up, Vp and gs
GET #4, , lat                          'read starting latitude   LOC 231-234
GET #4, , lon                          'read starting longitude  LOC 235-238
Yi = lat: Xi = lon                     'initial Aircraft position
ldt = dmx - dmy                        'time duration of loran file
idmy = LOC(4)
IF nscnl < (LOF(4) - 238) / 8 + .5 THEN STOP'LORAN nscnl error
nscnl = nscnl - 1
GET #4, LOF(4) - 7, late                    'ending latitude (deg)
```

```
GET #4, , lone: SEEK 4, idmy + 1                    'ending longitude (deg)
tinc = ldt / nscnl                                  'sec between lat/lon obs
dmx = (lat + late) / (2 * dr)                       'mean latitude (rad)
dmz = SQR(1 - .00669566# * SIN(dmx) ^ 2)
clat = 111320 / dmz                                 'latitude m/deg
clon = -clat * COS(dmx)                             'longitude m/deg (W is neg)
Vp = (late - lat) * clat / ldt                      'mean N aircraft velocity(m/s)
Up = (lone - lon) * clon / ldt                      'mean E aircraft velocity (m/s)
GS = SQR(Up * Up + Vp * Vp)                         'mean ground speed (m/s)
TC = Pi / 2 - ATN2(Up, Vp)                          'True Course
U = Tas * COS(Pi / 2 - ml(18) + MagVar) - Up        'E-W wind
V = Tas * SIN(Pi / 2 - ml(18) + MagVar) - Vp        'N-S wind
WS = SQR(U ^ 2 + V ^ 2)
WD = 270 - dr * ATN2(U, V): IF WD < 0 THEN WD = WD + 360

PRINT #6, : PRINT #6, TAB(25); "LORAN SUMMARY INFORMATION   "
PRINT #6, "SCANS=";nscnl; " @"; tinc; "s/scan "; TAB(40); "SYNC ERR = "; nse; ""
PRINT #6, "START LATITUDE="; DM$(lat); TAB(40); "END LATITUDE="; DM$(late)
PRINT #6, "START LONGITUDE="; DM$(lon); TAB(40); "END LONGITUDE="; DM$(lone)
PRINT #6, "LATITUDE meters/deg="; clat; TAB(40); "LONGITUDE meters/deg="; clon
PRINT #6, "PATH LENGTH="; INT(GS * dt); "(m)"; TAB(40);
PRINT #6, USING "AVG Up $ Vp ####.# ####.#"; Up; Vp
PRINT #6, USING "GROUND SPEED= ###.# (m/s)"; GS;
PRINT #6, TAB(40); "TRUE COURSE="; CINT(TC * dr)
PRINT #6, "START SNR " + MID$(sother, 4, 14); TAB(40);
PRINT #6, "END SNR " + MID$(eother, 4, 14)
PRINT #6,
PRINT #6, USING "PATH AVERAGE WIND ###.# m/s   at  #### Deg's"; WS; WD
skip:
IF NOT AnlSw OR nscn < 100 THEN EXIT SUB
PRINT #6, CHR$(12)
PRINT #6, TAB(25); "ANALYSIS OF FILE--"; infile$;
PRINT #6,
PRINT #6, "  COLLECTED "; fcdat; " "; HMS$(dstim); " to "; HMS$(detim);
PRINT #6, "     ANALYSIS "; fadat; " "; HMS$(astim)
PRINT #6,
PRINT #6, TAB(14); "DATA STATISTICS   #SCANS="; nscn; " SCAN RATE="; hz;
PRINT #6, "Hz"
PRINT #6,

'ADJUST b() to ALLOW FOR TIME TREND REMOVAL
FOR i = 1 TO nch
    IF TND(i) THEN B(i) = B(i) + nscn * mt(i) / 2
NEXT i

'FILL STOR BUFFER WITH FIRST SCAN's
SEEK 3, 500                                         'Move to start of data
inary.ds = VARSEG(stor(1))                          'Define data segment
inary.dx = VARPTR(stor(1))                          'Define buffer offset
```

```
inary.bx = FILEATTR(3, 2)                    'Define File Handle for #3
inary.ax = &H3F00                            'Select read interrupt service
inary.cx = Siz + 2 * nchs                    'Number of bytes to read
ptr = Siz / 2                                'set pointer
RETRIEVE                                     'get data
i3pt = 500 + outary.ax
ptr = 0                                      'reset pointer

'Initialize other third order loop constants
Zi = Palt: Wp = 0: Wpp = 0
Psi = r(18)
Yr = 3 * Fh * Psi: Zx = 0: Hx = 0
C3Xx = 0: C3Yx = 0: C3Zx = 0: C3Hx = 0
'Initialize covariance variables
RhoA = 0
ftr(1) = 1: flab$(1) = "W'W' (m2/s2)          "
ftr(2) = 1: flab$(2) = "W'U' (m2/s2)          "
ftr(3) = 1: flab$(3) = "W'V' (m2/s2)          "
ftr(4) = Cp: flab$(4) = "Heat flux (W/m2)     "
dmy = (597.3 - .564 * ml(17)) * 4.1876
ftr(5) = dmy: flab$(5) = "Latent flux (W/m2)  "
ftr(6) = 1: flab$(6) = "CO2 Flux (mg/m2)      "
ftr(7) = 1: flab$(7) = "O3 flux (ppm/m2)      "
ftr(8) = 1: flab$(8) = "CH4 flux (ppm/m2)     "
FOR i = 1 TO 8
    avg(i) = 0:  var(i) = 0
    cov(i) = 0:  cov2(i) = 0
NEXT i
'DEFINE SCALE AND LABELS FOR GRAPHIC DISPLAY OF COMPUTED X() VARIABLES
Xscal(1) = 5: Xscal(2) = 1: Xscal(3) = 1: Xscal(4) = 30:
Xscal(5) = 10: Xscal(6) = 5: Xscal(7) = 5: Xscal(8) = 0:
Xlb$(1) = "W   (m/s)": Xlb$(2) = "U   (m/s)": Xlb$(3) = "V   (m/s)"
Xlb$(4) = "Ta   (k)": Xlb$(5) = rlb$(12): Xlb$(6) = rlb$(13)
Xlb$(7) = rlb$(14): Xlb$(8) = rlb$(15)
'INITIALIZE RUNNING MEANS with first second of data
Xrm(1) = 0: Xrm(2) = U: Xrm(3) = V: Xrm(4) = 0
FOR i = 5 TO 8
    Xrm(i) = 0
    FOR j = 0 TO fsr - 1
        IF i = 5 THEN Xrm(4) = Xrm(4) + vf(8 + nchf * j)
        Xrm(i) = Xrm(i) + vf(7 + i + nchf * j)
    NEXT j
    Xrm(i) = Xrm(i) / fsr
NEXT i
Ta = Xrm(4) / fsr - ml(4) * Rftr
E = Rv * Xrm(5) * Ta                         'Water vapor pressure (mb)
RhoD = (Ps - E) / (Rdd * Ta)                 'Density of dry air (kg/m3)
Xrm(4) = Ta * (1000 / Ps) ^ C1               'Pot Temp (K)    c1=Rd/Cpd
Xrm(6) = Xrm(6) / RhoD: Xrm(7) = Xrm(7) / RhoD
```

```
Xrm(7) = Xrm(7) / RhoD

'Initialize temperature sensor response variables
Ta0 = Ta: Tap = Ta: Timm = Ta: Tim = Ta: Ti0 = Ta
CALL STATISTICS(1)
END SUB
```

```
SUB PROCESS STATIC
' ***********************************************************************
' *                                                                     *
' * PURPOSE:                                                            *
' * PROCESS HIGH SPEED DATA PRODUCING VELOCITY AND SPECIES CONCENTRATIONS *
' *                                                                     *
' * INPUT: r() as defined by setup table                                *
' *                                                                     *
' * COMPUTED:                                                           *
' * X(1)  - W' (m/s)                    X(2)  - U' (m/s)                *
' * X(3)  - V' (m/s)                    X(4)  - T' (pot temp K)         *
' * X(5)  - e' (g H2O/kg dry air)       X(6)  - CO2 mix ratio           *
' * X(7)  - O3 mix ratio                X(8)  - CH4 (ug/kg dry air)     *
' *                                                                     *
' * NOTES:                                                              *
' * Both aircraft and earth coordinate systems are right handed systems. *
' * Phi, theta & psi are positive to left, nose up and with compass.    *
' * Computed velocities are U (+ to east), V (+ to north) and W (+ up). *
' * Species fluctuations are corrected for temperature and moisture.    *
' ***********************************************************************
'DEFINE Mixing frequencies
CONST Fx = 6.28 / 45                        'X-mix freq = 45s
CONST Fy = 6.28 / 45                        'Y-mix freq = 45s
CONST Fz = 6.28 / 30                        'Z-mix freq = 30s

'DEFINE CONSTANTS--Third Order Blanchard System with three equal roots
CONST C1x = 3 * Fx: CONST C2x = 3 * Fx * Fx: CONST C3x = Fx * Fx * Fx
CONST C1y = 3 * Fy: CONST C2y = 3 * Fy * Fy: CONST C3y = Fy * Fy * Fy
CONST C1z = 3 * Fx: CONST C2z = 3 * Fz * Fz: CONST C3z = Fz * Fz * Fz
CONST C1h = 3 * Fh: CONST C2h = 3 * Fh * Fh: CONST C3h = Fh * Fh * Fh
CONST rm1 = .99975: CONST rm2 = 1 - rm1

'PROCESS ONE FAST SCAN OF DATA
FOR i = 1 TO nchf
idmy = i + ptr + lag(i)
IF idmy > Siz THEN idmy = idmy - Siz
r(i) = vf(idmy)
NEXT i
ptr = ptr + nchf
sec = sec + RHz

'FFT output
'iF kk < 9000 THEN
'    FOR i = 1 TO 8
'        PRINT #9, x(i);
'    NEXT i
'    PRINT #9,
'    kk = kk + 1
'END IF
```

```
'COMPUTE PRESSURE SPHERE STAGNATION, DYNAMIC PRESSURE AND PRESSURE ANGLES
dmy = SEftr * r(4)                          'position error correction (mb)
IF DelPSw THEN
    Ps = r(7) - dmy                         'corrected static pressure (mb)
ELSE
    Ps = r(nchf + 1) - dmy                  'corrected static pressure (mb)
END IF
Q = r(4) + dmy                              'corrected pitot pressure  (mb)
dmy = Kftr / Q
alpha = dmy * r(6)                          'airstream vert attack angle (rad)
beta = dmy * r(5)                           'airstream hor attack angle (rad)

'COMPUTE POTENTIAL TEMP/DENSITY,AND PRESSURE ALTITUDE
Palt = Tv0 / Gama * (1 - (Ps / Pr) ^ C0) + Zr 'Haltiner & Martin EQ 4-10
Ta = r(8) - Rftr * Q                        'Temperature (K)
CALL Response(Ta)                           'Adjust for time response
x(4) = Ta * (1000 / Ps) ^ C1                'Pot Temp (K)    c1=Rd/Cpd
E = Rv * r(12) * Ta                         'Water vapor pressure (mb)
RhoD = (Ps - E) / (Rdd * Ta)                'Density of dry air (kg/m3)
RhoA = RhoA + RhoD                          'Avg dry air density (kg/m3)
x(5) = r(12) / RhoD                         'H2O mixing ratio, g H2O/kg dry air
x(6) = r(13) / RhoD                         'CO2 mixing ratio,mg H2O/kg dry air
x(7) = r(14) / RhoD                         'O3 mixing ratio
x(8) = r(15) / RhoD                         'CH4 mixing ratio

'COMPUTE VELOCITY RELATIVE TO AIRCRAFT
dmy = C2 * ((1 + Q / Ps) ^ C1 - 1)          'Mach number^2 (m/s)
IF dmy < 0 THEN dmy = 0
Tas = SQR(C3 * Ta * dmy)                    'Aircraft Vel (m/s)
dmy = TAN(alpha)
dmx = TAN(beta)
Ua = -Tas / SQR(1 + dmy * dmy + dmx * dmx)
Va = Ua * dmx
Wa = -Ua * dmy

'ROTATE ACCELEROMETERS AND VELOCITIES TO EARTH COORDINATES
IF RotSw THEN
     ROTATE (r(10))                         '2-D rotation to remove roll
     ROTATE (r(9))                          '2-D rotation to remove pitch
     ROTATE (Psi - 1.5708 + MagVar)         '2-D rotation to east
ELSE
Wa = Ua * SIN(r(9) - alpha)
END IF

'COMPUTE AIRCRAFT VELOCITY CORRECTING WITH ALT & LORAN POSITION FEEDBACK
'USING THE BLANCHARD, 1971 THIRD ORDER SYSTEM
IF PosSW THEN
     C3Xx = C3Xx + C3x * Xerr * RHz              'Compute mixed Up (E-W)
     Up = Up + (r(1) - C2x * Xerr - C3Xx) * RHz  'Aircraft velocity (m/s)
```

```
     Xi = Xi + (Up - C1x * Xerr) / (hz * clon)   'Aircraft longitude (deg)

     Yi = Yi + (Vp - C1y * Yerr) / (hz * clat)   'Aircraft latitude (deg)
     C3Yx = C3Yx + C3y * Yerr * RHz              'Compute mixed Vp (N-S)
     Vp = Vp + (r(2) - C2y * Yerr - C3Yx) * RHz  'Aircraft velocity (m/S)

     Hx = Psi - r(18)                            'Feedback error (rad)
     C3Hx = C3Hx + C3h * Hx * RHz                'Compute mixed Psi heading
     Yr = Yr + (C1h * r(11) - C2h * Hx - C3Hx) * RHz 'Aircraft turn rate (rad/s)
     Psi = Psi + (Yr - C1h * Psi + r(11)) * RHz  'Aircraft heading
END IF
     C3Zx = C3Zx + C3z * Zx * RHz                 '
     Wp = Wp + (r(3) - g0 - C2z * Zx - C3Zx) * RHz 'Vertical velocity (m/s)
     Zx = Zi - Palt '- C4z * Wp                   'Feed back error
     Zi = Zi + (Wp - C1z * Zx) * RHz              'Inertial Altitude (m)

'COMPUTE VELOCITY RELATIVE TO EARTH COORDINATES
W = Wa + Wp: x(1) = W
U = Ua + Up: x(2) = U
V = Vp + Va: x(3) = V

'EDDY CO-VARIANCE COMPUTATIONS
Xrm(1) = rm1 * Xrm(1) + rm2 * x(1)
dmx = x(1) - Xrm(1)
FOR i = 2 TO 8
    Xrm(i) = rm1 * Xrm(i) + rm2 * x(i)
    dmy = x(i) - Xrm(i)
    avg(i) = avg(i) + dmy
    var(i) = var(i) + dmy ^ 2
    cov(i) = cov(i) + dmx * dmy
    cov2(i) = cov2(i) + (dmx * dmy) ^ 2
NEXT i
STATISTICS (2)
END SUB
```

```
SUB ROTATE (ang)

' ************************************************************************
' *                                                                      *
' * PURPOSE:                                                             *
' *      Three-dimensional coordinate rotation of Ax,Ay,Az and Ua,Va,Wa  *
' *      from aircraft to earth coordinates.                             *
' *                                                                      *
' * REMARKS:                                                             *
' *   Transforms from right handed aircraft coordinate system to right   *
' *   handed earth coordinate system.  Phi, theta and psi are positive   *
' *   to left , nose up and with compass. East and not north is zero.    *
' *   Three calls required for complete 3-D rotation.  Order of each 2-D *
' *   coordinate rotation is Roll (phi), Pitch (theta) and heading (psi) *
' *                                                                      *
' ************************************************************************
'
SWAP r(1), r(2): SWAP r(2), r(3)        'swap accelerations
sang = SIN(ang): cang = COS(ang)        'rotate accelerations
dmy = r(1) * cang + r(2) * sang
r(2) = -r(1) * sang + r(2) * cang
r(1) = dmy
SWAP Ua, Va: SWAP Va, Wa                'swap velocities
dmy = Ua * cang + Va * sang             'rotate velocities
Va = -Ua * sang + Va * cang
Ua = dmy
END SUB


SUB LORAN STATIC
'
' ************************************************************************
' *                                                                      *
' * PURPOSE:                                                             *
' *      TO READ LORAN LAT/LON  DATA AND COMPUTE Ua,Va CORRECTION FACTORS *
' *                                                                      *
' * INPUT:                                                               *
' *      FILE #4=LORAN LAT/LON DATA                                      *
' *                                                                      *
' * OUTPUT:                                                              *
' *      tn   -valid time for new lat/lon0 (sec from file start)         *
' *      lat  -latitude reference at time (DEG)                          *
' *      lon  -longitude location at time (deg)                          *
' *                                                                      *
' * Note at 55m/s the change in lat/long is only about .0004 deg/s       *
' ************************************************************************
'
CONST LnLag = 0                         'Lag in loran data
'GET NEW LORAN COORDINATES AND TIME
```

```
lct = lct + 1                          '# of loran lat/lon read
tn = lct * tinc + LnLag + dstim        'time of reading
lon0 = lon: lat0 = lat
GET #4, , lat                          'read new latitude
GET #4, , lon                          'read new longitude
Yerr = clat * (Yi - lat)               'Yerr=Loran lat - Aircraft lat
Xerr = clon * (Xi - lon)               'Xerr=Loran - Aircraft lon
XerrB = XerrB + Xerr                   'Sum for computation of path avg error
YerrB = YerrB + Yerr                   'Sum for computation of path avg error
END SUB
```